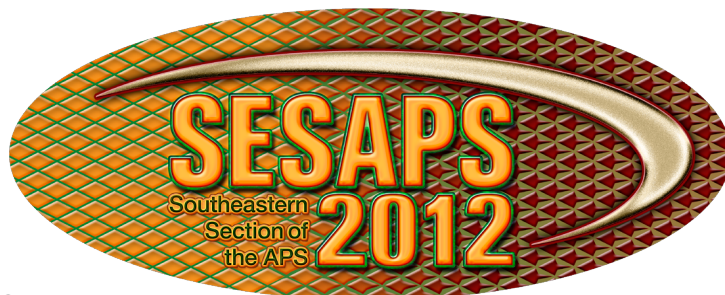


# BULLETIN

## of the American Physical Society

79<sup>th</sup> Annual Meeting of the Southeastern Section of the APS  
Wednesday–Saturday, November 14<sup>th</sup>–17<sup>th</sup>, 2012, in Tallahassee, Florida



November 2012  
Volume 57, No. 16



---

On the cover: Upper photograph shows the Westcott Building on the Florida State University Campus; Lower photograph is the Center for Plasma Science and Technology (FAMU), located at Innovation Park.

The SESAPS12 logo was designed by Scott Baxter, graphics designer in the Department of Physics at Florida State University. It depicts snake skin on the left in the FAMU colors of orange and green, transitioning to spearheads in the FSU colors of garnet and gold on the right.

# Bulletin of the American Physical Society

79th Annual Meeting of the Southeastern Section of the APS Volume 57, Number 16

Wednesday-Saturday, November 14-17, 2012; Tallahassee, Florida

## Contents

<b>SESSION AA: Registration (4:00-6:00PM)</b>	
<i>16:00 Wednesday Afternoon</i>	1
<b>SESSION AB: Reception</b>	
<i>17:00 Wednesday Evening</i>	1
<b>SESSION AC: Public Lecture I: The Higgs Particle and the Destiny of the Universe</b>	
<i>19:30 Wednesday Evening</i>	1
<b>SESSION BA: Results from LHC I</b>	
<i>08:30 Thursday Morning</i>	1
<b>SESSION BC: National High-Field Magnet Laboratory I</b>	
<i>08:30 Thursday Morning</i>	3
<b>SESSION CA: Atomic, Molecular, and Optical Physics I</b>	
<i>10:45 Thursday Morning</i>	6
<b>SESSION CB: Panel Discussion: The Under-Represented Majority</b>	
<i>10:45 Thursday Morning</i>	8
<b>SESSION CC: Condensed Matter Physics I</b>	
<i>10:45 Thursday Morning</i>	8
<b>SESSION DA: Applied Physics I</b>	
<i>13:30 Thursday Afternoon</i>	11
<b>SESSION DB: Mathematical and Computational Physics</b>	
<i>13:30 Thursday Afternoon</i>	13
<b>SESSION DC: Nuclear Physics I</b>	
<i>13:30 Thursday Afternoon</i>	15
<b>SESSION EA: Nanoscale Physics</b>	
<i>15:45 Thursday Afternoon</i>	17
<b>SESSION EB: Undergraduate Talks</b>	
<i>15:45 Thursday Afternoon</i>	18
<b>SESSION EC: Particle Physics I</b>	
<i>15:45 Thursday Afternoon</i>	20
<b>SESSION FA: Banquet</b>	
<i>18:00 Thursday Evening</i>	21
<b>SESSION FB: Public Lecture II: SUSY and the Lords of the Ring</b>	
<i>20:00 Thursday Evening</i>	21
<b>SESSION GA: Results from LHC II</b>	
<i>08:30 Friday Morning</i>	22
<b>SESSION GB: Statistical and Nonlinear Physics</b>	
<i>08:30 Friday Morning</i>	23

<b>SESSION GC: Biological Physics</b>	
<i>08:30 Friday Morning</i>	<b>26</b>
<b>SESSION HA: Applied Physics II</b>	
<i>10:45 Friday Morning</i>	<b>28</b>
<b>SESSION HB: Atomic, Molecular, and Optical Physics II</b>	
<i>10:45 Friday Morning</i>	<b>29</b>
<b>SESSION HC: Nuclear Physics II</b>	
<i>10:45 Friday Morning</i>	<b>31</b>
<b>SESSION IA: Tours of Facilities</b>	
<i>13:45 Friday Afternoon</i>	<b>33</b>
<b>SESSION JA: Executive Committee Meeting</b>	
<i>16:00 Friday Afternoon</i>	<b>34</b>
<b>SESSION JB: SESAPS Business Meeting</b>	
<i>17:30 Friday Evening</i>	<b>34</b>
<b>SESSION KA: Poster Session (6:00-10:00PM)</b>	
<i>18:00 Friday Evening</i>	<b>34</b>
<b>SESSION LB: Condensed Matter Physics II</b>	
<i>08:30 Saturday Morning</i>	<b>53</b>
<b>SESSION MB: Particle Physics II</b>	
<i>10:45 Saturday Morning</i>	<b>55</b>
<b>SESSION MC: National High-Field Magnet Laboratory II</b>	
<i>10:45 Saturday Morning</i>	<b>57</b>

---



**General Information.** The 79th Annual Meeting of the Southeastern Section of the American Physical Society will be held November 14 - 17, 2012 (Wednesday - Saturday) at The Double Tree Hotel in Downtown Tallahassee. The meeting is hosted by the Department of Physics at Florida Agricultural and Mechanical University and the Department of Physics at Florida State University. Detailed, up-to-date information about the meeting can be found at <http://sesaps12.fsu.edu/SESAPS12>.

**Scientific Program.** The program includes contributed and invited talks on astronomy, astrophysics, atomic physics, biophysics, complex fluids, computational physics, condensed matter physics, education in physics, energy, gravitation, high energy physics, nanophysics, national laboratories, neutrino physics, nuclear physics, statistical and nonlinear physics, string theory, and superconductivity.

- There will be a welcome reception Wednesday evening at the Double Tree Hotel from 17:00-19:00pm.
- There will be a public lecture on “The Higgs Particle and the Destiny of the Universe” at the nearby Challenger Learning Center (see map on page vi) at 19:30 on Wednesday evening. The lecture will be given by Professor Harrison Prosper of Florida State University.
- The conference banquet will take place at the Double Tree Hotel on Thursday evening. Presentation of the Beams, Pegram, and Slack awards will be made at the banquet. This will be followed by a public lecture at the Challenger Learning Center by Professor James Sylvester Gates from the University of Maryland on “SUSY and the Lords of the Ring.”
- There will be a panel discussion on “The Under-Represented Majority” in Physics on Thursday morning at 10:45am. Modest treats will be provided.
- Tours of local research facilities will take place immediately after lunch on Friday afternoon. The first bus will leave the hotel at 13:30. The last bus will leave Innovation Park at 17:00 to return to the hotel.
- A poster session will be held Friday evening from 18:00 - 22:00pm.

**SESAPS 2012 Mugs.** Mugs with the SESAPS 2012 logo are available for purchase at the registration desk Wednesday 4:00-7:00pm, and Thursday and Friday mornings from 8:00 - 10:00am.

**Information for Speakers.** All meeting rooms will be equipped with LCD projectors and speakers are strongly encouraged to use electronic projection. You may use your laptop for driving the projector. However, in order to save setup time, it is strongly preferred that speakers use the conference computer for presentation. We recommend that you bring the electronic file for your presentation either on a CD or a memory stick. All speakers using electronic projection in contributed talk sessions should plan to arrive at the meeting room at least 30 minutes prior to the start of the session to check that the technology will work with minimum delay between speakers. Overhead projectors will also be available for those who prefer using transparencies.

**Meeting Site, Transportation and Accommodations.** The scientific sessions will take place at The Double Tree Hotel. Participants are responsible for making their own reservations. A room block has been established for your convenience at The Double Tree Hotel (Phone: 850-224-5000). Lodging rooms are being offered at \$104 per room/per night. Please ask for the “APS” room block. Reservations are to be made no later than Friday, October 20, 2012. The Double Tree Hotel is located at 101 South Adams Street, in Tallahassee, Florida. The closest airport is Tallahassee Regional Airport (TLH). The Double Tree Hotel provides free airport shuttle service, depending on the availability of the shuttle. Call the hotel for service. Taxi service is also available.

## Conference Facilities Map:



For sightseeing ideas during your stay, please visit the Visit Tallahassee website (<http://www.visittallahassee.com>). A short walk from the meeting venue will take you to the Capitol Complex. On the 22nd floor, you will be treated to a panoramic view of Tallahassee.

**Registration.** Preregistration is strongly encouraged. See the conference web site for details. On-site registration desks will be open on Wednesday 4:00-7:00pm, and Thursday and Friday mornings from 8:00 - 10:00am. Only cash and checks can be accepted during on-site registration.

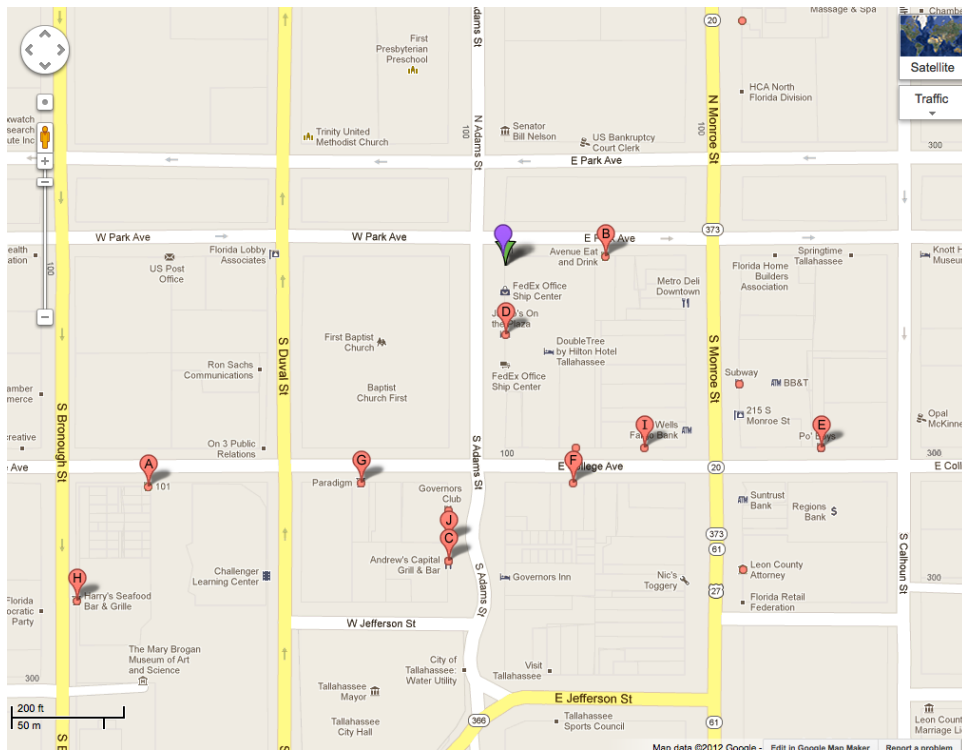
**Special Programs for Undergraduates.** SESAPS will offer a boxed set of the Feynman Lectures in Physics each for “Best Undergraduate Poster” and “Best Undergraduate Oral Presentation.” If you wish to have your submission judged for either prize during the meeting, please indicate this by typing “Undergraduate Poster” or “Undergraduate Oral Presentation” in the Special Instructions box on the APS Abstract Submission page. There will also be an opportunity for on-site registration of your submission.

**Future Meetings.** The next annual meeting of SESAPS will be hosted by Western Kentucky University. Please contact Prof. Edward J. Kintzel, Department of Physics and Astronomy, WKU, ([edward.kintzel@wku.edu](mailto:edward.kintzel@wku.edu)) for more information.

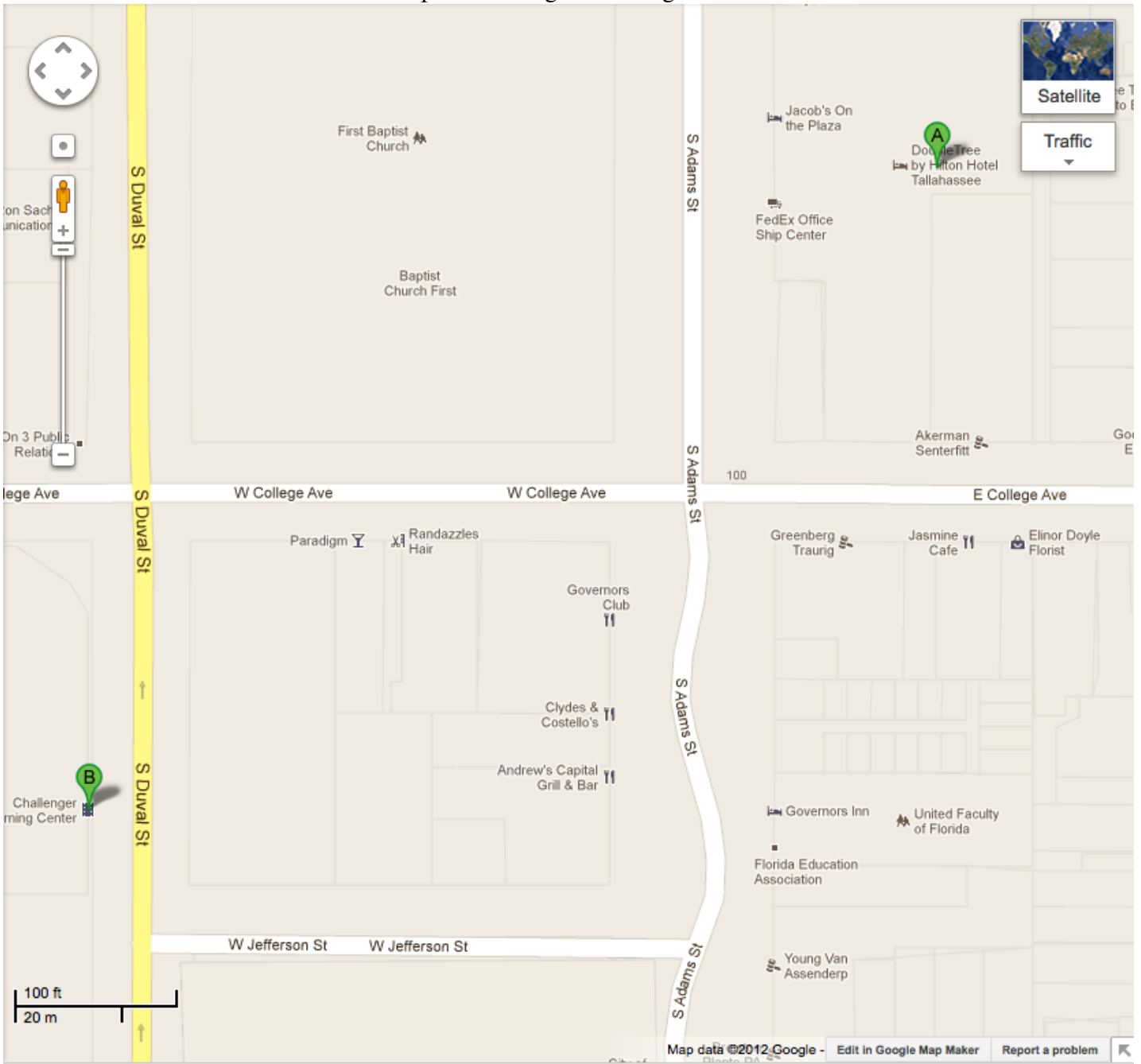
**For help or further information** The local SESAPS12 meeting contacts are Prof. Charles Weatherford ([charles.weatherford@famuedu](mailto:charles.weatherford@famuedu)), Prof. Mark Jack ([mark.a.jack@gmail.com](mailto:mark.a.jack@gmail.com)), Prof. Lewis Johnson ([lewis@cepast.famuedu](mailto:lewis@cepast.famuedu)), Prof. Paul Eugenio ([eugenio@fsu.edu](mailto:eugenio@fsu.edu)) and Prof. Winston Roberts ([wroberts@fsu.edu](mailto:wroberts@fsu.edu)). The chair of the Program Committee is Prof. Richard Haglund ([richard.haglund@vanderbilt.edu](mailto:richard.haglund@vanderbilt.edu)).

## Nearby Restaurants:

- A. 101 Restaurant, 215 West College Avenue, 0.1 mi SW, The Tallahassee Center, (850) 391-1309, 101tallahassee.com
- B. Avenue Eat and Drink, 115 East Park Avenue, 179 ft E, (850) 224-0115, avenueeatanddrink.com
- C. Andrew's Capital Grill & Bar, 228 South Adams Street, 0.1 mi S, (850) 222-3444, andrewsdowntown.com
- D. Jacob's On the Plaza, 101 South Adams Street, 123 ft S, (850) 224-7200, doubletree1.hilton.com
- E. Po' Boys, 224 East College Avenue, 0.1 mi SE, (850) 224-5400, poboys.com
- F. Jasmine Cafe, 109 East College Avenue, 404 ft S, (850) 681-6868, jasmine-cafe.com
- G. Paradigm, 115 West College Avenue, 462 ft SW, (850) 224-9980, clubparadigm.com
- H. Harry's Seafood Bar & Grille, 301 South Bronough Street, 0.2 mi SW, (850) 222-3976, hookedonharrys.com
- I. Goodies Eatery, 116 East College Avenue, 407 ft SE, (850) 681-3888
- J. Clydes & Costello's, 210 South Adams Street, 501 ft S, (850) 224-2173



# Map to Challenger Learning Center



---

## **SESSION AA: Registration (4:00-6:00PM)**

*16:00 Wednesday Afternoon*

Salon A

---

## **SESSION AB: Reception**

*17:00 Wednesday Evening*

Ballroom

---

## **SESSION AC: Public Lecture I: The Higgs Particle and the Destiny of the Universe**

*19:30 Wednesday Evening*

Challenger Learning Center

Chair: Winston Roberts, Florida State University

19:30 AC 01 *The Higgs Particle and the Destiny of the Universe*

**Prosper, Harrison;** ( Invited Speaker ) Florida State University

On July 4th 2012, scientists at the European Laboratory for Particle Physics announced the discovery of a particle with properties consistent with the elusive Higgs boson. If the particle is indeed the Higgs boson, its discovery would be the most significant event in the field of high energy physics in more than forty years. In this talk, we shall answer the following questions. What is the Higgs boson? How did we look for it? What did we find? Why is it important? Along the way, we shall provide a panoramic view of our current understanding of matter, energy, and forces and end with a discussion of how the destiny of the universe is linked to this most mysterious of particles.

---

## **SESSION BA: Results from LHC I**

*08:30 Thursday Morning*

Ballroom

Chair: Takemichi Okui, Florida State University

08:30 BA 01 *ATLAS 2.0: an update*

**Arce, Ayana;** ( Invited Speaker ) Duke University, ATLAS Collaboration

With the discovery of a new boson by the Large Hadron Collider experiments ATLAS and CMS, the ATLAS experiment has entered a new phase. Regardless of whether the theoretical landscape in particle physics is

narrowed or broadened with this discovery, some new, concrete challenges have become central to the ATLAS physics program. In this talk, I will report on relevant results of ATLAS searches and measurements over the past year and discuss how the experiment must continue to evolve to meet these challenges.

09:00 BA 02 *Overview of the Physics Program of the CMS Experiment*

**Neu, Chris;** ( Invited Speaker ) University of Virginia

The exceptional performance of the Large Hadron Collider has allowed unprecedented study of the phenomena of the fundamental world. The Compact Muon Solenoid experiment (CMS) is using the data collected in the 2011 and 2012 campaigns to pursue some of the most important questions in modern physics: What is the origin of mass? What is dark matter? Are there really only 4 forces in the physical world? How did the matter-antimatter asymmetry of the universe arise? Are there additional dynamics in the fundamental world that we have not yet observed? Does the universe possess dimensions beyond the 3+1D world we are familiar with? In this talk, the physics program of the CMS experiment will be discussed, highlighting the measurements and searches that attempt to address these crucial open questions.

09:30 BA 03 *Search for Heavy Stable Charged Particles at CMS*

**Veeraraghavan, Venkatesh;** (On behalf of the CMS collaboration) Florida State University

Several models of new physics, including split supersymmetry, predict the existence of a heavy particle, which is long-lived on timescales of the bunch spacing of the LHC. Such a particle would be observable using the Compact Muon Solenoid (CMS) at the Large Hadron Collider (LHC), and although produced at high momentum, it would travel slowly due to its large mass. We describe a search for these particles, using the experimental techniques of time of flight and dE/dx measurement. Results are presented based on data recorded with CMS in 2011, and possibly 2012.

09:42 BA 04 *Search for Higgs Production in Association with Top Quarks at CMS*

**Wood, John;** University of Virginia

Recent observations of a new boson with mass of 125 GeV are generally consistent with the Higgs of the Standard Model. The properties of this new particle must now be understood in detail in order to say anything conclusive about its relationship to a SM Higgs. The observation of this new particle in association with top quarks would allow the couplings of this particle to top and bottom quarks to be measured. ttH production, with H to bb, is an excellent channel to explore, given the well-understood ttbar kinematics and efficient b-tagging at CMS. However, this channel presents some difficult challenges due to a low signal to background ratio and uncertainties of SM background processes. This talk describes the search for the SM Higgs boson in association with top quarks at CMS, focusing on our background modeling and signal extraction techniques.

09:54 BA 05 *Pseudoscalar Higgs production in association with heavy-quark pairs at hadron colliders*

**Hartanto, Heribertus; Reina, Laura;** Florida State University **Jackson, Christopher;** University of Texas at Arlington

We present the next-to-leading order QCD predictions for the pseudoscalar Higgs production in association with heavy-quark pairs at hadron colliders ( $pp(p\bar{p}) \rightarrow Q\bar{Q}A^0$ ) where both the top and bottom quark pairs in the final states are considered. We compare the total cross sections as well as some differential distributions against the scalar Higgs case.

10:06 BA 06 *Threshold Resummation and Global Fits for Parton Distribution Functions*

(This work is supported by DOE Grant No. DE-FG02-97ER41022)

**Westmark, David;** Florida State University

QCD calculations for hard scattering hadronic processes involve convolutions of partonic cross sections with parton distribution functions (PDFs). In regions of phase space near partonic thresholds it is known that there are large threshold logarithms that can be resummed using soft-gluon resummation techniques. Deep inelastic scattering (DIS) and lepton pair production (LPP) are primary sources of information on PDFs. Due to the differing kinematics for DIS and LPP, the threshold resummation effects contribute differently to the two processes.

Recent global fits for PDFs have used DIS data from the large Bjorken  $x$ , moderate  $Q^2$  region where threshold effects are known to be large. It is the purpose of the present project to explore the effects of simultaneously incorporating threshold resummation in both DIS and LPP and to evaluate the effects of such additions on global fits. The status of the progress to date will be reviewed.

10:18 BA 07 *Threshold resummation in direct photon production.*

**Sato, Nobuo**; Florida State University

The precise knowledge of momentum distribution inside nucleons plays a key factor for the physics of hadron-hadron collisions such as LHC. In particular, the process of direct photon production with high transverse momentum can be used to constrain the momentum distribution of gluons inside nucleons because of the dominant contribution from Compton scattering  $qg \rightarrow \gamma q$ . Over the last three decades, this process has been extensively measured by several experiments at different energies. The comparison between the experimental data and the theoretical predictions has shown satisfactory agreement at high energies and inconsistencies at low energies, leading to the necessity to improve the theoretical predictions. This talk will discuss one kind of improvement called “threshold resummation” and its impact on predictions of the global set of direct photon data.

---

## SESSION BC: National High-Field Magnet Laboratory I

*08:30 Thursday Morning*

Adams-Park

Chair: James Brooks, Florida State University

08:30 BC 01 *Evolution of the Fermi Surface of Chromium at High Pressure and High Magnetic Fields*

**Stillwell, Ryan**; National High Magnetic Field Laboratory, Florida State University **Graf, David**; **Coniglio, William**; **Murphy, Timothy**; **Palm, Eric**; **Park, Ju-Hyun**; National High Magnetic Field Laboratory **Schlottmann, Pedro**; **Whalen, Jeffrey**; **Vasquez, Rafael**; **Siegrist, T.M.**; National High Magnetic Field Laboratory, Florida State University **Tozer, Stanley**; National High Magnetic Field Laboratory

Results on the pressure dependence of the Fermi surface of chromium will be presented. Employing plastic turnbuckle diamond anvil pressure cells in pulsed magnetic fields and metal diamond anvil cells in DC magnetic fields, skin depth measurements of chromium were made at low temperatures which yielded Shubnikov-de Haas oscillations. By performing in situ rotations of the pressure cell we are able to map out the Fermi surfaces as we move towards the quantum critical point at which the antiferromagnetic phase is suppressed.

08:42 BC 02 *High Field Measurements of the Peierls and Spin-Peierls Transition in the Organic Conductor  $(Per)_2[Pt(mnt)_2]$  Using a Tunnel Diode Oscillator*

(Work supported in part by the NSF, DOE, and the State of Florida.)

**Winter, Laurel**; **Brooks, James**; Florida State University, National High Magnetic Field Laboratory

Recently, we have used a tunnel diode oscillator (TDO) to investigate the organic conductor  $(Per)_2[Pt(mnt)_2]$ , which undergoes both a Peierls (charge density wave - CDW) and spin-Peierls (SP) transition. Previously performed temperature dependent studies such as resistivity, specific heat, and susceptibility all show a common transition at  $T_c \sim 6 - 8$  K. Since these two transitions appear to occur exactly at the same temperature, the question of coupling between the two chains remains open. In addition, since each method is primarily sensitive to either the CDW transition or the SP transition it is possible some small temperature difference separating the two is not evident from these techniques. In this situation, the TDO technique is ideal to investigate the possible temperature difference between the two transitions, due to its high sensitivity and ability to simultaneously measure both changes in electrical transport and magnetic properties of a material. It is in this context that we will discuss the current TDO developed phase diagram of  $(Per)_2[Pt(mnt)_2]$  at fields up to and above 15 T, as well as discuss what exactly the TDO is measuring since it is a vital part of understanding the results of the study.



08:54 BC 03 *Magnetic Field and Temperature Dependence of Decoherence in a High Mobility Landau Quantized 2DEG*

**Curtis, Jeremy**; University of Alabama at Birmingham **Tokumoto, T.T.**; University of Alabama at Birmingham **Cherian, J.G.**; Florida State University **Wang, X.**; Rice University **McClintock, Luke**; University of Alabama at Birmingham **Reno, J.L.**; Sandia National Laboratories **Belyanin, A.**; Texas A&M University **Kono, J.**; Rice University **McGill, S.A.**; National High Magnetic Field Laboratory **Hilton, D.J.**; University of Alabama

We apply a perpendicular magnetic field to a high mobility ( $\mu = 3.4 \times 10^6 \text{ cm}^2 \text{ V}^{-1} \text{ s}^{-1}$ ) two dimensional electron gas (2DEG) which splits the Fermi surface into a spectrum of Landau levels (LL). The highest filled and lowest unfilled LLs are coherently coupled by an incident THz pulse. The time required for carriers in this superposition state to become out of phase is the decoherence time. The focus of our work is to measure this decoherence time over a wide range of temperatures (0.4 K-100 K) and magnetic fields (1.25 T-17.5 T). Using THz time-domain spectroscopy (TTDS), we map the decoherence as a function of B and T. This talk will review previous work done at 0.4 K and 1.25 T; furthermore, we will discuss current work being done to increase our B dependence to 17.5 T using superconducting magnet 3 at the National High Magnetic Field Lab at Florida State University. This work utilizes a novel *reflection* TTDS system.

09:06 BC 04 *Magneto-transport properties of the ternary topological insulator  $(\text{Bi}_{0.5}\text{Sb}_{0.5})_2\text{Te}_3$  in the presence of electrostatic gating and magnetic impurity*

**Yu, Liuqi**; **Barreda, Jorge**; **Hu, Longqian**; **Xiong, Peng**; Florida State University **Guan, Tong**; **He, Xiaoyue**; **Wu, K.**; **Li, Y.**; Chinese Academy of Sciences

A three-dimensional ternary topological insulator,  $(\text{Bi}_{0.5}\text{Sb}_{0.5})_2\text{Te}_3$ , is used to characterize the unique electronic properties of the spin helical conducting surface state. Epitaxial films are grown via MBE on (111)  $\text{SrTiO}_3$  substrate, which serves as the gate dielectric. Magnetoresistance (MR) and Hall effect measurements have been performed in a broad range of back gate voltages. Ambipolar field effect has been observed, enabling effective tuning of the Fermi level across the band gap and identification of the surface transport in the topological transport regime. Weak antilocalization effect is identified and used to differentiate the surface state. The Hikami-Larkin-Nagaoka (HLN) equation is used to analyze the MR data and the results show the top and bottom surfaces become decoupled when the Fermi level is in the bulk band gap. We also examine the effects of paramagnetic impurity (MI), which introduces time reversal symmetry breaking scattering on the TI surface states. Taking advantage of the unique capability of *in situ* deposition of Cr atoms in a customized dilution refrigerator, MI was incrementally quench-condensed onto the sample surface and transport measurements were performed at each MI density. Pronounced changes in the weak antilocalization effect and the sample carrier density with increasing MI concentration were observed. Possible origins of these observations will be discussed.

09:18 BC 05 *Unusual Hall effect of  $\text{La}_{0.67}\text{Ca}_{0.33}\text{MnO}_3$  thin films with percolative phase transition*

**Yu, Liuqi**; **Zhang, Xiaohang**; **von Molnar, Stephan**; **Xiong, Peng**; Florida State University **Wang, Lingfei**; **Wu, W.**; USTC

Detailed transport measurements have been performed on three PLD-grown epitaxial  $\text{La}_{0.67}\text{Ca}_{0.33}\text{MnO}_3$  (LCMO) thin films on  $\text{NdGaO}_3$  (NGO) substrate. The films were grown under identical conditions ( $735^\circ\text{C}$  substrate temperature and 45 Pa  $\text{O}_2$  pressure) but post-annealed at  $780^\circ\text{C}$  in flowing  $\text{O}_2$  for 1, 10 and 20 hours respectively to produce increasing degrees of strain relaxation which could lead to charge-ordered states.(Z. Huang et al., JAP 105, 113919(2009)) In all three samples, the Hall resistivity in the paramagnetic phase takes on two distinct slopes: a negative slope at low fields which decreases with increasing temperature, and an almost temperature-independent positive slope at high fields. It is found that the switch in the Hall resistivity slope occurs at the same critical magnetization regardless of both temperature and magnetic field, which we interpret as an indicator of the percolative nature of the phase transitions.(X. Zhang et al., PRL 103, 106602 (2009)) In the two strain-relaxed samples, pronounced dips in the Hall resistivity are observed near the transition temperature. The apparent correlation of the appearance of the dips with increasing strain relaxation and their suppression by increasing in-plane magnetic field suggests a possible connection of the Hall resistivity dips with the presence of the charge ordered state.

Work supported in part by NSF DMR-0908625.

09:30 BC 06 *Mechanical and Physical Measurement Tools and Techniques Related to High Field Magnets*

**Walsh, Robert**; National High Magnetic Field Laboratory

Materials properties are the physical limitation in the achievement of higher magnetic fields and the construction of bigger magnets. High-field magnet designers try to use the newest generation of materials (structural and conductors) and design magnets with factors not acceptable in typical machine design or civil engineering applications. Examples of material property limitations on magnet design are introduced that set the stage for the state-of-the-art facilities necessary for characterizing the materials used in NHMFL magnets. Conventional strain measuring techniques (strain gages are the workhorses) are extended to low temperature tests by using cryogenic compatible materials and low temperature calibrations. For structural materials, strain gage based sensors provide accurate determination of yield strength, ductility, fracture toughness and fatigue life data necessary for efficient/reliable design of the magnets. Superconductors (LTS and HTS) are sensitive materials that often require non-contact strain sensing at cryogenic temperatures. A 3D-Digital Image Correlation system is a non-contact strain measuring system that provides whole-field strain measurement and is currently being extended to cryogenic applications of testing superconductors. Additionally, accurate dimensional characterization of test specimens, before and after testing, is enhanced with a contemporary CNC inspection microscope.

09:42 BC 07 *Enhanced grain connectivity in K-doped ferropnictide Ba-122 bulks and wires with high transport critical current density*

**Weiss, Jeremy; Tarantini, Chiara; Jiang, Jianyu; Kametani, Fumitake; Polyanskii, Anatolii; Larbalestier, David; Hellstrom, Eric**; National High Magnetic Field Laboratory Applied Superconductivity Center

We present very much improved properties of  $(\text{Ba}_{0.6}\text{K}_{0.4})\text{Fe}_2\text{As}_2$  (Ba-122) made as round wires in which transport critical current densities  $J_c$  (4.2 K, SF) in excess of  $0.12 \text{ MAcm}^{-2}$ , which is approximately 5 times higher than any other ferropnictide wire, have been obtained. Careful low-temperature synthesis was used to eradicate extrinsic current-blocking phases and cracks, which also had the effect of producing fine grain size ( $<200\text{nm}$ ) and a high grain boundary density. Very high magnetic field evaluations showed that the upper critical field  $H_{c2}$  was well above 50 T and  $H_{c2}$  anisotropy was significantly less than 2. This low anisotropy suggests that high vortex stiffness and perhaps less suppression of the grain boundary (GB) order parameter occur in this compound compared to the planar GBs of Co-doped Ba-122 used for bicrystal experiments, which showed weak link behavior that limits critical current across GBs like in other high-temperature superconductors.

09:54 BC 08 *Electron spin resonance measurements using on-chip cavities at low temperature*

(NSF Cooperative Agreement Grant No. DMR-0654118 NSF grant No. DMR-0645408 and DMR-1206267)

**Martens, Matthew; Serniak, Kyle**; Florida State University **Bertaina, Sylvain**; Universite Aix-Marseille **Chiorescu, Irinel**; Florida State University

We describe an Electron Spin Resonance (ESR) measurement technique utilizing a balanced bridge, similar to a “magic-T,” in conjunction with a lock-in detector. The setup uses a microstrip line, since this type of approach is highly sensitive and has been gaining more and more interest as of late. We describe the functioning principle and demonstrate that the setup has a high sensitivity, with a low noise baseline. ESR measurements were performed on a  $s=1/2$  DPPH sample at room temperature. Electronic spin excitation of the sample was achieved through use of an “omega” shaped microstrip cavity with resonant frequency of 17.4 GHz. Signal detection was done with a homemade heterodyne detector with and without the magic-T bridge and lock-in detector. For comparison, direct measurements were performed using a fast digital acquisition card.

10:06 BC 09 *Spin Configurations in the 2D Frustrated Spin System  $\text{YBaCo}_4\text{O}_7$  Using NMR*

(Work supported in part by NSF, DOE, and the State of Florida)

**Yuan, S.; Hoch, M.J.R.; Kuhns, P.L.; Besara, T.; Whalen, J.B.; Siegrist, T.M.; Reyes, A.P.; Brooks, James**; Florida State University **Zheng, H.; Mitchell, J.F.**; Argonne National Laboratory

The system  $\text{YBaCo}_4\text{O}_7$  has frustrated kagome spin planes which are separated by triangular AF spin layers. The configurations of the cobalt spins have been studied by neutron scattering at various temperatures, below

$TN=106$  K. In our low temperature NMR experiments on both a powder sample and a single crystal, non-equivalent cobalt sites are associated with distinct peaks in the zero field frequency scan spectra. Information about the internal hyperfine field orientations for both kagome and triangular layers has been obtained in two experiments, (1) rotating the sample with respect to the RF pulse field (zero applied field experiment) and (2) rotating the sample with respect to a small external field (in-field experiment). These approaches can be used to determine the spin configurations. Orthogonal orientations for the kagome hyperfine field and the triangular hyperfine field have been shown in both two experiments. Our low TAF spin alignment for the triangular layers is in agreement with the spin configuration in the neutron findings at 5 K, but for spins in kagome layers our orthogonal spin configuration does not agree with the neutron results.

10:18 BC 10 *Low-energy spectroscopy on molecular materials under high pressures*

**Thirunavukkuarasu, K.**; National High Magnetic Field Laboratory **Kuntscher, C.A.**; University of Augsburg **Bee-  
dle, C.C.**; National High Magnetic Field Laboratory **Winter, Stephen**; University of Waterloo **Kamarás, K.**; Wigner  
Research Center for Physics, Budapest, Hungary **Hennrich, F.**; Karlsruhe Institute of Technology, Eggenstein-Leopoldshafen,  
Germany **Kovalev, A.**; National High Magnetic Field Laboratory **Tozer, Stanley**; National High Magnetic Field Labo-  
ratory **Oakley, R.T.**; University of Waterloo **Hill, S.**; National High Magnetic Field Laboratory

Low-energy spectroscopy at extreme conditions opens doors to discovery and understanding of novel phenomena in condensed matter physics. In particular, applying hydrostatic pressure is the ideal way to continuously induce structural perturbations such as changes in intermolecular distances, and thereby control the various exchange interactions in novel materials. Among low-energy spectroscopic techniques, infrared and electron spin resonance (ESR) spectroscopy are powerful tools to probe the charge and spin degrees of freedom, respectively, and provide important information on the fundamental energy scales involved in various novel phenomena. However, use of these techniques to investigate materials at high pressures involves a high level of difficulty. In this talk, uncommon combinations of high pressure with IR spectroscopy and multi-frequency ESR spectroscopy, and their application to the study of molecular materials will be discussed. Depending on the availability of time, the strength of these techniques will be illustrated with examples.

---

## SESSION CA: Atomic, Molecular, and Optical Physics I

*10:45 Thursday Morning*

Ballroom

Chair: John Yukich, Davidson College

10:45 CA 01 *Controlled Dipole-Dipole Interactions in a Cold Rydberg Gas*

(This work is supported by the National Science Foundation.)

**Jones, Robert**; ( Invited Speaker ) University of Virginia

The great spatial extent of highly-excited Rydberg atoms endows them with large dipole moments and electric polarizabilities, making them extremely sensitive to external fields and neighboring atoms. We use cold diffuse ensembles of Rydberg atoms to explore few-and many-body dipole-dipole interactions at long range. Such systems are of potential interest for quantum computing platforms. We focus on time-domain methods and utilize pulsed lasers and electric fields to create specific electronic superposition states and control the evolution of the excited atoms. We have confirmed that electronic coherence can persist for long times ( $> 10 \mu\text{s}$  in our samples and have evidence that the coherence may be extended through the application of the appropriate control fields. We are exploring methods which exploit the dipole-dipole coupling to transport electronic coherence between atoms and to manipulate the relative positions of atoms in a magneto optical trap.

11:15 CA 02 *Measurements of the Polarization of Spectral Lines of Highly Ionized Ions Using a Two-Crystal Technique*

(We gratefully acknowledge support by US DOE under contract No. DE-FG02-98ER-14877 to Morehouse College and LLNL Research Collaborations Program for HBCU's.)

**Smith, A.J.**; Morehouse College **Beiersdorfer, P.**; **Reed, K.J.**; Lawrence Livermore National Laboratory

We Have measured the polarization of various spectral lines of highly ionized ion species including the inter-combination line of heliumlike vanadium, the resonance lines of heliumlike and lithiumlike sulphur as well as of neonlike and fluorinelike iron. The lines were excited directly by electron impact in the LLNL electron beam ion trap (EBIT-I or EBIT-II) and the polarization measurements carried out using a two-crystal technique. The results of our measurements are important for the diagnostics of astrophysical as well as of laser-produced plasmas. In this presentation we compare our results with theory.

11:27 CA 03 *CO<sub>2</sub> Laser enhanced lifetime of femtosecond and nanosecond produced air plasmas*

**Martinez, Jorge**; **Akpovo, Charlemagne**; **Lewis, Dawn**; **Brown, Staci**; **Johnson, Lewis**; Florida A&M University

Air produced plasmas generated from a 20 mJ femtosecond pulse at 800 nm and a 5 mJ nanosecond pulse at 532 nm were orthogonally enhanced with a 3 J defocused CO<sub>2</sub> pulse to study the effect of interpulse delay on plasma lifetime. When interpulse delay was optimized with respect to the CO<sub>2</sub> pulse, both the femtosecond and nanosecond plasmas exhibited longer lifetimes. The impact of CO<sub>2</sub> laser pulse energy was explored by maintaining a fixed CO<sub>2</sub> laser fluence at the interaction point. The femtosecond/CO<sub>2</sub> combination exhibited the same relationship as with the defocused 3 J pulse with a substantial lengthening of plasma lifetime and luminance. The effect of the enhancing wavelength was studied by replacing the CO<sub>2</sub> laser with a 1064 nm nanosecond laser pulse to monitor any differences in the laser generated air plasmas. The femtosecond/nanosecond combination exhibited quenching of the generated plasma with almost no change in plasma lifetime. A study of these interactions will broaden the understanding of the role of pulse duration and wavelength when considering the phenomena that occur in laser generated plasmas such as inverse bremsstrahlung processes, multi-photon ionization, and collisional heating.

11:39 CA 04 *UV Photoprotection of Ammonia and Adenine Studied by Time-resolved Photoelectron and Photofragmentation Spectroscopy*

(This work was funded by NSF grant CHE-0924456)

**Ullrich, Susanne**; ( Invited Speaker ) University of Georgia

The UV photostability of molecules is determined by excited state electronic relaxation mechanisms that must operate on ultrafast time scales in order to dominate over competing photochemical processes that potentially lead to destruction of the molecule. Electronic excited states with notable  $\sigma^*$  character, centered at X - H (where X = O or N) bonds, may play a particular important role in efficient photoprotection of many (bio)molecules.

We have investigated the photophysics of UV excited ammonia and adenine using three complementary femtosecond (fs) pump-probe techniques: time-resolved photoelectron (TRPES), ion-yield (TRIY) and photofragment translational spectroscopy (TRPTS).

Ammonia, a prototypical amine group which appears in a number of organic molecules, is resonantly excited to specific vibrational levels of its first electronic excited state of  $n\sigma^*$  character. Three deactivation paths are available along the N-H stretching coordinate: Non-adiabatic crossing through a conical intersection leads to either repopulation of the NH<sub>3</sub> ground state or dissociation into ground state NH<sub>2</sub> and H photoproducts whereas adiabatic avoidance correlates with excited state NH<sub>2</sub> and ground state H. TRPES spectra give direct spectroscopic evidence of  $\sigma^*$  mediated relaxation in form of combination bands of the umbrella mode and symmetric stretch. TRPTS measurements of H-atom appearance times provide time constants of < 75 fs to 350 fs for the relaxation, which increase with the amount of internal energy partitioned into the NH<sub>2</sub>co-fragment.

Adenine, a purine DNA base, is shown to undergo similarly efficient  $\pi\sigma^*$  mediated relaxation in competition

with a ring puckering pathway following 200nm photoexcitation to a bright  $^1\pi\pi^*$  state. H-atom photoproducts from the NH-stretching pathway are observed within  $<200$ fs, whereas deactivation along the ring puckering pathway takes  $\sim 700$ fs.

N. L. Evans, H. Yu, G. M. Roberts, V. G. Stavros, S. Ullrich: Observation of Ultrafast  $\text{NH}_3$  ( $\tilde{A}$ ) State Relaxation Dynamics using a Combination of Time-resolved Photoelectron Spectroscopy and Photoproduct Detection, *Phys. Chem. Chem. Phys.*, 2012, **14**, 10401

N. L. Evans, S. Ullrich: Wavelength Dependence of Electronic Relaxation in Isolated Adenine Using UV Femtosecond Time-Resolved Photoelectron Spectroscopy, *J. Phys. Chem. A*, 2010, **114**, 11225

12:09 CA 05 *Excited state dynamics in imidazole, pyrazole and pyrrole studied by femtosecond time-resolved spectroscopy*

**Yu, Hui; Evans, Nicholas; Ullrich, Susanne;** University of Georgia

In many biomolecules including nucleic acids and amino acids, ultrafast ( $<200$ fs) relaxation from an electronically excited state back to the ground state provides a self-protection mechanism against harmful ultraviolet radiation. The excited state dynamics of gas-phase imidazole, a basic five-membered heterocyclic subunit of the above mentioned biomolecules, is thus investigated experimentally to determine its contribution to the photo-protection. The imidazole photophysics are compared to structurally similar pyrrole and pyrazole that are less common in biological chromophores. Time-resolved photofragment translational spectroscopy and H-atom total kinetic release methods have been applied to follow the deactivation dynamics in real time. All three molecules display two competing pathways that operate on femtosecond timescales: A  $\pi\sigma^*$  (N-H dissociation) and a  $\pi\pi^*$  (ring deformation) mechanism are identified based on observation of H-atom and larger photoproducts, with an energetic onset specific to the individual molecule.

---

## SESSION CB: Panel Discussion: The Under-Represented Majority

*10:45 Thursday Morning*

Salon AB

Chair: Roxanne Springer, Duke University

10:45 CB 01 *PANEL DISCUSSION*

What can we do as a community to ensure that our members are provided with equal opportunities to succeed in physics? What steps can each of us take to ensure our own success? All are welcome to this discussion.

---

## SESSION CC: Condensed Matter Physics I

*10:45 Thursday Morning*

Adams-Park

Chair: David Hilton, University of Alabama-Birmingham

10:45 CC 01 *The source of holes in p-type  $\text{In}_x\text{Ga}_{1-x}\text{N}$  films*

(The work is supported by the National Science Foundation, DMR-1006163.)

**Zvanut, Mary Ellen; Willoughby, William;** University of Alabama at Birmingham

InGaN is an important alloy for many optoelectronic applications due to its tunable bandgap, which can range from  $\sim 1$ -3 eV, corresponding to wavelengths of  $\sim 400$ -1200 nm.  $\text{In}_x\text{Ga}_{1-x}\text{N}$  films, with x between 0.02 and

0.11, are studied at 4 K using electron paramagnetic resonance (EPR) spectroscopy. The films were made p-type by doping with Mg to a concentration of  $2\text{-}3 \times 10^{19} \text{ cm}^{-3}$ , and the thickness of each film was between 0.25 and 0.44  $\mu\text{m}$ . Hall measurements show that the hole density of a film increases with increasing In mole fraction, as expected, but the measured EPR intensity of the Mg-related signal is found to decrease. This trend is opposite of what is observed in other nitrides. Because the Mg-related EPR signal intensity represents the amount of unionized Mg, the amount of EPR detected Mg at low temperatures ( $\sim 4\text{K}$ ) tracks the hole concentration at room temperature in p-type GaN films. Together, compensating defects and a lowering of the acceptor level may explain the decrease in EPR intensity and the increase in hole density observed as the In mole fraction is increased.

10:57 CC 02 *Non linear quantum decoherence behavior in the molecular magnet V15*

**Bertaina, Sylvain**; CNRS - IM2NP **Shim, J.**; **Gambarelli, S.**; LCIB - CEA **Mitra, T.**; Bielefeld University **Tsukerblat, B.**; Ben Gurion University **Muller, A.**; Bielefeld University **Baibekov, E.**; **Malkin, B.**; Kazan Federal University **Barbara, B.**; Neel Institut

Molecular magnets attract a great interest for many years since their potential application in quantum information processing. Quantum coherence, the property needed to create a qubit (fundamental piece of a quantum computer) has shown recently in V15 [1]. Since, the studies of decoherence behavior in molecular magnets have been extremely active. In the present talk, we will present a non linear microwave power dependence of the decoherence in V15 [2]. Generally, the decoherence probed but electron spin resonance increase linearly when the microwave field increase. Here we will show how the nuclear spin bath could dramatically change this dynamic. When the Rabi frequency is close to the nuclear Zeeman frequency coherence form the electron spin in transferred to the nuclear spin and is dissipated reducing the macroscopic electron spin coherence.

[1] Bertaina, S., Gambarelli, S., Mitra, T., Tsukerblat, B., Müller, A., & Barbara, B. (2008). Quantum oscillations in a molecular magnet. *Nature*, 453(7192), 203–6.

[2] Shim, J., Bertaina, S., Gambarelli, S., Mitra, T., Müller, a., Baibekov, E., Malkin, B., et al. (2012). Decoherence Window and Electron-Nuclear Cross Relaxation in the Molecular Magnet V15. *Physical Review Letters*, 109(5), 1–5.

11:09 CC 03 *Construction of a THz-Time Domain Spectrometer in Reflection Geometry*

**McClintock, Luke**; **Curtis, Jeremy**; **Hilton, D.J.**; University of Alabama at Birmingham

We have constructed a terahertz (THz) time-domain spectrometer in reflection geometry. THz time-domain spectroscopy (TTDS) is an ultrafast sampling technique that utilizes nonlinear optics to generate and detect the electric field reflected THz radiation. This unique sampling technique allows us to probe dynamics of materials that have absorption features in the THz frequency range at picosecond time scales. We have demonstrated the determination of optical constants of gallium arsenide using this spectrometer in the reflection geometry, which shows that this design overcomes many of the experimental difficulties traditionally associated with coherent terahertz measurements in the reflection geometry.

11:21 CC 04 *Inductive Critical Currents in Nb/Ni bilayers*

**Broussard, Phillip**; **Davis, Emily**; **Ahrenholz, Timothy**; Covenant College

We have carried out measurements of inductive critical currents in Nb/Ni bilayers. The films were grown by magnetron sputtering onto room temperature silicon substrates from separate sources. The bilayers were composed of an initial 33 nm Nb layer followed by a Ni layer, which was varied from 0-7 nm. Inductive critical currents were measured using a third harmonic technique at 1 kHz.  $J_c$  varies as  $(1 - t)^\gamma$  with  $\gamma$  being  $3/2$  as expected for pure Nb films, but decreasing as the Ni layer is increased (here  $t$  is the reduced temperature,  $T/T_c$ ). Our pure Nb film had a  $T_c$  of 7.7 K with an inferred  $J_c(0)$  of 61 MA/cm<sup>2</sup>. As the Ni layer is increased, we see a marked reduction in the critical current which continues as the Ni layer is increased. Unlike the  $T_c$ 's for these samples, we do not see nonmonotonic behavior in the critical current, with  $J_c(0)$  reducing to a constant value as Ni thickness goes beyond 3 nm.

11:33 CC 05 *Tunable bands in biased multilayer epitaxial graphene*

(Work supported by NSF under grants PREM DMR-0934142, MRSEC DMR-0820382, and CREST HRD-1137751 and AFOSR under grant FA9550-10-1-0254.)

**Williams, Michael D.; Samarakoon, Duminda K.;** Clark Atlanta University **Hess, Dennis W.;** Georgia Institute of Technology **Wang, Xiao-Qian;** Clark Atlanta University

We have studied the electronic characteristics of multilayer epitaxial graphene under an electric bias. Ultraviolet photoemission spectroscopy measurements reveal that there is a notable increase of the electronic density-of-states in valence bands near the Fermi level. The evolution of electronic structure of rotational-stacked multilayer epitaxial graphene as a function of the applied electric bias is investigated using first-principles density-functional theory including interlayer van der Waals interactions. The tailoring of electronic band structure is shown to correlate with the interlayer coupling tuned by the applied bias. The implications of tunable electronic structure of rotational-stacked epitaxial graphene grown on the C-face of SiC for future device applications are discussed.

Nanoscale DOI:10.1039/c2nr1199a

11:45 CC 06 *Free flux flow: irradiation-induced effects and restricted geometries*

(Funded by an RUI grant from the National Science Foundation.)

**Gafarov, O.; Alexander, J.A.; Gapud, A.A.;** University of South Alabama **Christen, D.K.;** Oak Ridge National Laboratory (retired) **Wu, J.Z.;** University of Kansas

The field-dependent core size of magnetic flux quanta – fluxons – in the mixed state of Type II superconductors has a distinctive effect on free flux flow (FFF), the dissipative motion of fluxons in the absence of pinning. These core size effects have been previously observed by confirming a modification to the traditional Bardeen-Stephen flux-flow (BSFF) model by Kogan and Zelezhina (KZ) using high-density transport currents in weak-pinning, isotropic, low- $T_c$  compounds. Further exploration to provide insight into these phenomena are proposed: (1) Irradiation-induced effects on carrier scattering: FFF is affected by the electronic structure of the normal flux-core states; there is interest in how the flux dynamics could be altered by the modification of core states using low-level irradiation as a tool for incremental control of carrier scattering. (2) Restricted-geometry flux flow: Simulations of granular flow via FFF had been proposed previously; specifically, there is interest in observing the dynamics of flux flow through a narrow channel that has a two-dimensional “hopper” geometry, for comparison with known results from granular-flow studies.

11:57 CC 07 *Alkanethiol Coated Nanosprings for the Detection of Nitrogen-Rich Explosives*

**Hall, Jessica; Larin, Alexander; Sowell, Dewayne; Dobrokhoto, Vladimir;** Applied Physics Institute

In battle fields without clearly drawn lines such as Iraq and Afghanistan the detection of Improvised Explosive Device (IED) requires the use of advanced detection methods. A method of detection is to use alkanethiol coated nanosprings for the detection of nitrogen-rich explosives. The intent was to functionalize the nanospring mats for the detection of TNT, but through experimentation it was found that they are significantly more sensitive and selective to ammonium nitrate. Ammonium nitrate is the explosive component of fertilizer found in many IEDs. There is potential to incorporate these functionalized nanospring mats into an integrated system for the detection of IEDs.

12:09 CC 08 *Morphology and conductivity studies on carbazole based GUMBOS thin films*

(LEQSF(2011-14-RD-A-07), NASA (2011)-DART-44, Dr. K. M. Johnson (AES Corporation), NSF DMR 0843962)

**Kanakamedala, Kalyan; Siraj, Noureen; Divakar, Madhavi; Hasan, Farhana; Das, Susmita; Warner, Isiah; Daniels-Race, Theda;** Louisiana State University

The use of thin films in opto-electronic devices such as organic light emitting diodes (OLEDs) and solar cells has been widely investigated. Historically with respect to the latter, multiple methods have been under study to improve device efficiency, yet the cost of production to meet general-purpose applications is still high. Addressing this challenge, we investigate the feasibility of carbazole based thin films as may be applied to future solar cell



production. Based upon the recently discovered Group of Uniform Materials Based on Organic Salts (GUMBOS) [1], carbazole based GUMBOS and their nanoparticles were used in the preparation of thin films involving various techniques such as drop casting, vacuum drying, electrospraying and electrospinning. Via comparative studies of morphology and conductivity, we present results indicative of the potential opto-electronic functionality of these unique materials.

[1] A. Tesfai, B. El-Zahab, D.K. Bwambok, G.A. Baker, S.O. Fakayode, M. Lowry, I.M. Warner, Controllable formation of ionic liquid micro- and nanoparticles via a melt-emulsion-quench approach, *Nano Letters*, 8 (2008) 897-901.

12:21 CC 09 *Adhesion measurement of carbon nanotube films deposited on silicon substrates*  
(LEQSF(RD-A-07; PFUND233), NASA, KM Johnson (AES))

**Sarkar, Anirban; Daniels-Race, Theda;** Louisiana State University

Electrophoretic deposition (EPD) has attracted substantial interest as a room temperature based economical and versatile processing technique. EPD has been used in the fabrication of thin and thick films of carbon nanotubes (CNTs) on conducting substrates. However, in this work, to the best of our knowledge, for the first time EPD of CNTs on semiconducting substrates—both bare and coated (Si/SiO<sub>2</sub>, Si/Si<sub>3</sub>N<sub>4</sub>) silicon — has been investigated in detail. The process resulted in CNT film thicknesses of up to  $\sim 15 \mu\text{m}$  from aqueous suspensions at low deposition voltages (5-30 V). A thin layer of metal film ( $\sim 300 \text{ nm}$  of aluminum), thermally evaporated on the samples, promotes adhesion between the CNTs in the EPD suspension and the intended target surfaces. In this study, post-EPD measurements have been investigated to assess the adhesion strength of the fabricated films. The qualitative measurements include the Peel Test (as per the American Society for Testing and Materials (ASTM) D-3359-97 standard) and ultrasonication tests. Direct pull off and nitrogen gas impingement tests have been developed for quantitative estimation. Experimental results indicate interfacial adhesion strength greater than 0.5-1 MPa between the fabricated films and substrates. Values reported are indicative of the applicability of electrophoretically fabricated CNT films for silicon based micro-electronics and MEMS development.

---

## **SESSION DA: Applied Physics I**

*13:30 Thursday Afternoon*

Ballroom

Chair: Richard Haglund, Vanderbilt University

13:30 DA 01 *Electrical Disturbances in Near-Earth Orbits due to Space Plasmas*

**Atkinson, William;** ( Invited Speaker ) Boeing Company

A Simulator is presented that models the disturbance of electrical circuits by high energy electrons trapped in earth's radiation belts; the model components are a module computing the electron fluence rate given the altitude, the time of the year, and the sunspot number, a module that models the interaction of the electrons with the materials of the electrical component, and a module that computes the charge and the magnitude of electrical field in the insulating materials as a function of time. The Adameic-Calderwood equation is used to model the relationship between the electrical conductivity of dielectric materials and the electric field intensity, making the charging/discharging equations highly non-linear. The non-linearity of the charging equations becomes especially pronounced in magnetic storms during intense solar flares. The results show that the electric field intensity can approach the dielectric breakdown strength in materials commonly used as dielectrics in space-based systems and that the fields can be sustained at high levels for as long as an hour.

14:00 DA 02 *Transdisciplinary Research Opportunities at the Western Kentucky University Nondestructive Analysis Center*

**Kintzel, Edward;** ( Invited Speaker ) Western Kentucky University

The Western Kentucky University (WKU) Nondestructive Analysis (NOVA) Center has been established within the Commonwealth of Kentucky. The acquisition of the Large Chamber-Scanning Electron Microscope (LC-SEM) has positioned WKU as the only university in North America with an instrument of this type. As envisioned, the NOVA Center will be a national focal point for nondestructive measurements. The reach of this Center is to provide analytical services, by being the only educational institution within North America to offer non-destructive SEM analysis. Transdisciplinary studies will be presented that highlight the extensive suite of materials characterization techniques available at the WKU NOVA Center.

14:30 DA 03 *Development of an In-Situ Load Frame in a Large Chamber Scanning Electron Microscope*

**Leszczewicz, Jason; Kintzel, Edward; Woracek, Robin;** Western Kentucky University **Penumadu, Dayakar;** University of Tennessee-Knoxville **Young, Stephen;** Western Kentucky University

A high capacity custom designed uniaxial (tension-compression) mechanical testing system has been developed and integrated in to a 1.5 meter Large Chamber Scanning Electron Microscope (LC-SEM). This testing system provides unique ability to apply large axial force (up to 90 kN) for imaging deforming materials using various imaging modalities possible with electrons (secondary, back-scattered, and diffracted) using a close-loop control interface using National Instruments hardware and software. A wide spectrum of specimen sizes and materials can be accommodated and there is no limitation to using small sized specimen, as usually required in traditional SEM based tensile stages offered through vendors such as Gatan. This system is integrated for user access at the recently established Nondestructive Analysis Center (NOVA) at Western Kentucky University (WKU) that offers LC-SEM for advanced material analysis. The LC-SEM is also equipped with Focused Ion Beam (FIB), Energy Dispersive X-ray Spectrometry (EDS), Fourier Transform-Infrared (FT-IR) Spectroscopy and can operate under variable pressure mode. Initial results will be presented in this paper for metallic and polymeric composite materials using secondary electron based images.

14:42 DA 04 *Investigation of nanofibers in the interfacial transition zone of concrete*

**Palmer, Jahi; Palmquist, Shane; Cruz, Linda; Andrew, Keith; Kintzel, Edward;** Western Kentucky University Mechanical properties of concrete are most commonly determined using destructive tests including: compression, flexure, and fracture notch specimen tests. However, nondestructive tests exist for evaluating the properties of concrete such as ultrasonic pulse velocity and impact echo tests. One of major issues with concrete is that unlike steel it is quasi-brittle material. It tends to want to crack when tensile stresses develop. These cracks generally develop at the interfacial transition zone (ITZ) between the cement paste and the aggregate. Fibers have been added to concrete for many years to help with temperature and shrinkage cracks. In more recent years, the concepts of adding fibers with enhanced properties such as carbon and glassy nanofibers (NFs), to concrete have been explored. Some possibilities include developing concrete that may be more durable, flexible, stronger, less permeable, and potentially “crack free” than traditional concrete. Based on SEM images and quantitative data taken using the Large Chamber Scanning Electron Microscope at Western Kentucky University, this study examines the ITZ of concrete made with NFs. Results provide greater understanding on the nature of the ITZ region in concrete made with NFs.

14:54 DA 05 *Shock Formation and Disintegration in Fluids with Non-Convex Equations of State* (NSF grant CBET-0625015)

**Bahmani, Fatemeh; Cramer, Mark;** Virginia Polytechnic Institute and State University

We consider the steady, two-dimensional, inviscid, high-speed, flow around thin turbine blade profiles with special attention given to fluids having a non-convex equation of state; such fluids are commonly known as Bethe-Zel'dovich-Thompson (BZT) fluids. We show that the essential flow physics can be described by an inviscid Burgers equation having quartic nonlinearity rather than the quadratic nonlinearity of perfect gases. In order to illustrate the flow behavior, a fifth-order WENO (weighted essentially non-oscillatory) numerical

scheme is employed. New results of interest include the formation of oblique expansion shocks, shock-splitting induced by the interaction of a single shock with Mach waves, the capture of shock-fan combinations, and the collision of oblique compression and expansion shocks.

15:06 DA 06 *Evolution of Turbulence in High Temperature Plasmas*

(Work supported in part by grants to FAMU and to UW from Fusion Energy Sciences at DOE)

**Titus, James B.; Alexander, Alonzo B.; Mezonlin, Ephrem;** Florida A&M University **Almagri, Abdulgader;** University of Wisconsin - Madison

Turbulence measurements have been made in high temperature plasma in the Madison Symmetric Torus (MST) at the University of Wisconsin–Madison. Techniques from Fourier analysis and chaos theory are used to characterize magnetic turbulence in different plasma regimes, including magnetic reconnection and increased confinement. The Fourier components measure: the driving wavenumbers associated with instabilities, the amount of energy in different scales, and the rate at which that energy moves between scales. The chaos components measure the complexity of the fluctuations. More specifically, the Beta model for intermittency in 3D turbulence suggests that the fractal dimension, needed to account for non-space filling, can modify Kolmogorov’s 5/3 Law. The correlation dimension is used to estimate the fractal dimension during the evolution of different plasma events. During magnetic reconnection, it has been seen that as the magnetic energy decreases during a sawtooth crash, the energy in the ion-cyclotron frequency range (or dissipation region) increases and the fractal dimension sharply peaks. This suggests that complexity may play a role during the redistribution of energy through turbulence. These techniques will be the stepping-stones for turbulence studies at the Spheromak Turbulent Physics Experiment (STPX) at Florida A&M University.

---

## **SESSION DB: Mathematical and Computational Physics**

*13:30 Thursday Afternoon*

Salon AB

Chair: Lilia Woods, University of South Florida

13:30 DB 01 *Graviton Corrections to Maxwell’s Equations*

(NSF grant PHY-0855021)

**Leonard, Katie; Woodard, Richard;** University of Florida

We use dimensional regularization to compute the one loop quantum gravitational contribution to the vacuum polarization on flat space background. Adding the appropriate BPHZ counterterm gives a fully renormalized result which we employ to quantum correct Maxwell’s equations. These equations are solved to show that dynamical photons are unchanged, provided the free state wave functional is appropriately corrected. The response to the instantaneous appearance of a point dipole reveals a perturbative version of the long-conjectured, “smearing of the light-cone.” There is no change in the far radiation field produced by an alternating dipole. However, the correction to the static electric field of a point charge shows strengthening at short distances, in contrast to expectations based on the renormalization group. We check for gauge dependence by working out the vacuum polarization in a general 3-parameter family of covariant gauges.

13:42 DB 02 *The Partition Function for Semiclassical Gravity and Cosmic Strings*

**Duston, Christopher;** Florida State University

This talk will present a partition function for semiclassical gravity, constructed by representing smooth 4-manifolds as branched covers of the 4-sphere. By a result of Piergallini [1994], these manifolds are branched over immersed surfaces, so we will present several examples of codimension-2 foliations of the 4-sphere to illustrate the procedure for calculating the Einstein-Hilbert action. We will make this as general as possible by using the Weierstrass representation of surfaces, which can be taken flat with conical singularities. These con-

ical singularities can be interpreted as cosmic strings, making a connection between semiclassical gravity and symmetry breaking in the early universe.

13:54 DB 03 *Nuclear pairing problem with configuration-space Monte-Carlo approach*

(This work is supported by the US Department of Energy under Grant No. DE-FG02-92ER40750.)

**Lingle, Mark; Volya, Alexander;** Florida State University

Pairing correlations play an important part in the dynamics of nuclei. We present a Monte Carlo algorithm that allows for the large-scale pairing problem to be handled. The approach does not suffer from the limitations of other methods, such as problems with particle number conservation or issues related to the limit where the pairing interaction is weak. The configuration space Monte Carlo procedure for pairing treats the components of the wave function as probabilities; due to boson-like nature of nucleonic pairs the approach is not subject to the sign problem. The application of the algorithm to various cases of pairing are discussed and results for large model systems are presented.

14:06 DB 04 *Tuned Dynamic Damping of Structural Resonance*

**Yukich, John; Migirditch, Sam; Lim, Kyung Taek;** Davidson College

We have constructed and tested a tuned mass damper in an HO 1:87-scale structure to demonstrate dynamic damping of a building undergoing oscillations caused by simulated earthquake tremors. The apparatus is simple and inexpensive. The experiment, suitable for an undergraduate laboratory, demonstrates principles of physics as well as structural engineering.

14:18 DB 05 *A Question of Gravity: Forces from the Planets*

**Mendoza, William;** Florida State College at Jacksonville

The question of gravitational forces from the major celestial bodies of the Solar system will be considered in the context of a question posed in an introductory calculus-based physics course: is the gravitational force between obstetrician and infant at one meter of separation truly greater than that of any planet in the Earth-Sun system? Nearly all of the major celestial bodies will be quantitatively considered including the largest asteroids and planetary moons. The range of force from each body will be reported based on separation distances, and geometric considerations from the plane of the orbit. In addition to consideration of the central force issue, the tidal forces from the celestial bodies will also be quantitatively described and tabulated.

14:30 DB 06 *Bringing Mathematical Functions to Life*

**Engelhardt, Larry;** Francis Marion University

Mathematical functions play an extremely important role in all areas of physics. As such, it is important to be able to communicate the meaning and properties of these functions both effectively and efficiently. In this talk, we will demonstrate software that we have developed for precisely this purpose. This software is open source (free), and it can be downloaded as a platform-independent executable Java (.JAR) file from [www.compadre.org/OSP/items/detail.cfm?ID=11593](http://www.compadre.org/OSP/items/detail.cfm?ID=11593).

See also L. Engelhardt, *The Physics Teacher*, Vol. 50, pp. 402, October 2012 ([http://tpt.aapt.org/resource/1/phteah/v50/i7/p402\\_s1](http://tpt.aapt.org/resource/1/phteah/v50/i7/p402_s1)).

---

## SESSION DC: Nuclear Physics I

*13:30 Thursday Afternoon*

Adams-Park

Chair: Jorge Piekarewicz, Florida State University

13:30 DC 01 *Search for Exotic Mesons in  $\gamma p \rightarrow \Delta^{++} \pi^+ \pi^- \pi^-$  with CLAS at Jefferson Lab*

**Tsaris, Aristeidis**; Florida State University

Apart from the mesons that the constituent quark model predicts, QCD allows for additional states beyond the  $q\bar{q}$  system. By studying the following reaction  $\gamma p \rightarrow \Delta^{++} \pi^+ \pi^- \pi^-$  we are analyzing a large data set of three charged pion system. An event selection has been made to this data set in order to search for the spin-parity exotic  $\pi_1(1600)$  meson. Those events will be subject to PWA in search for this exotic meson. The experiment took place at Jefferson Lab using the CLAS spectrometer, a liquid hydrogen target was used and a tagged photon beam in a range of 4.4 – 5.5 GeV. Preliminary results will be shown, describing the data quality, kinematics and Monte Carlo simulation of the reaction.

13:42 DC 02 *The Photoproduction of Strangeness in  $\gamma p \rightarrow \Lambda K^+ \pi^+ \pi^-$  with CLAS at Jefferson Lab*

**Al Ghouli, Hussein**; Florida State University

Following the prediction of exotic states by Quantum Chromodynamics, the search for new and exotic mesons has become a priority in nuclear physics. The g12 Experiment, using the CEBAF Large Acceptance Spectrometer (CLAS) at Jefferson Lab, has provided a large photoproduction dataset. This experiment used a liquid hydrogen target, a 4 - 5.5 GeV tagged photon beam, and acquired 26 billion events. The reaction  $\gamma p \rightarrow \Lambda K^+ \pi^+ \pi^-$  provides an opportunity for searching for excited strange mesons using the g12 dataset. In this reaction, the  $\Lambda$  is identified via the  $p \pi^-$  decay where  $\pi^-$  is identified using the energy-momentum conservation. Studies indicate two dominating decay modes: the  $K^*(982)\pi$  mode, and the  $K^+\rho$  mode. Preliminary results will be presented in this talk, along with the kinematics and dynamics of this reaction. Future plans, including partial wave analysis, will be discussed briefly.

13:54 DC 03 WITHDRAWN

14:06 DC 04 *A Neutron-Antineutron Oscillation Search Experiment for Fermi National Accelerator Laboratory's Project X*

**Phillips, David**; North Carolina State University, NNBarX

Neutron-antineutron oscillation experiments with free neutrons provide a sensitive search for baryon number violating interactions with  $\Delta B = 2$ . Observation of  $n - \bar{n}$  oscillation would provide insight into the origin of baryon asymmetry in the universe and would change our ideas on the energy scales relevant for quark-lepton unification and neutrino mass generation. We present the concept for a  $n - \bar{n}$  experiment at Fermilab's Project X. The first stage of such an experiment would be similar to the most precise experiment to date, performed at the Institut Laue Langevin (ILL). Improvements to the neutron reflectors and cold neutron extraction efficiency would be made in an attempt to meet the science-driven goals of more than an order of magnitude sensitivity increase over the ILL experiment and to exceed  $n - \bar{n}$  oscillation limits obtained in intranuclear searches at Super-Kamiokande. A potential second stage would use a vertical configuration and lower energy neutrons to increase the sensitivity. We review the motivation and strategies for a next generation  $n - \bar{n}$  oscillation experiment with an emphasis on the technologies needed to achieve the desired sensitivity.

14:18 DC 05 *Noise Analysis of the Forward Gem Tracker at STAR*

**Osborn, Joe**; Star Collaboration

The Forward Gem Tracker (FGT) is an upgrade to the Solenoidal Tracker Detector (STAR) at the Relativistic

Heavy Ion Collider (RHIC) at Brookhaven National Lab. The FGT is designed to extend the current mid-rapidity tracking capabilities of STAR into the forward region ( $1 < \eta < 2$ ) covered by the Endcap Electromagnetic Calorimeter (EEMC). The combination of the EEMC and FGT will permit detection of decay  $e^- (e^+)$  from  $W^- (W^+)$  particles produced in polarized proton collisions at  $\sqrt{s} = 500$  GeV. Measurements of the parity violating asymmetry from W decays will provide important constraints on the sea quark  $\bar{u}/\bar{d}$  helicity distributions in the proton and ultimately provide insight into the possible flavor asymmetry of the light sea. The FGT was partially installed in the fall of 2011 and operated during the 2012 RHIC run. Analysis of run 12 data, specifically cluster characteristics and noise patterns, will be presented. The current installation status and plans for future running with the FGT at STAR will be discussed.

14:30 DC 06 *PEN Experiment: Towards a New Measurement of the Pion Branching Ratio*

**Lehman, Martin;** University of Virginia, PEN

The experimental determination of the  $\pi^+ \rightarrow e^+ \nu(\gamma)$  decay branching ratio currently provides the most accurate test of lepton universality. The PEN experiment at PSI, Switzerland, aims to improve the experimental precision of  $3.3 \times 10^{-3}$  to  $5 \times 10^{-4}$  using a stopped beam approach. During runs in 2008-10, PEN has acquired over  $2 \times 10^7$   $\pi_{e2}$  events. The experiment includes active beam detectors (degrader, mini TPC, target), central MWPC tracking with plastic scintillator hodoscopes, and a spherical pure CsI electromagnetic shower calorimeter. A progress update on key aspects of the analysis will be presented.

14:42 DC 07 *Spin Light Polarimeter for the EIC*

(Supported by the JSA Research Fellowship Grant and DOE Grant DE-FG02-07ER41528)

**Mohanmurthy, Prajwal; Dutta, Dipankar;** Mississippi State University

We plan to develop a realistic design for a novel polarimeter which will go a long way in satisfying the requirements of the precision experiments envisioned for the Electron Ion Collider (EIC). The Spin Light polarimeter is foreseen to be a non-invasive and continuous beam diagnostic instrument. A polarimeter based on the asymmetry in the spacial distribution of the spin light component of synchrotron radiation will make for a fine addition to the conventional Möller and Compton polarimeters. The spin light polarimeter consists of a set of wiggler magnet along the beam that generate synchrotron radiation. The spacial distribution of synchrotron radiation will be measured by an ionization chamber after being collimated. As a part of the design process, simulation of the effects of fringe field of the 3-pole wiggler magnet that forms the primary component of the polarimeter is underway. The fringe field was simulated using LANL Poisson Superfish mesh EM solver. The results from the beam motion studies, the preliminary design parameters of the polarimeter and GEANT4 simulation of the ionization chamber will be discussed.

14:54 DC 08 *First (d,p) experiment using active target detector ANASEN*

**Santiago-Gonzalez, Daniel; Wiedenhöfer, Ingo; Baby, L.T.; Koshchiy, E.; Rogachev, G.V.;** Florida State University

The energetic location of the  $d_{3/2}$ -orbital in neutron-rich nuclei is of particular interest as it determines the location of the drip-line in the oxygen isotopes. Its behavior has recently been discussed as a consequence of three-body forces [1]. Manifestations of such forces are traced through the location of the  $d_{3/2}$  orbital, which closer to stability leads to highly excited states. In order to study the location and fragmentation of this orbital in  $^{20}\text{O}$ , we performed an experiment at the RESOLUT radioactive beam facility of the Florida State University accelerator laboratory. We produced a beam of the short-lived  $^{19}\text{O}$  isotope with an intensity of  $1 \times 10^5$  pps, 65% purity and 4.4 MeV/u. This beam was used to study the spectroscopic factors of bound and unbound states of  $^{20}\text{O}$  using the  $(d, p)$  reaction in inverse kinematics and the new ANASEN active-target detector. We will present the methods used and compare our results with the ones recently published in [2].

[1] T. Otsuka et al., Phys. Rev. Lett 105, 032501 (2010)

[2] C. R. Hoffman et al., Phys. Rev. C 85, 054318 (2012)

15:06 DC 09 *Experimental techniques to use the (d,n) reaction for spectroscopy of low-lying proton-resonances*  
**Kuvin, Sean; Wiedenhöver, Ingo; Baby, L.T.; Santiago-Gonzalez, Daniel; Baker, Jessica;** Florida State University  
**Perdikakis, Georgios;** NSCL, Michigan State University **Gay, Dennis;** University of North Florida **Ebong, Imeh;** Office of Research, University of North Florida

Studies of rp-process nucleosynthesis in stellar explosions show that establishing the lowest  $l=0$  and  $l=1$  resonances is the most important step to determine reaction rates in the astrophysical rp-process path. At the RESOLUT facility, we have used the (d,n) reaction to populate the lowest p-resonances in  $^{26}\text{Si}$ , and demonstrated the usefulness of this approach to populate the resonances of astrophysical interest [1]. In order to establish the (d,n) reaction as a standard technique for the spectroscopy of astrophysical resonances, we have developed a compact setup of low-energy Neutron-detectors, ResoNeut and tested it with the stable beam reaction  $^{12}\text{C}(d,n)^{13}\text{N}$  in inverse kinematics. Performance data from this test-experiment and future plans for this setup will be presented.

[1] P.N. Peplowski et al. Phys.Rev. 79, 032801 (2009)

---

## SESSION EA: Nanoscale Physics

*15:45 Thursday Afternoon*

Ballroom

Chair: Mark Jack, Florida A&M University

15:45 EA 01 *Synthesis, structure and electrical properties of carbon nanotube junctions*

(This work is supported partially by the National Science Foundation under grant DMR#0548061 and partially by the American Chemical Society under grant PRF#51766-ND10.)

**Li, Wenzhi;** ( Invited Speaker ) Florida International University

Carbon nanotubes have great promise for applications in electronics, optics, materials science, energy storage, and sensor technology due to their interesting electronic and mechanical properties which are determined by their unique morphologies and structures. In this presentation, the growth mechanism, structure, and electrical property of multi-walled carbon nanotube junctions as well as the mechanical property of single-walled carbon nanotubes will be discussed. Specifically, this talk will discuss (1) the influence of the carbon precursor (thiophene) vapor concentration on the formation of the carbon nanotube junctions during the chemical vapor deposition process, (2) the correlation between the electrical property and the structure of the carbon nanotube junctions, and (3) the radial elasticity of individual single-walled carbon nanotubes measured by using atomic force microscopy (AFM).

16:15 EA 02 *Van der Waals Interactions in Graphene Nanoribbons – Important Implications revealed via Theoretical Investigations*

**Woods, Lilia;** ( Invited Speaker ) University of South Florida

Graphene nanoribbons (GNRs) are quasi-one dimensional structures with planar geometry. They have extraordinary properties suitable for novel technological applications, especially for high speed electronics. Of particular importance is how GNRs interact with each other and other materials not only to understand their fundamental science, but also to help interpret experimental data and design better devices. Because of their inertness and nature of CC bonding, van der Waals (vdW) forces at small separations dominate GNR interactions. I will present studies revealing the collective microscopic nature of GNR vdW interactions based on a discrete dipole approximation. Calculations utilizing Density Functional Theory (DFT) with semi-empirical correction for the vdW interactions will also be presented for folded GNRs. In all cases, the emphasis will be on understanding the peculiarities of the vdW force in terms of registry dependence, strength, and role in mechanical manipulations involving GNRs. Furthermore, I will emphasize electronic structure modulations in terms of overall changes, energy gaps, magnetic states in various folded configurations as obtained via DFT.



16:45 EA 03 *Electronic Transport Investigations of Reduced Graphene Oxide Sheet*

(In collaboration with Saiful I. Khondaker, Nanosceince Technology Center, Department of Physics, and School of Electrical Engineering and Computer Science, University of Central Florida)

**Joung, Daeha;** ( Invited Speaker ) University of Central Florida

Reduced graphene oxide (RGO) sheet, a chemically functionalized atomically thin carbon sheet, provides a convenient pathway for producing large quantities of graphene via solution processing. The easy processibility of RGO sheet and its composites offer interesting electronic, chemical and mechanical properties that are currently being explored for advanced electronics and energy based materials. However, a clear understanding of electron transport properties of RGO sheet is lacking which is of great significance for determining its potential application. In this talk, we will present fabrication of high-yield solution based graphene field effects transistor (FET) using AC dielectrophoresis (DEP) and investigate the detailed electronic transport properties of the fabricated devices. The majority of the devices show ambipolar FET properties at room temperature. However, the mobility values are found to be lower than pristine graphene due to a large amount of residual defects in RGO sheets. We calculated the density of these defects by analyzing the low temperature (300 to 77K) charge transport data using space charge limited conduction (SCLC) with exponential trap distribution. At very low temperature (down to 4.2 K), we observe Coulomb blockade (CB) and Efros-Shklovskii variable range hopping (ES-VRH) conduction in RGO implying that RGO can be considered as a graphene quantum dots array (GQD), where graphene domains act like QDs while oxidized domains behave like tunnel barriers between QDs. This was further confirmed by studying RGO sheets of varying carbon  $sp^2$  fraction from 55%-80% and found that both the localization length and CB can be tuned. From the localization length and using two band Kane model, we estimate tunable band gap of RGO sheets with varying carbon  $sp^2$  fraction.

17:15 EA 04 *Electron interaction effects in graphene*

**Sheehy, Daniel;** ( Invited Speaker ) Louisiana State University

Graphene, a one-atom thick sheet of graphite, has received a large amount of attention following its recent experimental isolation. At low energies, graphene possesses an emergent relativistic symmetry, and can be described in terms of linearly-dispersing massless “Dirac” fermions, with a velocity that is determined by band structure and experimentally measured to be 300 times smaller than the speed of light. This approximate relativistic behavior is, however, broken by the presence of the long-ranged Coulomb interaction, although many experiments can be explained in terms of a non-interacting picture. I will discuss how the Coulomb interaction will be manifested in various experimentally observable quantities, including the heat capacity, diamagnetic response, and optical conductivity. I will also discuss the implications of recent experiments on the optical transparency of graphene.

---

## **SESSION EB: Undergraduate Talks**

### *15:45 Thursday Afternoon*

Salon AB

Chair: Mary Ellen Zvanut, University of Alabama at Birmingham

15:45 EB 01 *Computational Tools for Exploring Cosmology*

**Stone, Keenan; Moldenhauer, Jacob; Engelhardt, Larry; Shuler, Ezekiel;** Francis Marion University

We describe a set of interactive simulations built for fitting cosmological models to experimental data sets. Current versions allow users to generate personalized dark energy based models (e.g. LCDM) while providing means of both visual and numerical comparison to observational results from various surveys. Additionally, we present progress towards the development of new programs that enable testing of a more general spectrum of models. These will feature minimization routines and improved interface to complement existing functionality, with aspiration that they may be found useful to researchers and educators alike.

15:57 EB 02 *Observability of Neutrinos from Failed Supernovae and Black Hole-Neutron Star Mergers*

**Liang, Jason; Lim, Halston;** North Carolina School of Science and Mathematics **Scholberg, Kate;** Duke University  
Neutrino astronomy is an indispensable tool for studying astrophysical phenomena such as failed supernovae (fSN) and black hole-neutron star mergers (BHNSM) and would allow for the observation of black hole and short-period GRB formation. We conducted a comprehensive study of the observability of neutrinos from fSN and BHNSM in future and proposed detectors that incorporates realistic detector responses. SNOwGLoBES, event calculation software that takes into account fluxes, cross sections, detector smearing, and post-smearing efficiencies, was utilized. For fSN and BHNSM, we determined the flux of each neutrino flavor and calculated the observed neutrino spectrum in various detectors as a function of distance. Additionally, for the fSN we generated time dependent models of the neutrino signal up until black hole formation. Our results indicate that observation of neutrinos from fSN and BHNSM in the galactic neighborhood is very feasible. In addition, the neutrino signals are distinguishable from the signal produced by typical SN, which has future implications for the study of the origin of high energy astrophysical neutrinos.

16:09 EB 03 *Investigating Failed Supernovae and Black Hole-Neutron Star Mergers Using Neutron Signals*

**Lim, Halston; Liang, Jason;** North Carolina School of Science and Mathematics **Scholberg, Kate;** Duke University  
Failed supernovae (fSN) and black hole-neutron star mergers (BHNSM) are unique high energy astrophysical events that can be studied in novel ways through their copious neutrino emissions. Using SNOwGLoBES, we were able to calculate the observed neutrino spectrum of fSN and BHNSM in various detectors, including Super-Kamiokande and LBNE. We analyzed the sensitivity of the observed neutrino spectrum to the source emission parameters and determined how flavor tagging influenced this sensitivity. Our results show that it is possible to discriminate between the average energies of electron and antielectron neutrinos from the observed neutrino signal, which sheds light on nucleosynthesis processes within fSN and BHNSM. We also found that in both the water Cherenkov detector Super-Kamiokande and the proposed liquid argon detector LBNE, the fSN neutronization burst produces a peak in the neutrino event rates after applying directional cuts (for water only) and event tagging, demonstrating the viability of using neutrinos to study the internal processes of fSN. Our assessment of tagging methods and determination of the promise for neutrino detectors for observing fSN and BHNSM will aid physicists in future neutrino astrophysics experiments.

16:21 EB 04 *Generation of Electricity from the Wind Draft of Cars*

**Pudukodu, Harish;** North Carolina School of Science and Mathematics

We developed a theoretical turbine power output model dependent on automobile speed and turbine distance from cars. Analysis of the data from experimental field tests with rush hour traffic, controlled single-car testing, and CFD modeling showed that our turbines generated electricity, but did not support our theoretical model, which assumed laminar flow and spherical cars. Our study represents a creative implementation of wind power that may have significant economic/environmental implications for the future of renewable energy.

16:33 EB 05 *Minimum-Bias Studies Using the Energy Scan Data from the Fermilab Tevatron Collider*

**Wilson, David;** University of Virginia, CDF **Group, Craig;** University of Virginia & Fermilab, CDF **Field, Rick;** University of Florida, CDF

We report on an analysis of the minimum-bias event data (that is, events with the least selective trigger criteria) taken at the Tevatron collider at Fermilab, in particular an energy scan recording collisions at  $\sqrt{s} = 0.3, 0.9,$  and  $1.96$  TeV. This data set represents a rare chance to analyze the energy dependence of several minimum-bias observables; for example, the pseudorapidity ( $dN/d\eta$ ) distribution. We present the results of a comparison of these observables with the PYTHIA Monte Carlo simulation.

16:45 EB 06 *Studies of Silicon Photomultipliers for their use in the Mu2e Experiment at Fermilab*

**Henderson, Alyssa;** University of Virginia **Group, Craig; Oksuzian, Yuri;** University of Virginia, Fermilab **Rubinov, Paul;** Fermilab

Silicon Photomultipliers (SiPMs), a relatively novel technology, are able to detect single photons and convert them into electrical signals when used within a proper voltage range. In order to learn more about SiPMs for

their use in the Mu2e experiment, we find a few characteristics of the SiPM at the Silicon Detector facility at Fermilab. We connected several SiPMs, one at a time, to a Keithley 2400 Sourcemeter that was programmed to vary the voltage automatically. In this way, we were able to apply our desired voltage range and the sourcemeter provided the corresponding current. We also conducted these experiments with the SiPMs in a dark chamber, which we used to control the temperature of the environment. We applied a voltage and measured the corresponding current at four temperatures and measured three characteristics: breakdown voltage, the operating voltage range, and the resistor value at each, as well as how they vary with temperature, time, and between two brands.

16:57 EB 07 *Molecular and Atomic Hydrogen Cloud Correlations in the Interstellar Medium of the Galaxy*

**Howard, Ward**; Union University **Gibson, Steven**; Western KY University **Brunt, Christopher**; Exeter University **Jolly, Christian**; Gatton Academy

A key question in Galactic astrophysics is how the cold, relatively dense clouds that form new stars are assembled from the warmer, more diffuse interstellar medium (ISM). We are investigating the relationship between neutral atomic hydrogen (HI) and molecular hydrogen (H<sub>2</sub>) gas to find where molecules may be actively forming in cooling

clouds prior to star formation. We use HI 21cm-line self-absorption (HISA) to identify the coldest atomic gas that is most likely associated with forming molecules, and we use carbon monoxide (CO) 2.6mm line emission as a proxy for H<sub>2</sub>, which does not have suitable ground-state transitions for direct mapping. We have measured the fraction of HISA with CO emission and CO with HISA in a variety of different Galactic plane survey data sets. We see a stronger correspondence of HISA and CO in the inner parts of the Galaxy, and a weaker correspondence elsewhere.

However, this trend may arise from chance alignments of unrelated clouds being more likely in the inner Galaxy rather than true physical correlation.

---

## SESSION EC: Particle Physics I

*15:45 Thursday Afternoon*

Adams-Park

Chair: Ayana Arce, Duke University

15:45 EC 01 *Recent Results on Spectroscopy from Belle*

**Wang, Xiao Long**; Virginia Tech, Belle

I will review recent results on spectroscopy from the Belle experiment that include measurements of the  $Z_b$  charged and neutral states, the newly discovered  $\psi_2$  charmonium state, and studies of  $e^+e^- \rightarrow \eta J/\psi$  with initial state radiation.

15:57 EC 02 WITHDRAWN

16:09 EC 03 *Determination of Low Energy  $\pi \rightarrow e\nu$  Electromagnetic Tail via Multivariate Cut Analysis*

**Frlez, Emil**; University of Virginia, PEN

The PEN experiment at the Paul Scherrer Institute aims to measure the leptonic decay  $\pi^+ \rightarrow e^+\nu(\gamma)$  branching ratio with  $5 \cdot 10^{-4}$  relative uncertainty. Electromagnetic shower leakage for 70 MeV monoenergetic positrons in the pure Csi electromagnetic calorimeter is of the order of 2% for  $E_{CALO} < 50$  MeV and presents an important systematic uncertainty. We have explored a set of cuts via multivariate analysis to determine the best algorithm for extracting the almost background-free set of  $\pi_{e2}$  tail events.

16:21 EC 04 *An Integrated Theory of Everything (TOE)*

**Colella, Antonio;** (My article “An Integrated Theory of Everything” was published on the Internet. My book “Master Big Bangs through Black Holes in Four Hours - An Integrated Theory of Everything Introduction” is in book production.) Retired

An Integrated TOE unifies all known physical phenomena from the Planck cube to the Super Universe. Each of 129 fundamental matter and force particles is represented by its unique Planck cube string. Any object can be represented by a volume of contiguous Planck cubes. Super force string singularities at the center of Planck cubes existed at the start of all universes. The foundations of an Integrated TOE are twenty independent existing theories including; string, spontaneous symmetry breaking, Higgs forces/supersymmetric Higgs particles, dark matter, dark energy, stellar black holes, and baryogenesis. The premise of an Integrated TOE is without sacrificing their integrities; these twenty independent existing theories are replaced by twenty interrelated amplified theories (Table IV). Amplification of Higgs forces to 64 supersymmetric Higgs particles is essential for an Integrated TOE. Additional amplifications include: Higgs force particles are residual super force particles; matter particles and their associated Higgs forces are one and inseparable; spontaneous symmetry breaking is bidirectional; 17 super force condensations occur at 17 different temperatures; and the sum of 8 permanent Higgs force energies is dark energy.

---

## **SESSION FA: Banquet**

*18:00 Thursday Evening*

Ballroom/Salon A/Salon B

---

## **SESSION FB: Public Lecture II: SUSY and the Lords of the Ring**

*20:00 Thursday Evening*

Challenger Learning Center

Chair: Charles Weatherford, Florida A&M University

20:00 FB 01 *SUSY and the Lords of the Ring*

**Gates, James Sylvester;** ( Invited Speaker ) University of Maryland

The last decade in physics has led to an array of new ideas including one called supersymmetry (SUSY for short). If valid, Nature may soon begin to reveal the existence of “superpartners,” new forms of matter and energy. At the CERN laboratory in Geneva, Switzerland is a ring that will rule upon them all. It is called the LHC (Large Hadron Collider), and has recently been in the news. Come to this lecture and learn about this Fellowship of the Ring.

---

## SESSION GA: Results from LHC II

*08:30 Friday Morning*

Ballroom

Chair: Laura Reina, Florida State University

08:30 GA 01 *Physics at the Tevatron in the LHC Era*

(Work done with Susan Blessing, Florida State University, and the D0 and CDF Collaborations.)

**Hoang, Trang;** ( Invited Speaker ) Florida State University

The Tevatron is now the second-highest-energy collider in the world. However, there are still many Tevatron measurements that are competitive with or better than those currently done at the LHC. I will discuss some of these analyses.

08:42 GA 02 *The LHC and New Physics Beyond the Standard Model*

**Matchev, Konstantin;** ( Invited Speaker ) University of Florida

This talk will review several scenarios for new physics beyond the standard model and the current status of the corresponding searches at the LHC.

08:54 GA 03 *Visualizing the Matrix Element Method*

**Gainer, James; Matchev, Konstantin;** University of Florida

The Matrix Element Method (MEM) is an increasingly popular technique in experimental particle physics. In this method, the squared matrix elements for producing the observed final state using various hypotheses, such as a signal hypothesis and a background hypothesis, are calculated. The resulting matrix elements can be used to quantify when events are more “signal-like” or “background-like,” thus allowing more sensitive searches for new physics. We provide an introduction to this method. We then demonstrate a simple interpretation of signal and background matrix elements, which is appealing visually and may inspire novel searches for new physics.

09:06 GA 04 *Caustics for High-Precision Mass Measurement and its application to W & Higgs*

(US National Science Foundation, grant NSF-PHY-0969510, the LHC Theory Initiative)

**Cho, Won Sang; Matchev, Konstantin;** University of Florida

We introduce a mixed events variable called “Mass Caustics”  $\tilde{M}$  for measuring the masses of resonant particles. By its construction, the mass caustics  $\tilde{M}$  has a super-sharp singular peak structure which generalizes the ordinary invariant and transverse masses while preserving the Lorentz boost invariance of resonance mass peak positions. In result, the information on the mass peak position is statistically amplified in compared to the variables at present, and high precision mass measurement can be achieved. Such precision of mass spectrometry opens the door to numerous applications in the fields dealing with relativistic particles, in particular when parts of the relic particles are invisible with limited event statistics. We demonstrate this technique for mass measurement of the W and Higgs bosons which decay with missing neutrino.

09:18 GA 05 *Parton distributions and the W mass measurement*

**Quackenbush, Seth;** Florida State University **Sullivan, Zack;** Illinois Institute of Technology

Errors arising from parton distributions are the dominant source of theoretical error in the W mass measurement at the Tevatron and LHC. With the large W cross section and steadily rising LHC luminosity, parton distributions are expected to become the limiting factor in measuring the W mass at the LHC. We examine the origins of these errors and discuss methods to minimize them. Naive theoretical analyses dramatically underestimate the error, primarily due to the influence of showering and detector resolution on shape of the W transverse mass distribution.

09:30 GA 06 *Search for a Fourth Generation Top-Like Quark with Single Charged Lepton Final States in 7 TeV pp Collisions*

(This work supported in part by DoE Grant DE-FG-96ER4097.)

**Jenkins, Charles;** University of South Alabama, CMS

The CMS Experiment at the LHC recorded 7 TeV center of mass energy pp collisions in the 2011 run. One search conducted in this data was for a fourth generation top-like quark decaying as:  $t' \rightarrow W b$ . A fourth generation is disfavored by a 125 GeV Standard Model Higgs boson, which is consistent with the observation of a new Higgs-like boson at 125 GeV at the LHC. However, extended Higgs theories allow  $t'$  quarks and there are other models with non-chiral top-like quarks that have similar decay signatures used in this search. This analysis searches for strong top-like quark production which decay into  $Wb$ , where one of the W bosons decays leptonically ( $W \rightarrow l\nu$ ), the other hadronically ( $W \rightarrow q \bar{q}$ ). This analysis studies two channels:  $\mu$ +jets and electron+jets. Results from a sample of  $4.9 \text{ fb}^{-1} \mu$ +jets and  $5.0 \text{ fb}^{-1}$  electrons+jets will be presented.

---

## **SESSION GB: Statistical and Nonlinear Physics**

*08:30 Friday Morning*

Salon AB

Chair: Mark Jack, Florida A&M University

08:30 GB 01 *Surface critical behavior at a nonequilibrium phase transition*

(Supported by the US National Science Foundation through Grants DMR-0904999 and DMR-1205309.)

**Park, Hyunhang; Pleimling, Michel;** Virginia Tech

We study the local critical phenomena at a dynamic phase transition by means of numerical simulations of the kinetic Ising models with surfaces subjected to a periodic oscillating field. We examine layer-dependent quantities, such as the period-averaged magnetization per layer  $Q(z)$  and the layer susceptibility  $\chi_Q(z)$ , and determine local critical exponents through finite size scaling. Both for two and three dimensions, we find that the values of the surface exponents differ from those of the equilibrium critical surface. It is revealed that the surface phase diagram of the nonequilibrium system is not identical to that of the equilibrium system in three dimensions.

08:42 GB 02 *Non-equilibrium steady states in a two-temperature Ising ring with Kawasaki dynamics*

(Supported by the US National Science Foundation through Grants DMR-0904999, DMR-1205309, and DMR-1244666)

**Borchers, Nick; Pleimling, Michel;** Virginia Tech **Zia, R.K.P.;** Virginia Tech, Iowa State University

From complex biological systems to a simple simmering pot, thermodynamic systems held out of equilibrium are exceedingly common in nature. Despite this, a general theory to describe these types of phenomena remains elusive. In this talk, we explore a simple modification of the venerable Ising model in hopes of shedding some light on these issues. While it was shown by Ising that there is no phase transition in the one-dimensional Ising model, a system attached to two heat reservoirs exhibits many of the hallmarks of phase transition. When the system settles into a non-equilibrium steady-state it exhibits numerous interesting phenomena, including an unexpected “freezing by heating.” These phenomena will be explored and possible approaches to understanding the behavior will be suggested.

08:54 GB 03 *Shape Comparison Between Non-equilibrium Droplets and Equilibrium Crystal Shapes for the 2D Ising Model*

(This research was supported by NSF grant OCI-1005117 as a part of the REU in scientific computing at Marshall University, [www.marshall.edu/reu](http://www.marshall.edu/reu).)

**Richards, Howard**; Marshall University **Shields, Austin**; Richard Stockton College of NJ **Germiller, Austin**; Oklahoma Baptist University **Raffield, Jesse**; Florida State University

We use the Boost Graph Library to identify droplets in the single-droplet region of metastable decay for the 2D Ising model (using a single-spin flip algorithm), and likewise for equilibrium crystals (using Kawasaki dynamics). As a quantitative way of comparing shapes, we measure the number of broken bonds for the droplets/crystals and also (using the `igraph` library) the graph-theoretic diameter. Both measurements show that the droplets and crystals have the same shapes on average. This is consistent with earlier research, which used the nucleation rate of droplets to compare their surface free energy with the free energy of equilibrium crystals. The advantage of the present method is that it can be extended to nucleation and growth on irregular lattices.

09:06 GB 04 *Random Network Models of Power Grids*

(Supported in part by NSF DMR-1104829.)

**Rikvold, Per Arne**; **Abou Hamad, Ibrahim**; Florida State University **Poroseva, Svetlana V.**; Univeristy of New Mexico

Power grids are complex engineering systems of vital importance to modern societies, and it is important to understand how to improve their resilience to various kinds of damage. However, it is often difficult to obtain detailed data on the structures, generating capacities, and power demands for real power systems. In order to be able to test network-analysis algorithms under a variety of conditions, it is therefore useful to develop artificial models that can be tuned to reflect properties of real grids, and that also can be scaled to study effects of the grid size and shape. Here we present a methodology to use Monte Carlo simulations to generate random grids that agree with the degree distribution for the vertices (power plants and consumers) and the length distribution for the transmission lines in the Florida high-voltage power grid. These model grids are used to test the performance of algorithms to partition the grid into semi-independent islands. We find that it is more difficult to partition the model grids than the real Florida grid, suggesting that the real grid contains correlations that are absent in our current generation of models.

09:18 GB 05 *Relaxation dynamics of magnetic flux lines subject to correlated disorder*

(Research supported by the U.S. Department of Energy, Office of Basic Energy Sciences, Division of Materials Sciences and Engineering under Award DE-FG02-09ER46613.)

**Dobramysl, Ulrich**; **Assi, Hiba**; **Pleimling, Michel**; **Täuber, Uwe C.**; Virginia Tech

Technological applications of type-II superconductors in magnetic fields require a careful investigation and characterization of the stationary and transient properties of vortex matter. Naturally occurring disorder and artificially introduced crystal defects acting as pinning sites, together with repulsive vortex-vortex interactions lead to rich and complex physics. We study the out-of-equilibrium relaxation of a system of vortex lines, subject to columnar pinning sites, and characterize the transient behavior via two-time quantities. To this end, we model these vortex lines as interacting elastic lines and employ a Langevin molecular dynamics algorithm to simulate the dynamics of the discretized system. In particular, we compare the flux line relaxation in the presence of correlated, columnar pinning sites to previously obtained data on randomly-placed pinning sites. By varying the flux line length, we investigate the differences in the relaxation between point-like vortices and extended vortex lines.

09:30 GB 06 *Exact Results on Potts Model in a Generalized External Field*

**Xu, Yan**; Florida State University **Shrock, Robert Ellsworth**; Stony Brook University

The  $q$ -state Potts model is a spin model that has been of longstanding interest as a many-body system in statistical physics. A natural generalization is to consider this model in a generalized external field that favors or disfavors



spin values in a subset  $I_s = \{1, \dots, s\}$  of the total set of  $q$ -state spin values. We obtain a powerful exact formula (Shrock formula) for the partition function of this generalized Potts model on various families of graphs  $G$ ,  $Z(G, q, s, v, w)$ , where  $v$  and  $w$  are temperature- and field-dependent Boltzmann variables. An important property of this formula is that it expresses  $Z(G, q, s, v, w)$  in a graph-theoretic manner as a sum of contributions from spanning subgraphs  $G'$  of the graph  $G$ , rather than as a sum over spin configurations. Using this general formula, we derive a number of exact properties of  $Z(G, q, s, v, w)$ . We also analyze an interesting special case of the zero-temperature Potts antiferromagnet, corresponding to a set-weighted chromatic polynomial  $Ph(G, q, s, w) \equiv Z(G, q, s, -1, w)$  that counts the number of colorings of the vertices of  $G$  subject to the condition that colors of adjacent vertices are different, with a weighting  $w$  that favors or disfavors colors in the interval  $I_s$ .

09:42 GB 07 *Improved method of calculation of mode lifetime in low dimension*

(Support from the Dept. of Energy under grant DE-SC0008487.)

**Gao, Yang; Daw, Murray;** Clemson University

While vibrational mode lifetimes is an important property of materials, the method of calculation is surprisingly undeveloped. Recently, Dickel and Daw [1,2] proposed a theory to do the calculation efficiently. It is developed based on the Liouvillian and the recursion method. The mode lifetime can be represented in terms of moments of the power spectrum of Liouvillian.

To verify the theory numerically, we applied this method and molecular dynamics to three different models of low dimension. Calculations are done by molecular dynamics(MD) and Monte Carlo(MC), and the result shows that the relation between mode lifetime  $\tau$  and moments can be found,

$$\tau = F(\mu_2, \mu_4, \mu_6, \dots)$$

and also lifetime can be approximated nicely with some low order moments:

$$\tau = \tau_2 \tilde{F}(\gamma_4, \gamma_6, \dots), \tau_2 = \sqrt{\frac{1}{\mu_2}}, \gamma_n = \frac{\mu_n}{\mu_2^{\frac{n}{2}}}$$

[1] D. Dickel & M. S. Daw. Improved calculation of mode lifetimes, part i: Theory. *Comp. Mat. Sci.*, 47:698, 2009.

[2] D. Dickel & M. S. Daw. Improved calculation of mode lifetimes, part ii: Numerical Result *Comp. Mat. Sci.*, 2010.

09:54 GB 08 *Neutral species domination on different lattices for the symmetric stochastic cyclic competition of four species*

(Supported by the US National Science Foundation through Grants DMR-0904999 and DMR-1205309.)

**Intoy, Ben;** Virginia Tech **Dorosz, Sven;** University of Luxembourg **Pleimling, Michel;** Virginia Tech

Although the mean-field solution for four species in cyclic competition is generally in good agreement with stochastic results, it fails to describe the extinction and absorbing states that finite size systems inevitably fall into. We study the effects of dimension, lattice type, and swapping rate between particles on the time it takes for the system to go into a static absorbing state, which consists of a neutral species pair. The lattice types discussed include the well mixed environment, one-dimensional line with periodic and closed boundary conditions, the Sierpinski triangle, and the two-dimensional square with periodic and closed boundary conditions. All simulations are run with less than a thousand sites, as in the symmetric case extinction time dramatically increases with lattice size. We find that for some of the studied lattices there are long and short lived configurations.

10:06 GB 09 *Preliminary Analysis of the Inverse-x Oscillator*

**Oyedeji, 'Kale;** Morehouse College **Mickens, Ronald E.;** Clark Atlanta University

The inverse-x oscillator has the following equation

$$\ddot{x} + \frac{1}{x} = 0.$$

While the motion is singular at  $x = 0$ , nevertheless, all of the solutions are bounded in  $x$  and periodic in time. In addition to proving these behaviors, we calculate the exact period and present a (preliminary) analysis of the periodic solutions with respect to the construction of analytic approximations. The procedures used involve phase-space methods and harmonic balance.

10:18 GB 10 *Dynamics of Oscillatory Systems Having A Fractional Power Damping Force*

(This work was supported in part by the CAU School of Arts and Sciences professional Development Funds Program and by NSF Award 0420516 to the Center of Physics and Chemistry of Materials at Fisk University.)

**Mickens, Ronald E.**; Clark Atlanta University

In standard mathematical models of dynamic systems the effects of dissipation/damping is represented by a linear term proportional to the velocity, i.e., if  $x$  is a relevant coordinate, then this force is  $F = -\lambda\dot{x}$ , where  $\lambda$  is a positive parameter, and the over-dot denotes differentiation in time. For a conservative system, the application of such a force produces motions for which  $x$  goes to zero in an infinite time. We demonstrate that the use of a nonlinear dissipation/damping force proportional to  $\dot{x}$  raised to a fractional power, i.e.,

$$F = -\lambda [\text{sgn}(\dot{x})] |\dot{x}|^a, \quad 0 < a < 1,$$

gives rise to dynamics for which the motion ceases in a finite time. Using the example of the Duffing equation and the method of first-order averaging, we illustrate this phenomenon. We also discuss the application of these results to the analysis of vibrations in nano-tubes and graphene sheets.

---

## SESSION GC: Biological Physics

*08:30 Friday Morning*

Adams-Park

Chair: Richard Haglund, Vanderbilt University

08:30 GC 01 *Measuring looping probability of short double-stranded DNA*

**Kim, Harold**; ( Invited Speaker ) Georgia Institute of Technology

Bending of double-stranded DNA (dsDNA) is associated with fundamental biological processes such as genome packaging and gene regulation, and therefore studying sequence-dependent dsDNA bending is a key to understanding biological impact of DNA sequence beyond the genetic code. Average mechanical behavior of long dsDNA is well described by the wormlike chain model, but the behavior of dsDNA at length scales around or below its persistence length remains controversial. In this talk, I will explain how we can measure looping probability of dsDNA using a fluorescence technique called FRET (Förster Resonance Energy Transfer) and infer its elastic properties. I will also explain how we compare the experimental results against a discrete wormlike chain model which successfully explains the behavior of long dsDNA. I will show that the behavior of short dsDNA (<200 base pairs) cannot be described by the wormlike chain model, but demonstrates subelastic deformation mechanism.

09:00 GC 02 *Managing surroundings: cell adaptations to 2D and 3D surfaces that promote movement*

**Rericha, Erin**; ( Invited Speaker ) Vanderbilt University

In the canonical model of amoeboid cell migration, the bounds of motility are set by cell-surface adhesion; surface attraction is required for actin mediated extension of pseudopods to push the cell center of mass forward, yet it must be sufficiently low to allow cells to de-adhere and retract their rear [1]. When collective migration occurs the balance of resistive adhesion forces with protrusive forces is presumably altered as cell-cell contact provides an additional mass to push against [2]. Specific integrin binding sites are known to impact focal adhesions during individual migration [3]. In the absence of specific binding sites such as in the social amoeba *Dictyostelium*, we envision that hydrophobic attraction and electrostatics works in a similar manner [4]. We

studied the ability of Dictyostelium discoideum, which migrate individually and collectively, to move on surfaces of varying hydrophobicity and charge. We found that these cells actively regulate their surface contact such that individuals adhere and migrate equally well on surfaces of dramatically varying properties without changing cell shape, indicating the cells “sense” the surface. To find the timing of this adaptation we examine the spreading behavior at the initial surface contact and when the cells transition from one surface to another. In 3D collagen networks cells modify the environment by degrading and crosslinking the surrounding network as well as secreting additional collagen. We present direct visualization of the early network modifications by cancer cell lines in an effort to determine the boundary conditions of the collagen on a cell embedded in a network.

09:30 GC 03 *Electrokinetic trapping of a single fluorescent nanobead*

**King, Jason K.; Canfield, Brian K.; Davis, Lloyd M.;** University of Tennessee Space Institute

We demonstrate electrokinetic control and confinement of a single 40 nm fluorescent latex bead in 25% glycerol-water solution. Fluorescent beads are excited with a diode laser and imaged by a custom forward-illumination microscope onto a low-light CCD. The sample is loaded between two pairs of electrodes arranged in a crossed configuration on separate planes that allow generation of an electric field of variable orientation and strength. These electrodes consist of sputtered platinum over chrome patterned onto #1.5 microscope coverslips. Astigmatism is introduced to the focus of the microscope tube lens to modify the point spread function (PSF) as a function of axial position, allowing determination of the particle position in three dimensions. By collapsing the rows and columns of the acquired image to one-dimensional arrays and fitting a Gaussian to each, the planar position and width can be determined with sub-pixel precision. The axial position can be calculated from the measured PSF ellipticity combined with calibration measurements performed on immobilized fluorescent beads at fixed distances from the focal plane. With this information we can apply appropriate voltages to counteract Brownian motion and further characterize the setup for use in single-molecule trapping.

09:42 GC 04 *Single Emitter Localization using a Four-focus Confocal Fluorescence Microscope*

**Germann, James A.; Canfield, Brian K.; Davis, Lloyd M.;** University of Tennessee Space Institute

We demonstrate that four spatially separated and temporally pulsed laser foci can be used to detect and localize a single fluorescent emitter to below the diffraction limit in a confocal microscope. Optical excitation is accomplished using LabVIEW Real-Time to control sequential pulsing of four laser diodes. The beams are coupled collinearly through three beam splitters and focused in a custom confocal microscope. The individual foci are positioned at the vertices of a micron-sized tetrahedron, which establish a Cartesian coordinate system. Fluorescence photons are counted by a single-photon avalanche diode and time-gated based on the pulse excitation sequence. Emitter location is estimated from the count rates generated at the four foci using Maximum Likelihood techniques. Preliminary results for tracking a fluorescently labeled nanoparticle in an aqueous/glycerol solution with a piezoelectric stage are presented. Future research with the four-focus microscope will concentrate on trapping a single fluorescent molecule.

09:54 GC 05 *Spectral Coupling of Nicotine-linked Au Nanoparticles for Surface Enhance Raman Scattering*

(This work at HU was supported by NSF HRD 1137747 and ARO W911NF-11-1-0177(HU).)

**Jackson, Ashley; Austin, Jasmine; Abdel-Fattah, Mahmoud; Tabibi, Bagher;** Hampton University **Kim, Wan-Joong;** Electronics and Telecommunications Research Institute **Jung, Sungsoo;** Korea Research Institute of Standards and Science **Seo, Jaetae;** Hampton University

Molecule-linked plasmonic nanoparticles have been of great interest because of large enhancement of fluorescence or scattering of vibrational modes because to localized field enhancement. Spherical metal nanoparticles without molecule linkage have a simple dipole plasmonic mode within dipole approximation. However, the molecule-linked plasmonic nanoparticles have longitudinal- or multi-modes of plasmonic oscillations which display strong SPR at longer wavelengths, as well as a hot spot between the nanoparticles with molecule linkage. A nicotine molecule has a strong affinity with gold nanoparticles because of the nitrogen lone-pair on the molecule. The nicotine-linked Au nanoparticle exhibits a localized surface plasmon resonance in the visible and near infrared region, and is coherently excited for large SERS enhancement. While inhaling nicotine can

speed lung cancer, it is also used in smoking cessation therapy. This presentation will include the spectral coherent coupling of nicotine-linked Au nanoparticles between the plasmonic mode at longer wavelength and optical excitation for large SERS enhancement, which can be utilized for the bio-chemical and bio-medical applications.

---

## **SESSION HA: Applied Physics II**

*10:45 Friday Morning*

Ballroom

Chair: Ed Kintzel, Western Kentucky University

10:45 HA 01 *The Progress and Promise of Advanced LIGO*

**Betzwieser, Joe;** ( Invited Speaker ) LIGO Livingston Laboratory

The three initial, and later enhanced, LIGO gravitational wave detectors in the Livingston, Louisiana and Hanford, Washington observatories collected over one year of triple coincidence data at or better than the initial LIGO design sensitivity during science runs from 2005 to 2010. Astrophysical population estimates placed the detection rate for the initial LIGO detectors at 1 every 10 years, so it was not surprising that these instruments did not make a detection. The Advanced LIGO interferometers have been designed to be a factor 10 more sensitive than the initial detectors, which will increase the volume searched by a factor of 1000. These upgrades are expected not only to provide that first, elusive detection, but we hope to also allow for routine detections, and thus to usher in an exciting age of gravitational wave astronomy. Installation of the Advanced LIGO interferometers began two years ago and it is now more than half complete. We will present an overview of the Advanced LIGO detectors, as well as the current status of the installation. We will also go over some of the exciting science that these detectors, combined with other next generation gravitational wave detectors around the world, hope to accomplish once completed.

11:15 HA 02 *High Resolution Dual Modality (Neutron and X-ray) Imaging of Granular Materials and Direct Numerical Simulations*

**Penumadu, Dayakar;** ( Invited Speaker ) University of Tennessee

This presentation will summarize the ongoing research of Mr. Felix Kim (PhD student of Dr. Penumadu) on the high resolution neutron ( $\sim 13.7 \mu\text{m}/\text{voxel}$ ) and X-ray ( $\sim 11.2 \mu\text{m}/\text{voxel}$ ) tomography imaging of partially water saturated compacted sand specimens. Neutron imaging work was performed at Helmholtz Zentrum Berlin (HZB) in collaborations with Drs. Kardjilov and Manke. Two different particle grain morphologies (round and angular) were used. Partially saturated granular assembly is a three phase material consisting of solid phase (Silica:  $\text{SiO}_2$ ), gas phase (air), and liquid phase (water). Due to different attenuation characteristics of neutrons and X-rays to these three phases of interest, neutron and X-ray images provided unique but complementary information. While the water phase contrast is well identified with cold neutron images without using a contrast agent, the detailed structure of silica sand phase is much clearly shown in X-ray images due to low attenuation of air/water phases to X-rays. This presentation will provide a detailed description of neutron and X-ray tomography techniques employed. An automatic approach to register the dual modality image in the same coordinate is also demonstrated. Direct numerical simulation technique based on the realistic pore geometry obtained from X-ray tomography of dry sand specimen is also demonstrated. Pore morphology method was used to predict capillary water distribution and capillary pressure - saturation curve as an example. Neutron imaging shows promise for interesting and multi-disciplinary research and the planned VENUS imaging beam line at the Spallation Neutron Source at Oak Ridge National Laboratory and the existing thermal imaging beam line at NIST will also be introduced.

Dr. Penumadu would like to acknowledge the support of DTRA award A12-1068 for this ongoing research.

11:45 HA 03 *New capabilities in helium-ion microscopy for nanofabrication and microanalysis at the Center for Nanophase Materials Sciences*

(Work done in collaboration with David Joy.)

**Rondinone, Adam;** ( Invited Speaker ) Oak Ridge National Lab

Electron microscopy is a critical technique for all types of nanoscience and basic materials research. However, it is now evident that future imaging needs at the nanoscale cannot be advanced purely by electron-beam instrumentation because enhancing one parameter of instrument performance, for example the spatial resolution, inevitably degrades some other parameter of performance, such as the depth-of-field. Minimizing these problems by techniques such as aberration correction is routine but raises the complexity and hence the cost of such electron-beam instruments to extraordinary levels. The technical advantages of using helium ions rather than electrons are clear - the ultra-short wavelength of ions compared to that of electrons of the same energy permits high resolution and high depth-of-field to be achieved simultaneously and, because the penetration depth of ions is 30 to 50x shorter than that for electrons, ion images are richer in surface detail. The Center for Nanophase Materials Sciences (CNMS) is commissioning the world's first helium-ion microscope tailored specifically for nanofabrication, to include imaging, FIB nanopatterning using helium/neon beams, and TOF-SIMS microanalysis. This instrument will be part of the user program and available to the general research community, and located within the CNMS cleanroom to accommodate fabrication and analysis of nanostructured devices within a clean environment.

12:15 HA 04 *Three-dimensional in situ nano manipulation and nano fabrication inside the scanning electron microscope*

**Cohn, Robert W.;** ( Invited Speaker ) University of Louisville

Beyond visualization and composition analysis, scanning electron microscopes (SEMs) provide limitless opportunities to probe, manipulate and fabricate materials and devices in real-time. Using a field emission electron microscope outfitted with a four arm nanomanipulator and numerous vacuum feedthroughs, a number of experiments and studies will be described, including bending and vibration mechanics of nanowires and polymer fibers, e-beam induced deflection and rotation of polymer nanofibers, selective growth of individual metallic nanowires from a room temperature alloy melt, field emission induced melting of sharpened tungsten tips and contact angle measurements of vacuum oils on nanowires.

---

## SESSION HB: Atomic, Molecular, and Optical Physics II

*10:45 Friday Morning*

Salon AB

Chair: John Yukich, Davidson College

10:45 HB 01 *Perfect Fluidity: From Strongly-Interacting Fermi Gases to Quark-Gluon Plasmas*

(Supported by NSF, DOE, ARO, and AFOSR.)

**Thomas, John;** ( Invited Speaker ) North Carolina State University

Strongly interacting atomic Fermi gases and quark-gluon plasmas share a common feature: They exhibit nearly ideal, minimum viscosity hydrodynamic expansion, which is a characteristic of a “perfect” fluid. A perfect fluid is defined to be a normal fluid (not a superfluid) with the minimum ratio of shear viscosity to entropy density permitted by the laws of quantum physics,  $\hbar/(4\pi k_B)$ , as derived recently using string-theory methods.

We measure both the shear viscosity and the entropy of an optically-trapped, strongly-interacting gas of spin  $1/2$ -up and spin  $1/2$ -down  ${}^6\text{Li}$  atoms. A bias magnetic field tunes the gas to a collisional (Feshbach) resonance, where the s-wave scattering length, for collisions between atoms of opposite spin, diverges. At resonance, the system is universal and scale-invariant, so that the thermodynamic and hydrodynamic properties are universal functions

of the density and temperature. Even though it is dilute, such an atomic Fermi is the most strongly interacting non-relativistic system known, enabling tests of recent theories in diverse disciplines from high temperature superconductors to nuclear matter, and even string- theory, via the minimum viscosity conjecture.

11:15 HB 02 *Time Resolved Analysis of the C, (C<sub>2</sub>) Swan and (CN) Violet Systems from Dicarboxylic Acids from Laser Induced Breakdown Spectroscopy*

**Brown, Staci; Akpovo, Charlemagne; Martinez, Jorge; Lewis, Dawn; Johnson, Lewis;** Florida A&M University

Laser Induced Breakdown Spectroscopy (LIBS) was used as a method for the detection of carbon, carbon-carbon and carbon- nitrogen molecular bonds from atmospheric recombination. Ablated samples were comprised of a series of dicarboxylic acids with an increasing number of carbon in their molecular structure from 2 to 7 (ex. Oxalic Acid, Malonic acid, Succinic Acid, etc). Accumulated pulses of a focused Nd:YAG q-switched laser beam operated at 532nm and an energy of approximately 5mJ at a repetition rate of 20 Hz were used to generate a plasma. The LIBS spectra were acquired using a high-resolution Czerny-Turner image spectrometer with an intensified charge-coupled device. Through a time resolved analysis of the emission spectra, we demonstrate the effects of the change in gate delay on the emission of the vibrational headbands for the Swan (C<sub>2</sub>) and Violet (CN) spectroscopic systems. We also, illustrate the effects that these constraints have on the peak intensities of the individual headbands in relation to each other and those of ionic Carbon and Nitrogen.

11:27 HB 03 *Atomic and Molecular Collisions using a Time-Dependent Close-Coupling Method*

(The work was supported in part by grants from the U.S. DOE and the U.S. NSF)

**Pindzola, M.S.;** ( Invited Speaker ) Auburn University

A non-perturbative time-dependent close-coupling method has been developed to handle quantal many-body Coulomb breakups found in photon-impact, electron-impact, and ion-impact ionization of atoms, molecules, and their ions. For atoms the time-dependent Schrodinger equation is solved using a 2D or 3D numerical lattice and an expansion in coupled spherical harmonics. For molecules the time-dependent Schrodinger equation is solved using a 4D numerical lattice and an expansion in rotational functions. For highly charged atomic ions the time-dependent Dirac equation is solved using a 2D numerical lattice and an expansion in coupled spin-orbit eigenfunctions. Theoretical cross sections are compared to experiment for a variety of atomic and molecular collisions, including the triple photoionization of the Li atom.

11:57 HB 04 *Optical Properties of Plasmon-Coupled Semiconductor Quantum Dots*

(This work at HU was supported by NSF HRD 1137747 and ARO W911NF-11-1-0177.)

**Ramdon, Roopchan; Abdel-Fattah, Mahmoud; Tabibi, Bagher;** Hampton University **Kim, Wan-Joong; Cho, Hyoyeong;** Electronics and Telecommunications Research Institute **Jung, Sungsoo;** Korea Research Institute of Standards and Science **Fudala, Rafal; Rich, Ryan;** University of North Texas Health Science Center **Gryczynski, Zygmunt;** Texas Christian University **Gryczynski, Ignacy;** University of North Texas Health Science Center **Yu, William;** Rice University **Wang, Andrew;** Ocean NanoTech **Seo, Jaetae;** Hampton University

Hybrid optical materials of semiconductor quantum dots (SQDs) in the vicinity of metal nanoparticles (MNPs) are of great interest for photonic applications because of their large fluorescence enhancement and wide tunability in the optical spectral region. When the SQDs are placed in the vicinity of plasmonic MNPs, excitons and plasmons are strongly coupled through Coulomb interactions that modify the optical properties of hybrid nanomaterials of SQDs and plasmonic MNPs. With optical excitation, both MNPs and SQDs can be excited to their higher energy states, and relax to the ground states through either radiative or non-radiative channels. However, if the energy transfer from SQDs to MNPs is much faster than radiative and non-radiative decays, the fluorescence can be largely enhanced by the reduction of the probability of non-radiative decays and large enhancement of local field. Therefore, the plasmon-exciton coupling modifies fluorescence intensity, lifetime, and polarization. This presentation will include the optical properties of CdSe/ZnS at ~620 nm by coupling with Au nanoparticles with diameter ~32 nm.

---

## SESSION HC: Nuclear Physics II

*10:45 Friday Morning*

Adams-Park

Chair: John Shriner, Tennessee Technological University

10:45 HC 01 *Giant Monopole Energies from a Constrained Relativistic Mean-Field Approach*

**Chen, Wei-Chia; Piekarewicz, Jorge;** Florida State University

Most nuclear energy density functionals (EDFs) are calibrated using exclusively data from nuclear experiments performed under normal nuclear densities and isospin asymmetries. Thus, when extrapolated to the extreme, the predictions differ significantly from model to model. In this work, we develop a constrained relativistic mean-field approach to compute giant monopole energies of nuclei with various isospin asymmetries. The results are compared against those obtained from a relativistic random phase approximation and excellent agreement is found. These results make viable the use of giant monopole energies into the calibration scheme of future nuclear EDFs.

10:57 HC 02 *Four-fold data analysis of  $^{252}\text{Cf}$  fission products*

**Wang, E.H.; Brewer, N.T.; Hamilton, J.H.; Ramayya, A.V.; Hwang, J.K.;** Vanderbilt University **Luo, Y.X.;** LBNL, Vanderbilt University **Rasmussen, J.O.;** LBNL **Zhu, S.J.;** Tsinghua University **Ter-Akopian, G.M.; Oganessian, Yu.Ts.;** JINR

Prompt gamma-ray 4-fold data were built to collect  $2 \times 10^{11}$   $\gamma - \gamma - \gamma - \gamma$  quadruple- and higher-fold  $\gamma$  - coincidence events from the spontaneous fission of  $^{252}\text{Cf}$  with Gammasphere detector arrays. The nuclei  $^{106}\text{Nb}$ ,  $^{142}\text{La}$ , Ba and Gd have been studied with these data. By using the new 4-fold data, we confirmed several weak tentative transitions in  $^{106}\text{Nb}$ ,  $^{142}\text{La}$ , Ba,  $^{148}\text{Ce}$  which were observed previously from the  $\gamma - \gamma - \gamma$  triple cube. Some new transitions in  $^{106}\text{Nb}$ ,  $^{142}\text{La}$  were identified by our new 4-fold data. Cascades in  $^{145}\text{Ba}$  are much clearer in four-fold data than the previous triple coincidence data. We will continue to study other nuclei by our 4-fold data with lower background than the previous triple cube. We thank M. Riley for urging us to build the 4-fold data set to get more accurate intensities.

11:09 HC 03 *ANC measurement on  $(^6\text{Li},d)$  reactions*

**Avila, M.L.; Rogachev, G.V.; Koshchiy, E.;** Florida State University

Direct measurement of many astrophysically important reactions cannot be done due to small cross sections. An alternative can be to obtain the Asymptotic Normalization Coefficient (ANC) as an effective method to determine the astrophysical S factor. Combination of the sub-Coulomb  $\alpha$ -transfer reaction and application of the ANC technique in the analysis of the experimental data practically eliminates all dependence of the result on model parameters, making this approach a very valuable tool for studies of astrophysically important reaction rates. In this study we report the ANC measurements of near threshold states for  $(^6\text{Li},d)$  reactions performed at sub-Coulomb energies at the Florida State University Tandem-LINAC facility. The reactions that were studied using this technique are  $^{16}\text{O}(^6\text{Li},d)^{20}\text{Ne}$ ,  $^{13}\text{C}(^6\text{Li},d)^{17}\text{O}$  and  $^{12}\text{C}(^6\text{Li},d)^{16}\text{O}$ .

11:21 HC 04 *The recent study of the structure of  $^{31}\text{Si}$*

**Tai, Pei-Luan; Hamilton, L.; Bender, P.; Tabor, Samuel; Tripathi, Vandana; Hoffman, C.;** Florida State University. **Clark, R.; Fallon, P.; Macchiavelli, A.; Paschalis, S.; Petri, M.;** Lawrence Berkeley National Laboratory **Carpenter, M.; Janssens, R.V.F.; Lauritsen, T.; McCutchan, E.; Seweryniak, D.; Zhu, S.; Chiara, C.;** Argonne National Laboratory **Chen, X.; Reviol, W.; Sarantites, D.;** Washington University

$^{31}\text{Si}$  was produced through the  $^{18}\text{O} (^{18}\text{O}, \alpha n)$  reaction at the beam energy of 25 MeV, which preferentially populates the high spin states. The  $\alpha$  particles were detected in Microball and the multiple  $\gamma$ -ray coincidences were detected by Gammashpere. There are 11 newly observed states and 22 new discovered  $\gamma$  transitions. A

strong competition is seen between negative-parity “intruder” states and positive-parity pure s-d states. Shell model calculations agree relatively well with both groups of states. Kinematic correction code for recoil is under development.

#### 11:33 HC 05 *Study of Neutron Deficient ${}^9\text{C}$*

**Belarge, Joseph; Rogachev, G.V.**; Florida State University **Blackmon, J.**; Louisiana State University **Wiedenhöver, Ingo; Baby, L.T.; Johnson, E.D.; Kuchera, A.N.; Koshchiy, E.**; Florida State University **Lai, J.; Linhardt, L.; Macon, K.; Matos, M.**; Louisiana State University **Santiago-Gonzalez, Daniel**; Florida State University

Development of theoretical framework that allows the combination of nuclear structure calculations with the continuum is an important objective of modern nuclear theory [1,2]. Due to the low binding energy of exotic isotopes even the lowest excited states are unbound and therefore it is essential to take the continuum into account. We studied the structure of the lightest bound carbon isotope,  ${}^9\text{C}$ , through  ${}^8\text{B}+p$  resonance scattering using the new active target detector ANASEN [3]. The experiment was performed at the John D. Fox Superconducting Accelerator Laboratory at FSU. A rare isotope beam of  ${}^8\text{B}$  ions was produced using the radioactive nuclear beam facility RESOLUT. Pure hydrogen gas was used as a target and also as an active medium for the gas proportional counters of the ANASEN detector. The analysis of the  $p+{}^8\text{B}$  excitation functions was performed using the R-Matrix approach. The preliminary results will be presented.

[1] A. Volya, Phys. Rev. C **79**, 044308 (2009).

[2] S. Quaglioni and P. Navrátil, PRL **101**, 092501 (2008).

[3] M. Matos, et al., Proc. Intern. Symposium on Nuclei in the Cosmos XI, July 19-23 2010, Heidelberg, Germany, p.226(2010)

#### 11:45 HC 06 *High Spin Structures in ${}^{25}\text{Na}$*

(Work supported in part by the National Science Foundation under grant NSF-10-64819; Bender currently at TRIUMF)

**VonMoss, Justin; Tabor, Samuel; Tripathi, Vandana; Bender, P.; Volya, Alexander; Tai, Pei-Luan**; Florida State University

High-spin states in  ${}^{25}\text{Na}$  were populated in the  ${}^9\text{Be}({}^{18}\text{O}, pn)$  reaction using a 35 MeV  ${}^{18}\text{O}$  beam from the John D. Fox Superconducting Accelerator Laboratory at Florida State University. Gamma rays were detected using the FSU compton-suppressed germanium array in coincidence with protons from the reaction. Two new states and seven new gamma transitions were observed. Additionally a doublet has been identified which resolves a conflict in the published works. Unobserved, and highly excited particle-hole states have been predicted using shell model calculations.

#### 11:57 HC 07 *Measurement of the ${}^{25}\text{Al}(d,n){}^{26}\text{Si}(p)$ reaction at RESOLUT: Spectroscopy of $l = 0$ and $l = 1$ resonances*

**Baker, Jessica; Wiedenhöver, Ingo; Rojas, Alexander; Baby, L.T.; Kuvin, Sean; Peplowski, Patrick; Santiago-Gonzalez, Daniel**; Florida State University **Perdikakis, Georgios**; National Superconducting Cyclotron Laboratory, Michigan State University **Gay, Dennis**; University of North Florida

Studies of rp-process nucleosynthesis in stellar explosions show that establishing the lowest  $l = 0$  and  $l = 1$  resonances is the most important step to determine reaction rates in the astrophysical rp-process path. In an experiment performed at the RESOLUT radioactive beam facility of Florida State University, we have studied the  ${}^{25}\text{Al}(d,n){}^{26}\text{Si}$  reaction in inverse kinematics to establish the spectrum of the lowest  $l = 0$  and  $l = 1$  resonances. The spectrum is consistent with a previous experiment using the same reaction at RESOLUT [1] and results obtained from recent stable beam experiments [2].

[1] P.N. Peplowski et al. Phys.Rev C **79**, 032801 (2009)

[2] K.A. Chipps et al. Phys.Rev C **28**, 045803 (2010)



12:09 HC 08 *The Proto-neutron star crust studied with an Ising approach*

(This work was supported in part by grants from the U.S. Department of Energy DE-FD05-92ER40750.)

**Hasnaoui, Karim; Piekarewicz, Jorge;** Florida State University

The thermodynamics of the proto-neutron stars crust is studied in this project. Obtaining information on the star matter thermodynamics will enhance the understanding of physical phenomena involved in the cooling of proto-neutron stars, and the formation of type II supernovae. The main goals of this project is to understand qualitatively, how the different structures of the crust, such as the well known “*nuclear pasta*” or the liquid and gas phases can be formed as function of the proton fraction  $X_p$ , the density  $\rho$ , or the temperature  $T$ . For this purpose, we have developed a classical model based on a Ising/Lattice-gas approach, where the short range nuclear interaction and the long range Coulomb interaction have been included. We are now able to perform simulation for a very large number of particles, and we will show that the signals of phase transitions between the *pasta* structures and the gas phase as function of the different conditions previously mentioned, can be clearly identified on the structure form factor  $S(k)$ , but also on the heat capacity  $C_v$ .

12:21 HC 09 *Monte Carlo simulation of secondary electron emission in the Nab experiment*

(Supported by grants from the National Science Foundation and the Department of Energy)

**McLaughlin, Chatham David;** University of Virginia, Nab

The Nab experiment aims at a precise measurement of  $a$ , the electron neutrino correlation parameter and  $b$  the Fierz interference term in neutron  $\beta$  decay. The measurement is to be performed at the Spallation Neutron Source (SNS) in Oak Ridge, TN using a asymmetric magneto-electrostatic spectrometer. One of the main challenges is the detection of the low energy proton resulting from the  $n \rightarrow e^- p \bar{\nu}_e$  decay. This can be accomplished in two ways: by placing the detector itself at a negative potential to accelerate the protons. Alternatively we detect the secondary emission electrons (SEEs), from multiple passages of the proton through a thin ( $\sim 100\text{nm}$ ) foil in front of the detector. The foil is at a high negative potential. The Poisson distributed SEEs are detected in segmented Si detectors with virtually no adverse effects due to the detector’s thin dead surface layer. Initial Monte Carlo simulation of the problem using GEANT4 indicates a mean of 8.7 secondary electrons are generated using a Al foil at -30kV. While most are immediately reabsorbed, a median of 2 electrons is detected per proton. Other suitable foil materials can increase the number of detected SEEs. Representative results of a full simulation in both detection modes will be presented.

---

## SESSION IA: Tours of Facilities

*13:45 Friday Afternoon*

Various Locations

13:45 IA 01 *TOURS OF FACILITIES*

The tours of local research facilities will take place immediately after lunch on Friday afternoon. The facilities that will be toured are the National High Magnetic Field Laboratory, The High Performance Materials Institute, and The Center for Plasma Science and Technology. Each tour will last between 45 minutes and an hour. Those taking the tours are free to tour one or all of the facilities, but everyone is reminded that the last bus will leave Innovation Park (the site of the three facilities) at 17:00. The first bus can be boarded in front of the hotel beginning at 13:30. The last bus will leave Innovation Park at 17:00 to return to the hotel.

---

## **SESSION JA: Executive Committee Meeting**

*16:00 Friday Afternoon*

Tallahassee

Chair: Roxanne Springer, Duke University

---

## **SESSION JB: SESAPS Business Meeting**

*17:30 Friday Evening*

Florida

Chair: Roxanne Springer, Duke University

---

## **SESSION KA: Poster Session (6:00-10:00PM)**

*18:00 Friday Evening*

Ballroom, Adams-Park, and adjacent hallways

### *KA 01 LiF Thermoluminescent Detectors for Proton and Neutron Dosimetry*

**Chambers, Erin**; Tennessee Technological University **Allgower, Chris**; Indiana University Health Proton Therapy Center **Klein, Susan**; Indiana University Bloomington

Measurements of proton and secondary neutron dose have been taken using LiF:Mg,Ti thermoluminescent dosimeters at the Indiana University Health Proton Therapy Center at Bloomington, IN. These measurements provide evidence for a lower secondary neutron dose from active beam modulation as opposed to passive modulation. An unexplained inconsistency in TLD proton dose response was identified. This research was funded by the National Science Foundation and supported by the Indiana University REU program.

### *KA 02 Width and Spacing Distributions in Nuclear Data*

**Johnson, T.L.**; (Supported by TTU URECA Program) **Shriner, Jr., J.F.**; Tennessee Technological University **Mitchell, G.E.**; (Supported by the US Department of Energy via grants No. DE-FG52-09NA29460 and No. DE-FG02-97-ER41042) North Carolina State University, TUNL

A recent study focusing on neutron resonance widths (P. E. Koehler, Phys. Rev. C **84**, 034312 (2011).) has called into question whether the Gaussian orthogonal ensemble (GOE) version of random matrix theory describes nuclear resonance data. The conclusion that the data are inconsistent with GOE seems in contradiction with the analysis of resonance spacing data. We wish to test the possibility that the distribution is not truly GOE but the spacing data by themselves still appear to be described by the GOE. We have simulated both width and spacing distributions that differ by varying amounts from the GOE distribution and determined how one estimate of GOE behavior, the fraction of missing levels, behaves as we deviate increasingly from a GOE distribution. Results will be presented.

KA 03 *Minimum-Bias Studies Using the Energy Scan Data from the Fermilab Tevatron Collider*

**Wilson, David; Group, Craig;** University of Virginia, CDF **Field, Rick;** University of Florida, CDF

We report on an analysis of the minimum-bias event data (that is, events with the least selective trigger criteria) taken at the Tevatron collider at Fermilab, in particular an energy scan recording collisions at  $\sqrt{s} = 0.3, 0.9,$  and 1.96 TeV. This data set represents a rare chance to analyze the energy dependence of several minimum-bias observables; for example, the pseudorapidity ( $dN/d\eta$ ) distribution. We present the results of a comparison of these observables with the PYTHIA Monte Carlo simulation.

KA 04 *Studies of Silicon Photomultipliers for their use in the Mu2e Experiment at Fermilab*

**Henderson, Alyssa;** University of Virginia **Group, Craig; Oksuzian, Yuri;** University of Virginia and Fermilab **Rubinov, Paul;** Fermilab

Silicon Photomultipliers (SiPMs), a relatively novel technology, are able to detect single photons and convert them into electrical signals when used within a proper voltage range. In order to learn more about SiPMs for their use in the Mu2e experiment, we find a few characteristics of the SiPM at the Silicon Detector facility at Fermilab. We connected several SiPMs, one at a time, to a Keithley 2400 Sourcemeter that was programmed to vary the voltage automatically. In this way, we were able to apply our desired voltage range and the sourcemeter provided the corresponding current. We also conducted these experiments with the SiPMs in a dark chamber, which we used to control the temperature of the environment. We applied a voltage and measured the corresponding current at four temperatures and measured three characteristics: breakdown voltage, the operating voltage range, and the resistor value at each, as well as how they vary with temperature, time, and between two brands.

KA 05 *Nuclear Effects in Polarized  $^3\text{He}$  Structure Functions and Asymmetries*

(I would like to acknowledge the Department of Energy for the funding of the Student Undergraduate Laboratory Internships (SULI) program in which this research was conducted.)

**Ethier, Jacob;** Stetson University **Melnitchouk, Wally;** Thomas Jefferson National Accelerator Facility

In polarized electron-nucleon scattering, spin structure functions (SSFs) give information about quark spin contributions to the total nucleon spin. Since free neutron targets are nonexistent, nuclei such as  $^3\text{He}$  (two protons and one neutron) and deuterium (one proton and one neutron) are commonly used as effective neutron targets to gather SF data. Given that the neutron is not free but is bound inside the nucleus results in consequences for its internal quark structure. The aim of this work was to study theoretical models of  $^3\text{He}$  SSFs and polarization asymmetries (ratios of polarized to unpolarized SFs) that account for these bound nucleon effects so that neutron information can be reliably extracted from nuclear data. The  $^3\text{He}$  SSFs and asymmetries can be calculated by smearing the proton and neutron SSFs with the light-cone momentum distributions of the nucleons in the nucleus. The full calculations of the  $^3\text{He}$  SSFs and asymmetries reveal a distinct difference in resonance structure compared to the free nucleon SSFs.

KA 06 *Metropolis-Hastings Algorithm Optimization Using Lag-1 Correlation Time and Chain Power Spectrum to Generate Nuclear Coordinates from Nuclei with Neutron Halo*

**Gordon, Emily; Novikov, Ivan;** Western Kentucky University

We extract parameters of nuclear density distribution for the  $^{11}\text{Li}$  nucleus by calculating interaction and reaction cross sections and comparing the results to experimental data. The cross section calculations are done in the framework of Glauber theory using Monte Carlo integration technique. The Metropolis-Hastings algorithm and other Markov Chain Monte Carlo (MCMC) approaches are used to create sequences of random numbers distributed according to a predefined distribution. The algorithm efficiency depends on exact expressions of the distribution of interest and proposal distribution. The goal of this study is to find the parameters of proposal distribution which maximize the efficiency of the Metropolis-Hastings algorithm. The algorithm performance was optimized using lag-1 correlation time and the shape of the power spectrum of the random number sequence.

*KA 07 Implementing a New Ion Chamber Design for Neutron Spin Rotation*

**Gardiner, Hannah;** Louisiana State University **Anderson, Eamon; Fry, Jason; Holley, Adam; Snow, Mike;** Indiana University

The quark-quark weak interaction is difficult to measure due to the presence of the strong force. However, low energy neutrons passing through liquid Helium-4 can be used to probe the nucleon-nucleon weak interaction, which is induced by the quark-quark weak interaction. The neutron spin rotation experiment seeks to measure the spin rotation angle of neutrons due to their weak interaction with Helium-4 nuclei. This rotation angle is translated into a neutron flux asymmetry with a neutron polarizer/analyzer pair. A segmented Helium-3 gas ionization chamber was developed to measure the resultant neutron flux. We report on the design and initial tests of that ionization chamber. This work is supported by the National Science Foundation REU program and NSF grant #PHY-0969490.

*KA 08 Use of Computational Simulations for Analysis of Parity Violation Experiments with Neutrons*

**Serpico, Jonathan; Novikov, Ivan;** Western Kentucky University

We developed and analyzed the results of computer simulations of experiments in which parity violating and parity conserving asymmetries are measured in nuclear reactions with neutrons. The software utilizes parallel computing technologies. The value of the parity violating and parity conserving asymmetries and their accuracies were obtained for various neutron beam parameters, targets, and configurations of detection systems. The energy dependence of parity violating and parity conserving amplitudes were obtained in the framework of reaction theory.

*KA 09 Characterization of a polymer based drug delivery system for the enhancement of wound healing*

**Widejko, Ryan;** Francis Marion University **Moore, Keith; Potts, Jay;** University of South Carolina School of Medicine

The field of Regenerative Medicine has seen an increase in the need to improve long term implant compatibility. To address this need we have combined microencapsulation and beneficial wound healing agents. The aim of the project was to develop and characterize a delivery system for the agent  $\alpha$ CT1. To enable the extended release of this peptide, alginate microcapsules coated in poly-l-ornithine (PLO) were explored as a means of delivery. These capsules were created via electro-spraying and characterized by phase contrast microscopy, scanning electron microscopy (SEM), atomic force microscopy (AFM), and release profiles. SEM analysis showed the addition of PLO did not change the overall geometry or topology of the microcapsules. AFM analysis showed that PLO affected the rigidity of the capsules by decreasing it from 54.26 pN to 46.11 pN. The release profile analysis revealed that over an 8 hr period the addition of PLO extended the  $\alpha$ CT-1 released by 146% over the release of alginate alone. Phase contrast microscopy revealed that the addition of PLO changed the average size of the capsules from 209  $\mu$ m to 187  $\mu$ m. The results of this project indicate that the use of alginate microcapsules as a drug delivery system for  $\alpha$ CT-1 is a viable method. This material is based upon the work performed in association with an REU Program hosted by the Biomedical Engineering Program at USC and supported by the NSF under the grant #EEC-1005138.

*KA 10 Measurement of coiled-coil stability by fluorescence resonance energy transfer*

**Pino, James; Kim, Bomi; Santiago, Manuel; Whitson, Stefanie; Whitson, Kristin;** University of Tennessee at Chattanooga

Alpha helical coiled-coils are common structural motifs by which proteins assemble into larger complexes. The leucine zipper-like oligomerization domain of heterogeneous nuclear ribonucleoprotein C (CLZ) assembles into an anti-parallel tetramer with a coiled-coil fold. Fluorescently-tagged CLZ peptides were designed and characterized as appropriate to perform measurements using fluorescence resonance energy transfer (FRET) to study the overall stability of the assembly. Experiments revealed that the appearance of FRET in a sample was time dependent and thus reflective of the kinetics of the tetramer's formation. Furthermore, FRET assays using varying concentrations of labeled peptides have allowed the first measurement of the equilibrium dissociation constant ( $K_D$ ) of the CLZ tetramer, which is representative of the strength of specific molecular interactions within the

oligomer. The method can be used to study effects of mutations in this coiled coil on the thermodynamic stability of the complex.

#### KA 11 *Sensitivity of Rayleigh-Taylor Instability growth rate due to thermal conductivity*

**Learn, Ryan; Plewa, Tomasz;** Florida State University **Zhiglo, Andrey;** NSC Kharkhov Institute of Physics and Technology

In many high energy density and astrophysical systems, the heat conduction plays an important role in the system evolution by redistributing the heat and modifying flow morphology. Thermal conduction is known to induce fluid flows in systems where materials of different densities are in pressure equilibrium. In situations when gravity is present, material discontinuities might be subject to the Rayleigh-Taylor instability. In that case, and in presence of thermal conduction, one may expect the interplay between the thermal conduction and the Rayleigh-Taylor Instability.

We explore this possibility and study Rayleigh-Taylor driven mixing in thermally conducting plasmas by means of multidimensional hydrodynamic simulations. The parameters used in our numerical experiments are based on proposed and completed experiments on the OMEGA and National Ignition Facility lasers.

#### KA 12 *Characterization of Zr-V-Fe Non-Evaporable Getter Strips for use in a Miniature Penning Trap*

(This project was funded by the REU grant US-NSF PHY-1062410 and the NSCL grant US-NSF PHY-1102511.)

**Baker, Robert;** Austin Peay State University **Bollen, Georg; Lincoln, David;** NSCL, Michigan State University **Redshaw, Matt;** NSCL, Central Michigan University **Ringle, Ryan; Schwarz, Stefan; Valverde, Adrian;** NSCL, Michigan State University

The Low Energy Beam and Ion Trap (LEBIT) group at the National Superconducting Cyclotron Laboratory (NSCL) performs high-precision mass measurements using a Penning trap. The current method involves measuring reference ions of known mass in order to calibrate the magnetic field. Because the reference measurements require us to stop the measurement of a rare isotope, we will optimize the use of beam time by installing a magnetometer to directly measure the magnetic field while conducting a rare isotope measurement. A miniature Penning trap (MiniTrap) will be mounted adjacent to the measurement trap to serve as a magnetometer. To reach the desired precision, the MiniTrap must be operated in very low pressures. We investigate using the SAES St707 (Zr-V-Fe) non-evaporable getter to pump out the MiniTrap to achieve an ultra-high vacuum. Excess hydrogen will be ionized into  $H_2^+$  and serve as the reference mass. We report a pumping speed for the activated getter material, partial pressures for the background gases after different pumping intervals, and discuss further work with the MiniTrap.

#### KA 13 *Computational analysis of odorant binding to OBPs*

**Kim, Bomi; Pino, James; Santiago, Manuel; Whitson, Stefanie; Whitson, Kristin;** University of Tennessee of Chattanooga

Humans can detect countless odors but the mechanism by which much of the pathway occurs is not elucidated. Odorant binding proteins (OBPs) carry hydrophobic odorants across aqueous mucus to be deposited at olfactory receptors, triggering a neuronal response. The active site within the beta-barrel structure is conducive for hydrophobic odorants, where a lysine residue has been implicated as essential for binding of aldehyde moieties. The studies herein aim to determine the relative stability of various odorant/OBP combinations by energy minimization and computational modeling with ligand docked to active sites in wild-type OBP2A, mutant OBP2A, or OBP2B. The results demonstrate other specific interactions between odorants and protein, revealing wild-type OBP2A may have two binding sites, with initial binding occurring near the barrel opening. Energies indicate protein stability though two ligands are present in the active site. In addition, ligands with similar structures bind the same location on the protein, indicating directionality of the protein in ligand binding.

KA 14 *Examination of Concrete with Carbon Nanotubes Using the Large Chamber Scanning Electron Microscope*

**Cruz, Linda; Palmquist, Shane; Palmer, Jahi; Andrew, Keith; Kintzel, Edward;** Western Kentucky University  
Mechanical properties of concrete are most commonly determined using destructive tests including: compression, flexure, and fracture notch specimen tests. However, nondestructive tests exist for evaluating the properties of concrete such as ultrasonic pulse velocity and impact echo tests. One of major issues with concrete is that unlike steel it is quasi-brittle material. It tends to want to crack when tensile stresses develop. These cracks generally develop at the interfacial transition zone (ITZ) between the cement paste and the aggregate. Fibers have been added to concrete for many years to help with temperature and shrinkage cracks. In more recent years, the concepts of adding fibers with enhanced properties such as carbon nanotubes (CNTs), to concrete have been explored. Some possibilities include developing concrete that may be more durable, flexible, stronger, less permeable, and potentially “crack free” than traditional concrete. Based on SEM images and quantitative data taken using the Large Chamber Scanning Electron Microscope at Western Kentucky University, this study examines the ITZ of concrete made with CNTs. Results provide greater understanding on the nature of the ITZ region in concrete made with CNTs.

KA 15 *Quantum Magnetism Software*

**Garland, Scott; Engelhardt, Larry;** Francis Marion University

We present an open-source (free), user-friendly computer program that generates theoretical magnetism data based on customizable quantum spin systems. A detailed knowledge of quantum mechanics is not required to use this program, making it suitable for students as well as researchers. FIT-MART, the Fully Integrated Tool for Magnetic Analysis and Research, is available for download as a platform-independent, executable java (.jar) file at: <http://www.opensourcephysics.org/items/detail.cfm?ID=12308>.

KA 16 *Ameliorating Computational Tools and Testing Cosmological Models*

**Shuler, Ezekiel;** (Undergraduate Poster Presentation) Francis Marion University

The Lambda-Cold Dark Matter (LCDM) model is the standard model for the universe. This model explains some key elements in the universe that cosmologists believe to be true, however this model also has some inconsistencies. Using the CosmoMC code along with the Palmetto Cluster, I will run jobs that will best test the LCDM model. I will also improve an EJS (Easy Java Simulations) program to require GRBs (Gamma-Ray Bursts) as apposed to just SN (Supernovae). Supernovae Type Ia are known as standard candles, and they are used to directly probe the expansion rate of the universe. Recently, GRBs (Gamma-Ray Bursts) have been explored more and have been proposed to be a complementary probe to Supernovae Type Ia. So far, GRBs are the most intense explosions in our universe. For this reason, the GRBs have much higher redshifts up to 8.1, but redshifts close to 10 or larger are expected. This simulation allows the user to discover the cosmological model that best-fits the recent supernovae and GRB datasets. After receiving the results from my jobs on the Palmetto cluster, I will conclude on the stasis of the LCDM model and be able to do a pulmonary test with the GRBs in the EJS program. I found that the LCDM model is a pretty good model for our universe, but we need more conclusive data to rule it out or keep it. The study of the evolution of the universe is extremely important to understand the cause of the accelerated expansion of the universe (cosmic acceleration).

KA 17 *Galaxy Collision Modeling*

(Palmetto Academy, a division of the NASA SC Space Grant)

**Thavayoganathan, Kirubaa;** Francis Marion University

This project is a study of colliding galaxies. Using a parallelized N-Body code called GADGET-2, we create a model of the collision between Milky Way galaxy and Sagittarius dwarf galaxy (SDG). The SDG system is one of the closet dwarf galaxies to the Milky Way and observations provide very accurate positional and kinematical data for computer modeling. Through varying the parameters of the starting location of the SDG system we are able to study the resulting position of the SDG after 1 billion years has passed. Using the position of the SDG system as observed today we will be able to modify the initial position of the SDG system to produce an even

better model.

#### KA 18 *Control Box for Sub-Orbital Telescope*

**Rhodes, Christian**; Francis Marion University, Atsa

One of the major obstacles for observational astronomers is the Earth's atmosphere. By sending telescopes outside of the atmosphere we can overcome this problem. However, this can be quite expensive, especially with billion dollar telescopes such as the Hubble. Reasonably, astronomers do not want to risk burning out the CCD on the valuable telescope by pointing it near the sun. Solutions such as using Black Brant rockets have arisen, yet still cost millions of dollars. By utilizing commercial spaceflights offered by XCOR, we can cut this cost to less than a couple hundred thousand dollars and get the telescope back at the end of the flight. To prove that this is possible, we are developing a telescope that can fit onto the passenger side of the spacecraft. Even though the telescope will be hand-steered, a programmed control box was needed to change the filters and to record. The control box sends commands via serial communication to a shell program that controls the CCD program and the filter wheel program. By creating a shell program that controls the CCD and filter program inside the Windows operating system, the shell program is easily adaptable to any CCD or filter wheel program. This control box allows you to manually and automatically change the filters and record as well as document the time in which all the actions occurred.

- This project was completed under the Palmetto Academy, a division of the NASA SC Space Grant Consortium

#### KA 19 *Optical Strain Indicators*

(NASA and SCSGC: Palmetto Academy 2012)

**Heath, Jonathan**; Francis Marion University **Anderson, Dakotah**; **Anker, Jeffrey**; Clemson University

Remote non-destructive methods to measure strain are need for many NASA projects e.g. for astronauts to check on exterior equipment without having to be exposed to space, ground observatories to monitor tension of bolts miles away in the sky, and scientists to monitor how effective an airbag would stand against full impact of 200lb individual. We designed prototype optical strain indicators to accurately measure the strain of various objects and materials through nondestructive measures. These indicators may be used to label structural components, such as bolts, so that improper strain can be seen by the eye or camera. Strain gauges with alternating bands of red and blue were created that appeared to change color when a "window pattern" with transparent and opaque regions was displaced relative to the colored bands below. The strain gauges were attached to various objects/materials as they moved, stretched, or bent. The fabricated optical strain gauges were found to be quite versatile for many applications. Future work includes minimalizing the alternating color lines printed on the indicators, constructing and testing a screw design, and pursuing additional tests that involve expansion and bending.

#### KA 20 *Development of a Pattern Simulator for Benchmarking a Near-field Holographic Image Processor*

(National Science Foundation Summer REU Program)

**Martin, Kate**; North Georgia College & State University **Beaudoin, Christopher**; MIT Haystack Observatory

Deformations of the reflector optics comprising a radio telescope can introduce station position errors that are significant in the context of VLBI2010. Radio holographic imaging is a technique that can be utilized to detect such deformations. In experiments involving large reflector antennas at relatively high frequencies, geosynchronous satellites are observed to conduct far-field radio holography since the stand-off ranges satisfy the far-field requirement. However, these sources are relatively fixed with respect to the radio telescope and this limitation does not facilitate the ability to characterize the deformations over the telescope's full field-of-view. The near-field holographic imaging technique overcomes this limitation of the satellite-based far-field technique since the source is under the control of the observer and may be placed in close proximity to the radio telescope in question. Additional complexities arise in this near-field scenario but these considerations have been addressed in the literature. In this report, a near-field antenna pattern simulator was developed to facilitate testing of a near-field holographic image processor. The results of this simulator have been compared against independent expectations to validate the simulator.

### KA 21 *Utilizing On-Chip Resonant Cavities for Magnetic Resonance Studies*

**Serniak, Kyle; Martens, Mathew;** Florida State University, National High Magnetic Field Laboratory **Bertaina, Sylvain;** Faculte des Sciences et Techniques and Universite Aix-Marseille **Chiorescu, Irinel;** Florida State University, National High Magnetic Field Laboratory

We studied an Electron Spin Resonance (ESR) setup utilizing a balanced bridge in conjunction with a lock-in detector to be used at the low temperature attained by a dilution refrigerator. ESR measurements were performed on a spin 1/2 DPPH sample at room temperature. The setup uses a microstrip line, which has recently attracted a lot of interest due to its high sensitivity and low noise baseline. Electronic spin excitation of the sample was achieved through use of an “omega” shaped microstrip cavity with resonant frequency of 17.4 GHz, which concentrates the magnetic field in a small region where the sample is placed. A homemade heterodyne detector was used for signal detection with and without a balanced magic-T bridge and lock-in amplifier. Direct measurements were also performed using a fast digital acquisition card.

### KA 22 *Four Harmonic Buncher For FSU LINAC*

**Moerland, Daniel; Wiedenhöfer, Ingo;** Florida State University

Florida State University’s John D. Fox Superconducting Accelerator Laboratory is operating a Tandem-Linac system for heavy ion beams at energies of 5-10 MeV/u. Recently, the accelerator has been used as the driver for the radioactive beam facility RESOLUT, which poses new demands on its high-intensity performance and time-resolution. These demands motivated us to optimize the RF bunching system and to switch the bunch frequency from 48.5 to 12.125MHz. We installed a four-harmonic resonant transformer to create 3-4 kV potential oscillations across a pair of wire-mesh grids. This setup is modulating the energy of the beam injected into the tandem accelerator, with the aim to create short bunches of beam particles. A sawtooth-like wave-form is created using the Fourier series method, by combining the basis sinusoidal wave of 12.125MHz and its 3 higher order harmonics, in a manner similar to the systems used at ATLAS and other RF-accelerators. A new aspect of our setup is the use of a digital 1GHz function generator, which allows us to optimize and stabilize the synthesized waveform. The control system was realized using LabView and integrated into the controls of the accelerator.

### KA 23 *Lagrange Meshes in Nuclear Physics*

**Hynds, Taylor;** Florida State University

We examine different methods of solving the Schrödinger equation for two and three-body systems. We begin by constructing variational wave functions, as expansions in a basis of orthogonal polynomials. This method has been found to give accurate results, given a sufficiently large basis. However, computationally this can become very cumbersome. We therefore employ the Lagrange-mesh method, which leads to a simple calculation of both potential and kinetic matrix elements that is both computationally efficient and results in little to no loss in accuracy.

This method has been applied to several problems with well known analytical solutions, and has given excellent results. The effectiveness of this method in analyzing bound states of quarks has yet to be demonstrated. In the future this method will be applied to the quantum-mechanical three-body problem.

### KA 24 *Lagrange Mesh in Hadronic Physics*

**Rosenfeld, Spencer; Roberts, Winston;** Florida State University

We used a variational method to solve a quantum mechanical three body problem. This is accomplished by computing the matrix representation of the Hamiltonian operator in a Lagrange mesh basis and minimizing the appropriate energy eigenvalues. The method was applied to an approximate potential for quark-quark interactions.



KA 25 *Characterization of  $^{10}\text{B}$  Lined Proportional Counters and Moderator Design*

(This work is supported in part by USDOE Grant Nos. DE-FG02-97ER4104, DE-FG02-97ER41033 and DTRA Grant No. HDTRA1-11-C-0001.)

**Silano, J.A.**; University of North Carolina-Chapel Hill, TUNL

An SA-B1-0824-101  $^{10}\text{B}$  lined neutron counter from G.E. Reuter-Stokes was characterized and moderator was designed and tested for detecting fast neutrons. The neutron counters are single-wire cylindrical proportional counters with a Boron tube lining enriched to 92%  $^{10}\text{B}$  and are filled with Ar gas. Thermalized neutrons interact with the Boron layer through the  $^{10}\text{B}(n,\alpha)^7\text{Li}$  reaction, and the reaction products deposit energy in the Ar gas. The deposited energy pulse is amplified by a proportional counter bias potential of 800 V, resulting in a detectable signal. The detector consisting of four tubes was simulated in Geant4 and the dependence of the detector efficiency on the thickness of the  $^{10}\text{B}$  layer was determined. The detector efficiency was measured experimentally with a  $^{241}\text{AmBe}$  source of known neutron activity. A modular design for the high density polyethylene moderator allows the detector to be composed of four proportional counters for optimum efficiency, or be split into two separate detectors for  $(\gamma, n)$  polarization measurements.

KA 26 *Effective R-matrix parameters of the Woods-Saxon nuclear potential*

(This work is supported by the Florida State University CRC DSA award.)

**Abrahamsen, Dylan; Volya, Alexander; Wiedenhöver, Ingo**; Florida State University

The phenomenological R-matrix approach is one of the most practical tools for the analysis of the multi-channel resonant scattering data. However, the relatively unconstrained phenomenological parameters of the R-matrix approach have been subjects of a continuous criticism. The goal of this research is to study the connection between the R-matrix channel radius and the reduced width and the parameters of the actual potential model. We evaluate the scattering observables of the Woods-Saxon potential [1] and do an R-matrix fit which allows for the reduced width and channel radius to be determined. The dependence of the R-matrix parameters on the diffuseness, spin-orbit interaction and on other parameters of the nuclear potential is discussed.

[1] N. Schwierz, I. Wiedenhöver, A. Volya, <http://arxiv.org/abs/0706.1628>

KA 27 *The Search for Large Extra Dimensions via Single Photon plus Missing Energy Final States*

**Gomez, Alicia**; Florida State University, DZero

In high energy particle physics there is a hierarchy problem in the standard mode. The force of gravity is orders of magnitude weaker than the other forces. A theorized solution to this problem is that the Kaluza-Klein graviton carries much of the gravitational force into another dimension. We are looking for evidence of large extra dimensions by analyzing quark antiquark collisions which result in the production of a single photon and missing transverse energy. The data we are using is from the D0 experiment at the Tevatron collider at Fermilab National Accelerator Laboratory. The method we are using for our analysis is to restrict the data by imposing certain quality requirements which are pertinent to our analysis. From this data sample, we analyze distance of closest approach histograms to determine which events are best for analysis. Using these events we will set limits on the fundamental mass scale for large extra dimensions.

KA 28 *W Boson Production Charge Asymmetry in the Electron Channel*

**Huff, Ashley; Blessing, Susan**; Florida State University, D0

We present a measurement of W Boson Production Charge Asymmetry in  $PP(\bar{p})$  collisions through  $W \rightarrow e-\nu_e$  decays. The collision of a u quark and a  $d(\bar{p})$ quark will produce a  $W^+$  Boson while the collision of an  $u(\bar{p})$  quark and a d quark will produce a  $W^-$  Boson. These particles decay rapidly but we are able to measure their asymmetry by studying the resulting electrons and neutrinos. These results will be used to further constrain PDF fits and improve the accuracy of future predictions for new physics.

### KA 29 *Dipole Magnets for Axion Research*

(Mississippi State Consortium)

**Fowler, Nicholas; Dutta, Dipangkar; Riehle, Robertsen; Mohanmurthy, Prajwal;** Mississippi State University, MASS

Axions are hypothetical particles which have been proposed by Peccei and Quinn as a solution to the strong CP problem. The Mississippi State Axion Search (MASS) project has involved the light shining through a wall (LSW) technique to test for the existence of axions particles. The setup involves two tuned vacuum cavities, one with a radio source and one with a radio detector. The two cavities are separated by a lead wall and placed in a very strong magnetic field. At the moment, we are still in the construction phase but we are very close to beginning experimentation. My contribution to the research has mainly involved the construction of the magnet.

### KA 30 *Mississippi State University Axion Search*

(This work is supported by Mississippi State Consortium.)

**Ray, Amy; Dutta, Dipangkar; Gaerlan, Mikhail; Mohanmurthy, Prajwal; Shabestari, Mitra; Riehle, Robertsen;** Mississippi State University, MASS

The Mississippi State Axion Search is a project that is searching for a dark matter candidate, an axion- like particle. A technique known as the “light shining through a wall” is used to search for this particle via the mechanism that two incident photons couple to form an axion which passes through a wall and then decays back into photons on the other side where they are recorded by a detector. The setup of this experiment consists of two vacuum cavities, one containing a strong EM field and the other housing detectors. The project is currently being set up and will soon be ready to record data. We will present an overview of the project, construction and characterization of the integrator electronics, and data acquisition (DAQ) based on National Instrument Lab View.

### KA 31 *The Construction of Mississippi State Axion Search*

(This work is supported by the Mississippi State Consortium)

**Powers, Adam; Dutta, Dipangkar; Riehle, Robertsen; Mohanmurthy, Prajwal;** Mississippi State University, MASS

Axions have been proposed by the Peccei-Quinn theory to be the solution to the strong CP problem. A great deal of the research toward axions has been in narrowing the range of the mass and the coupling constant in which they could be observed. The Mississippi State Axion Search is an exotic particle experiment which uses a light shining through a wall (LSW) technique. The experimental setup consists of two tuned vacuum cavities placed under a very strong magnetic field and separated by a lead wall. While one of the cavities houses a strong radio source, the other (dark) cavity houses the detector systems. Currently, we are piecing together the cavity with the magnets and the wall separating the chambers. The presentation will include a run through of the construction thus far and the purpose of our setup.

### KA 32 *CosmoEJS: Interactive Cosmological Data Fitting Simulations*

**Moldenhauer, Jacob; Engelhardt, Larry; Stone, Keenan; Shuler, Ezekiel;** Francis Marion University

We present a collection of cosmological modeling programs built with Easy Java Simulations for studying the accelerated expansion of the universe (cosmic acceleration). These interactive programs use real-time plotting and fitting of cosmological models with actual experimental data sets. The user can choose multiple models and data surveys to compare to one another at the same time. These programs can be found at <http://www.compadre.org/osp/items/detail.cfm?ID=12406>.

### KA 33 *Core-Collapse Supernova Explosion Mechanisms: SASI vs Neutrino Driven Convection*

(This research was supported by the NSF grant AST-1109113 and used resources of the National Energy Research Scientific Computing Center, which is supported by the Office of Science of the U.S. Dept. of Energy under Contract No. DE-AC02-05CH11123.)

**Handy, Timothy; Plewa, Tomasz;** Florida State University **Odrzywolek, Andrzej;** Jagiellonian University

Despite advances in theory and computer models, the explosion mechanisms in core collapse supernovae (ccSN)

are still under debate. In particular, the reported relative importance of the standing accretion shock instability (SASI), non-SASI turbulent fluctuations, and bulk convective motion due to neutrino heating varies between research groups, with no current consensus.

In this work we offer our own insight into the problem, utilizing an extensive database of 2D and 3D ccSN models tuned to match the energetics of SN 1987A. We propose, implement, and apply novel methods for characterizing the post-bounce evolution of the stellar core. Our analysis focuses on energy transport, convection, morphology of the flow, and statistical properties of fluid motions. We compare the results of our work to those reported by other groups. In particular, we find that our models indicate more vigorous explosions in 3D as compared to 2D for the same neutrino luminosity.

KA 34 *One equation describes galaxy redshift, the Pioneer Anomaly, and the Pound-Rebka experiment*

**Hodge, John**; Blue Ridge Community College

The Scalar Potential Model (SPM) suggests an equation to describe galaxy redshift that has a higher correlation coefficient than the Hubble Law model. The equation was applied to the Pioneer Anomaly (PA) in 2006. The SPM describes all the anomalies of the PA that no other model does. Data analysis in 2011 confirmed predictions of the equation. This paper shows the equation is consistent with the Pound-Rebka experiment result. <http://web.comporium.net/~scjh/>

KA 35 *Spheromak Turbulent Physics Experiment: Initial Physics*

(This work was supported by the Department of Energy.)

**Williams, K.M.**; Florida A&M University **Scime, Earl**; West Virginia University **Thomas, Edward**; Auburn University **Woodruff, Simon**; Woodruff Scientific, STPX

The Spheromak Turbulent Plasma Experiment (STPX) at Florida A & M University came online July 2012. The STPX is dedicated in part to examining turbulence and stability physics in the spheromak environment. Much of the research on STPX will be applied to astrophysical and fusion systems. In addition the STPX will serve as a platform for the design and testing of novel diagnostic techniques. Also, closely coupled modeling and experimentation will take place using the FAMU computational cluster. The STPX device will make use of a number of diagnostic systems that have been developed in partnership with our research collaborators. For this meeting, initial physics and STPX plasma characteristics will be discussed.

KA 36 *Design study for diverging supernova explosion experiment on NIF*

(This research was supported by the DOE grant DE-SC0008823. The research used resources of the National Energy Research Scientific Computing Center, which is supported by the U.S. DOE Office of Science under Contract No. DE-AC02-05CH11123.)

**Flaig, Markus**; **Plewa, Tomasz**; Florida State University **Grosskopf, Michael**; **Keiter, Paul**; **Drake, Paul**; **Kuranz, Carolyn**; University of Michigan **Park, Hye-Sook**; **Remington, Bruce**; Lawrence Livermore National Laboratory

We report on preliminary design simulations for the DivSNRT experiment, which is a spherically-diverging Rayleigh-Taylor experiment scaled to the core-collapse supernova conditions to be carried out at the National Ignition Facility (NIF). The simulations are done in cylindrical geometry, using the block-AMR multi-group radiative diffusion hydrodynamics code CRASH. We assess the sensitivity of the Rayleigh-Taylor instability growth on numerical discretization effects, variations in the laser drive energy and the manufacturing noise at the material interface. We find that for perturbations with well resolved wavelength, the CRASH code is able to account for the effects of the target manufacturing noise as long as its amplitude is larger than a single grid cell. We also explore different designs of the target mount in order to minimize its influence on the Rayleigh-Taylor instability evolution. These results will serve as the basis for more detailed, multi-interface target design optimization studies in the future.

KA 37 *Stratospheric Studies Using High Altitude Ballooning*

**Wood, Dylan; Oelgoetz, Justin;** Austin Peay State University

Stratospheric balloons serve as a relatively inexpensive and simple method to study a unique environment with extremely low temperatures and pressures, far above most of the atmosphere. Such balloons can be used to carry a wide variety of experiments ranging from Geiger counters for cosmic ray studies to simple environmental sounders. Austin Peay State University has built a flight system and conducted an initial high altitude balloon launch to test hardware and design feasibility. Through use of an Automatic Packet Reporting System (APRS) beacon, the first balloon was successfully tracked to a maximum altitude of approximately 95,000 feet and retrieved from its landing zone in rural Wilson County, TN. Subsequent launches are underway and will test on-board data acquisition hardware. Results of analysis of data from the on-board 3-axis accelerometer, 3-axis magnetometer, temperature probe, Global Positioning System (GPS) units, and camera will be presented, along with a sketch of future experimental plans.

KA 38 *Integrated Printed Moisture Sensors in Composite Structures*

**Bermes, Karen; Park, Jin Gyu; Liang, Zhiyong;** Florida State University

Moisture that is present in the ambient environment can break down composite structures, such as boats and aircraft, if they are subject to extended exposure. Therefore, these effects need to be monitored over the lifetime of the structure. We are attempting to do this by producing a moisture sensor that can be integrated into composite structures and have little impact on the structural integrity. To achieve a thin sensor, both printed electronics and nanotechnology were utilized. An open circuit was printed on polyimide (PI) using Ag nanoparticle ink. For some sensors, bucky paper (BP) was laid on top using acetone to flatten it, and on the others carbon nanotube (CNT) ink was printed on top of the Ag printed network. The samples were sintered and testing began in a Controlled Environment Chamber (CEC). We hypothesized that resistance would increase with increasing humidity because the water would impede current in the circuit. This is what occurred in the BP sensors; however the CNT printed sensor displayed the opposite behavior. We are currently looking into why printed materials exhibited opposite behaviors.

KA 39 *Analysis of residual stress in welds using electronic speckle-pattern interferometry (ESPI)*

**Craft, Sean; Ghimire, Bishwas; Thapa, Bidhan; Sasaki, T.; Yoshida, Sanichiro;** None

Residual stress is stress which is locked-in inside of a material and is independent of external load/force. The material under consideration is a welded metal sample consisting of two different constituent metals. In this case, the cause of the residual stress is the fact that the two metals, when cooled down from the high temperatures of the welding process, will contract at different rates and to differing degrees due to a difference in their respective coefficients of linear expansion. Of course, because they are now attached, the metals will try to deform one another, which creates internal forces at the weld site. The technique we will be using to analyze this residual stress is electronic speckle-pattern interferometry (ESPI). In unrelated experiments, ESPI has been successfully utilized to show areas of concentrated stress when external forces are applied to a sample metal. Our conjecture is that it can also be used to analyze the areas where residual stress is located within a sample such as that described above. Our method of analysis is based on the following hypothesis: if a slight tensile force is applied to the welded sample perpendicular to the weld, this will cause the sample to contract parallel to the weld. Near the weld site, on one side of the weld, the sample will resist this deformation, due to the fact that it is already deformed in this direction by the residual stress. And conversely, on the other side of the weld, the sample should welcome this deformation.

KA 40 *Measurement and Analysis of C<sub>2</sub> Swan Spectra Following Breakdown of Nitro Compound Simulants*

**Witte, M.; Parigger, C.G.;** University of Tennessee Space Institute **Bullock, N.A.; Merten, J.A.; Allen, S.D.;** Arkansas State University

Recent measurements of micro-plasma following laser-induced optical breakdown on 3-nitrobenzoic acid show well developed molecular spectra during the first several hundreds of nanoseconds. Analysis of Carbon Swan spectra for well-above breakdown threshold energy/pulse is accomplished using an accurate line strength file.

Moreover, presence of hydrogen-beta allows us to infer electron density in the plasma evolution. Computational challenges include accounting for background variation and appropriate modeling of hydrogen embedded in molecular spectra. Recorded and computed spectra agree nicely for time delays on the order of 1600 ns from optical breakdown when using a single temperature for local thermodynamic equilibrium plasma.

*KA 41 Self-absorption of hydrogen Balmer lines in laser induced plasma.*

**Rezaee, M.R.;** University of Tennessee **Parigger, C.G.;** University of Tennessee Space Institute

In the study of self-absorption phenomena in laser-induced hydrogen plasma we focus on  $H_\alpha$ ,  $H_\beta$  and  $H_\gamma$  of the Balmer series. Broadened line profiles, shifts and line intensity ratios are commonly measured for plasma characterization and diagnostics in laboratory scale micro-plasma, for example, laser-induced plasma but are also measured to explore inductively coupled plasma and extraterrestrial plasma. One can infer the electron density and plasma temperature from measured spectra. Accurate diagnostics is important for applications in magnetically confined plasma devices as well as in quantitative laser-induced breakdown spectroscopy. Moreover, stability of plasma in Tokamak chambers is a function of electron density and temperature, and optical spectroscopy is utilized to find these values. Self-absorption however can cause extra broadening and distortion in line profiles. Here we present results that reveal evidence of self-absorption in  $H_\alpha$ . We compare the electron density obtained from  $H_\alpha$  with the ones obtained from  $H_\beta$  and  $H_\gamma$ , and we also discuss the determination of temperature from Balmer Series lines.

*KA 42 Acquisition and Analysis of Titanium Monoxide Spectra in Plasma*

**Woods, A.C.;** **Parigger, C.G.;** University of Tennessee Space Institute

The recent use of titania ( $TiO_2$ ) nanoparticles for thin-film production has raised interest in the environment and properties of Ti containing particles in plasma. As a precursor to  $TiO_2$  in rapidly cooling plasma, the titanium monoxide ( $TiO$ ) molecule provides insight into the environment in which  $TiO_2$  nanoparticles are produced. The spectral transitions of the  $TiO$  molecule have long been studied and observed by astronomers. We discuss our efforts in the calculation of predicted spectra for the  $TiO$   $\gamma$  ( $A^3\Phi - X^3\Delta$ ),  $\gamma'$  ( $B^3\Pi - X^3\Delta$ ), and E-X  $\Delta v=0$  transitions as well as laser-induced breakdown spectroscopy (LIBS) as a technique for collecting time-resolved spectra. By nonlinear fitting to  $TiO$  molecular transitions measured in laser-induced plasma, computed spectra are used to infer the temperature of the observed  $TiO$ .

*KA 43 Investigation Into The Design Of An Accelerator Drive Reactor*

**Jones, Daniel;** **Womble, Phillip;** Western Kentucky University

Using the Monte Carlo N Particle (MCNP-4C2) code, we attempted to simulate an accelerator driven reactor that did not employ any highly enriched nuclear materials and used only high Z materials as reflector/moderators. We will discuss the results of a "toy model" that we created using Th, Pb, and U. Using a rectangular parallel-piped design, 55 MeV neutrons impinged upon a plate of  $^{232}Th$  to create fission neutrons. The fission neutrons out of the  $^{232}Th$  plate were moderated to energies around 1 MeV. These slower neutrons were introduced into a mass of fissionable material (such as  $^{235}U$ ) where the primary criticality would occur. We calculated the relative neutron yield from each section and investigated the practicality of a Pb neutron reflector assembly.

*KA 44 Characterization of adhesion mechanism of thin-film systems using two independent, but correlating techniques*

**Ghimire, Bishwas;** **Adhikari, Sushovit;** **Yoshida, Sanichiro;** **Kabza, Konrad;** Southeastern Louisiana University

Adhesion strength of thin-films to the substrate has been studied using two methods. The first is characterization of dynamic behavior of the film relative to the substrate surface based on an opto-acoustic technique. The thin-film specimen is configured as an end-mirror of a Michelson interferometer, and oscillated from the rear with an acoustic transducer. The resultant film surface displacement relative to the substrate is evaluated from the fringe shift of interference pattern behind the beam splitter. The second is surface energy analysis based on Young's contact angle measurement. Small drops of solutions with various surface tensions are placed on the substrate surface. The contact angle of each drop is measured, and its cosine is plotted as a function of the surface tension. The surface energy of the substrate is estimated through extrapolation of the plot to the zero-surface tension

limit. These methods have been applied to pairs of thin-film specimens of the same film (Au, Pt) and substrate material (Si) prepared with different pre-coating surface conditions (plasma-treated and untreated). The two methods show clear correlation indicating that the plasma-treatment strengthens the adhesion.

#### KA 45 *A Spontaneous Parametric Downconversion Source for Tests of Single Photon Quantum Mechanics*

**Smith, R. Seth**; Francis Marion University

During the spontaneous parametric downconversion process, a single photon of one frequency is converted into two photons of lower frequency in a nonlinear crystal. The input wave is referred to as the “pump” and the output waves are referred to as the “signal” and “idler”. The process is said to be “spontaneous” because there are no input signal or idler fields. Rather, these fields are generated spontaneously inside the nonlinear crystal. The process is “parametric” because it depends on the electric fields, rather than just their intensities. This creates a definite phase relationship between the input and output fields. It is called “downconversion” because the signal and idler fields are at a lower frequency than the pump field. The setup, operation, and performance of a spontaneous parametric downconversion source will be described, as well as future applications of this source for tests of single photon quantum mechanics.

#### KA 46 *Determining optical properties of black carbon by integrating cavity ring-down spectroscopy and nephelometry*

(We acknowledge support from the Department of Defense under grant #W911NF-11-1-0188.)

**Tedela, Getachew; Singh, Sujeta; Fiddler, Marc; Bililign, Solomon**; North Carolina Agricultural and Technical State University

Accurate measurement of optical properties of aerosols is crucial for quantifying the influence of aerosols on climate. Aerosols that scatter and absorb radiation can have a cooling or warming effect depending on the magnitude of the respective scattering and absorption terms. One example is black carbon known for its strong absorption. The reported refractive indices for black carbon particles, range from  $1.2+0i$  to  $2.75+1.44i$ . Our work attempts to measure extinction coefficient, and scattering coefficient of black carbon particles at different incident beam wavelengths using a cavity ring-down spectrometer and a Nephelometer and compare to Mie theory predictions. We report calibration results using polystyrene latex spheres and preliminary results on using commercial black carbon particles.

#### KA 47 *Spectroscopy of Aluminum Monoxide in Flames*

**Surmick, D.M.; Woods, A.C.; Parigger, C.G.**; University of Tennessee Space Institute **Height, J.; Donaldson, A.B.; Gill, W.**; Sandia National Laboratories\*

Application of optical spectroscopy is discussed in studies of combustion phenomena. Here we present recent experimental results from flame pool measurements. Analysis is accomplished using accurate line strength files. One of the goals of the current study is to infer temperature of combusting aluminum particles from the  $B^2\Sigma^+ \rightarrow X^2\Sigma^+$  transition of aluminum monoxide (AlO). An indicator of aluminum combustion is presence of AlO bands. The temperature of the flame for various positions is determined by fitting measured with computed spectra. Moreover, the background radiation is modeled using grey-body rather than standard black-body emissions. Computational efforts include comparisons of results from fitting diatomic AlO with results from fitting broadband background emissions.

\*Sandia is a multiprogram laboratory operated by Sandia Corporation, a Lockheed Martin Company, for the United States Department of Energy’s National Nuclear Security Administration under contract DEAC0494AL85000.

#### KA 48 *DNA electrophoresis in tri-block copolymer gels*

**Wei, Ling; Van Winkle, David**; Florida State University

Double-stranded DNA ladders were first separated in conventional agarose gel at room temperature. The lanes of well-separated DNA ladders in agarose were cut and trimmed before transferring to Pluronic<sup>®</sup> F 127, which is a triblock copolymer forming a gel-like phase of micelles arranged with cubic order at room temperature with

concentrations higher than 18%. The electrophoresis in F 127 was performed with the electric field perpendicular to the separation direction in agarose. A 10 bp DNA ladder consisting of 10 base pair repeats (10 bp-330 bp), 25 bp DNA ladder consisting of 19 blunt fragments ranging in length from 25 bp-450 bp (at 25 bp increments) plus a 500 bp band, and 250 bp DNA ladder consisting of 14 blunt fragments ranging in length from 250 bp-3500 bp (at 250 bp increments), were used as samples for this two dimensional gel electrophoresis. The continuously decreasing mobility with increasing length observed in the agarose separation is not duplicated in the Pluronic<sup>®</sup> F 127 separation. Rather, a complicated dependence of mobility on DNA length is observed whereby 100 – 125 bp fragments have the highest mobility and there is also a variation of mobility with length correlated to the micelle diameter.

*KA 49 An Investigation of Surface-Plasmon Mediated Emission from Functionalized Zinc Oxide Nanowires*

**Mayo, Daniel**; Vanderbilt University **Mu, Richard**; Fisk University **Haglund, Richard**; Vanderbilt University  
The exciton-plasmon coupling mechanisms responsible for enhancing photoluminescence in a three-dimensional, metal-coated ZnO nanowire architecture are examined using an insulating MgO interlayer. Vertically-oriented ZnO nanowires are grown by a modified vapor-solid method inside a vertical furnace. The sides of the nanowires are then coated with MgO and functionalized with Ag nanoparticles via electron-beam evaporation using a glancing-angle deposition apparatus. By varying the thickness of the MgO spacer layer, it is possible to elucidate the exciton-plasmon coupling mechanisms that mediate ZnO photoluminescence. For the visible emission, strong quenching occurs independent of the MgO thickness. In contrast, the band-edge emission displayed an enhancement factor of 20 as the nominal thickness of the MgO spacer was increased from 10 to 60 nm.

*KA 50 Nonlinear Plasmonics of Gold Nanospirals*

**Davidson, II, Roderick B.**; **Ziegler, Jed I.**; Vanderbilt University **Vargas, Guillermo**; Prairie View A&M University **Haglund, Richard**; Vanderbilt University

Archimedean nanospirals have been shown to have complex optical interactions characterized by wavelength- and polarization-sensitive intraparticle resonances. Due to their lack of any axis of inversion symmetry, nanospirals should also exhibit highly nonlinear behavior, such as second- and third-harmonic generation. The gold nanospirals in these experiments were created using electron beam lithography; the  $4\pi$  nanospirals have overall dimensions below 500 nm. The characteristic angular dependence of second harmonic emission (SHG) as a function of polarization angle is observed for linearly polarized light. The differences in SHG emission using linear and circular polarized excitation are also explored. Through these measurements we will characterize the strength of the second-order nonlinearity of the gold nanospirals relative to GaAs calibration materials. These measurements characterize an efficient second order non linear nanoparticle that does not have to meet the phase matching requirements of nonlinear crystals.

*KA 51 Cavity Perturbation Technique: The Effects of Crystal Size on the EPR Spectra of Fe8*

(This work is supported by the National Science Foundation (grant no. DMR-0804408). Work performed at the National High Magnetic Field Laboratory is supported by NSF Cooperative Agreement No. DMR-0654118 and by the State of Florida)

**Shiddiq, Muhandis**; **Liu, Junjie**; **Beedle, C.C.**; **Hill, S.**; National High Magnetic Field Laboratory, Florida State University

The Cavity Perturbation Technique (CPT) is a contact-free technique that measures the change of the characteristics of a cavity resonator upon the introduction of a foreign body (the sample under investigation). In this experiment, we study the effect of crystal size with regards to the CPT transmission spectra for single crystals of the single-molecule magnet Fe8. We have found that the frequency shift and transmission suppression become larger when the size of the sample is increased, suggesting a classical coupling between the Fe8 crystal and the resonator. From cavity perturbation theory, these phenomena may be explained by the following classical formula:  $\Delta\omega/\omega = -\beta\chi$ , where  $\omega$  is the complex frequency,  $\beta$  is the filling factor that depends on the sample volume and the resonant mode of the cavity, and  $\chi$  is the complex susceptibility.

#### KA 52 Tailoring electronic properties of SnO<sub>2</sub> nanobelts via thermal annealing

(References: [1] Yi Cheng et al., Appl. Phys. Lett. 89, 093114 (2006). [2] Yi Cheng et al., Nano Lett. 8, 4179-4184 (2008). [3] Yi Cheng et al., Biosensors and Bioelectronics 26, 4538-4544 (2011).)

**Barreda, Jorge; Keiper, Timothy; Kim, Joon-II; Xiong, Peng;** Florida State University **Zheng, Jim P.;** Florida A & M, Florida State University

Nanostructures of semiconducting metal oxides display many desirable characteristics for nano-electronics and sensing applications. Nanobelts (NBs) of SnO<sub>2</sub> have been synthesized using catalyst-free chemical vapor deposition of SnO powder. Channel-limited field-effect transistors (FETs) have been produced from the NBs and their use as effective gas [1], pH [2], and protein [3] sensors has been demonstrated. We investigate the control and optimization of the electronic properties of the NBs for biosensing applications by varying the oxygen stoichiometry via thermal annealing in oxygen and vacuum. Annealing our NBs in O<sub>2</sub> environment at 800°C for 2hrs prior to the FET fabrication produces devices with conductance in the range of millisiemens, suggesting an increase in oxygen vacancies. Subsequent vacuum annealing allows tuning of the conductivity of the NBs. We demonstrate significant modulation of the current through the FET channel with an applied backgate voltage, indicating our devices are acceptable candidates for sensing charged biomolecules. Silane chemistry is used for the selective biofunctionalization of the NB-FETs. Antibody-antigen binding is detected by a change in the NB conductance after exposure to an analyte containing the specific antigen.

#### KA 53 Novel Sensor Design based on Switchable Electromagnetic-Induced Transparency

**McGahan, Christina; Appavoo, Kannatassen;** Vanderbilt University **Shapera, Ethan Paul;** University of Cambridge **Haglund, Richard;** Vanderbilt University

We can increase detector sensitivity past that of conventional surface plasmon resonance (SPR) detectors by changing the local dielectric environment. Here we demonstrate a novel sensor design that combines SPR detection with a phase-changing element to increase detector sensitivity. Vanadium dioxide (VO<sub>2</sub>) modulates the near-field dielectric environment of the electromagnetically induced transparency (EIT) nanostructures via its insulator-to-metal transition, which shifts the nanostructures' plasmonic response. We obtain a sensor design using three-dimensional, finite-difference time-domain (FDTD) simulations to optimize the dimensions of a gold pi nanostructure exhibiting EIT due to its dipole-quadrupole interaction. To verify our simulations, we use electron-beam lithography to fabricate arrays of optimal structures on VO<sub>2</sub> films deposited on ITO covered glass by pulsed laser deposition or electron-beam evaporation. We tune the EIT by varying the dimensions of the pi structures, thus changing the strength of the dipole-quadrupole interaction. The resonance of the structures of different separation distances is experimentally verified through measuring broadband white-light transmission while the VO<sub>2</sub> is thermally modulated.

#### KA 54 Iron Nanoparticle Mössbauer Spectroscopy with Rare-Earth Permanent Magnets

**Swafford, L.D.; Parigger, C.G.; Hah, Hien-Yoong; Gray, S.; Cole, M.; Warnberg, D.; Johnson, C.E.; Johnson, J.A.;** University of Tennessee Space Institute **Shafranovsky, E.;** Russian Academy of Sciences

Properties of materials can be determined with a high degree of precision from Mössbauer spectra. Due to the recoil energy of free particles, Mössbauer spectroscopy is useful when the atoms are contained in a lattice structure. Resonance with the nucleus is achieved using gamma radiation. The Doppler effect is utilized by oscillating the radiation source thus modulating the energy of the gamma radiation. The recorded spectra show hyperfine splitting with intensities that depend on the angle of the gamma radiation with respect to the nuclear spin moment. For ferri- and ferro-magnets, the orientation of the magnetization and strength of the applied field can be inferred. For most paramagnets the magnetic susceptibility is on the order of 10<sup>-6</sup>, and application of Mössbauer spectroscopy requires low (a few Kelvin) temperature and large (a few Tesla) magnetic fields that are usually generated with superconducting magnets. However, for single-domain nanoparticles, or superparamagnets, with susceptibility on the order of 10<sup>-1</sup> to 10<sup>-2</sup>, a sizeable magnetization can be produced at room temperature in 1 Tesla fields. Such magnetic fields are obtainable with Nd-Fe-B permanent magnets. We present results of recent measurements on nanoparticles of iron.



#### KA 55 Upper Critical Fields in Nb/Ni Bilayers

**Davis, Emily; Ahrenholz, Timothy; Broussard, Phillip;** Covenant College

We studied the upper critical fields ( $H_{c2}$ ) of Nb/Ni bilayers. These bilayers had a constant Nb thickness of 33 nm, and the Ni thicknesses varied from 0-7 nm. For each sample, we took resistive measurements of the superconducting transition under fields ranging from 0-4360 G. From these measurements, we obtained the upper critical field slopes ( $H'_{c2}$ ) of each sample. The  $H'_{c2}$  of a simple Nb layer was 3710 G/K, while the  $H'_{c2}$  values for the bilayers ranged randomly from 4650-6840 G/K. While the critical temperatures ( $T_c$ ) of the samples seemed to exhibit a particular non-monotonic pattern as a function of Ni thickness (due to proximity effect), the  $H'_{c2}$  values as a function of Ni thickness formed no such clear pattern. We also analyzed the curvature of the  $H$  vs.  $T_c$  plots for each sample. Most of the plots were linear at lower applied fields, but many showed either positive or negative curvature as we applied higher fields. This curvature began anywhere between 2000 and 4000 G. Generally, bilayers with thinner Ni layers produced  $H$  vs.  $T_c$  plots with negative curvature, and bilayers with thicker Ni layers produced plots with positive curvature.

#### KA 56 Modeling time-dependent upconversion in Er-Yb doped sol-gel silicate glass

**Onken, Drew; Hampton, D.G.; Trennepohl, C.J.; Boye, D.M.; Silversmith, A.J.;** Davidson College

Examining pulsed IR to visible upconversion in  $\text{Er}^{3+}$ - $\text{Yb}^{3+}$  doped sol-gel silicate glass may lead to applications in fiber optic communication due to the similar time scale of its GHz bandwidth. Excited state absorption of  $\text{Er}^{3+}$  accompanying energy transfer from neighboring  $\text{Er}^{3+}$  and  $\text{Yb}^{3+}$  is responsible for the upconversion process. The dynamics of  $\text{Yb}^{3+}$  to  $\text{Er}^{3+}$  energy transfer are studied by observing green emission from the  $^4\text{F}_{7/2}$  and  $^4\text{S}_{3/2}$  levels of  $\text{Er}^{3+}$  after a 6-ns pulsed laser excitation of the  $^2\text{F}_{5/2}$  level of  $\text{Yb}^{3+}$  at 978nm. This study examines the time-dependence of the fluorescence emission by varying the  $\text{Yb}^{3+}$  concentrations and the annealing temperature. Our previous work has shown that the rare earth ions reside on the pore surface, and so the nanoporous nature of the sol-gel glass creates a finite reservoir of energy donors in each pore. These finite energy reservoirs foil the application of standard rate equation models and instead necessitate Monte Carlo simulations which can be used to determine the physical parameters of each energy transfer step in the upconversion chain.

#### KA 57 Spectral Selectivity of Photoinduced Effects in $\text{As}_x\text{S}_{100-x}$ Glass Thin Films

**York-Winegar, James;** Austin Peay State University **Pálka, Karel; Vlček, Miroslav;** University of Pardubice **Oelgoetz, Justin; Kovalskiy, Andriy;** Austin Peay State University

Spectral dependence of photoinduced effects in  $\text{As}_x\text{S}_{100-x}$  ( $x = 30, 35, 40$ ) amorphous thin films were studied using Raman spectroscopy, atomic force microscopy (AFM), and ellipsometry. Samples were exposed to LED light in an argon environment to avoid oxidation on the surface layer. AFM measurements reveal that our samples are of optical quality before and after exposure, allowing for application of these thin films. Ellipsometry was used measure exact penetration depths using the Beer-Lambert law. For all investigated compositions the Raman spectra taken after 375 and 405 nm exposures do not differ noticeably. The same conclusion holds for samples exposed to 450 and 525 nm light, however these two sets experienced different structural transformations. Irradiation of the virgin samples causes photopolymerization effect and significant widening of the vibrational bands. For stoichiometric comparison ( $x = 40$ ) the lower ratio between  $\text{As}_4\text{S}_3$  cages and  $\text{As}_4\text{S}_4$  units is observed for UV exposed sample in comparison with irradiated by band gap light. For all exposure wavelength there is also no evidence for S chains and  $\text{S}_8$  fragments after irradiation. Theoretical calculations using density functional theory are currently underway.

#### KA 58 Synthesizing and Size-Characteristics of Ferrofluids

**Maheswaranathan, Ponn; Talbert, Justin;** Winthrop University

Ferrofluids are colloidal suspension of magnetic nanoparticles (10-100 nm) utilized in various applications for their unique magnetic and thermodynamic properties. Ferrofluids contain magnetite ( $\text{Fe (II, III)}_3\text{O}_4$  or iron (II, III) oxide), a surfactant, and, in some cases a carrier. All traditional ferrofluid syntheses include a surfactant and establish that the surfactants play a significant role in their properties. In ferrofluid syntheses, a carrier is

not always utilized and its role is not clearly investigated. In the presence of a magnetic field, the ferrofluid reacts to the magnetic field by creating “spikes” of different shapes which depends on the size of the magnetite particles. For this to occur, the magnetite particles must be around ten nanometers in diameter. Therefore, the size of magnetite particles created during synthesis determines the extent of the ferrofluid’s magnetic and thermodynamic properties. In this research, ferrofluids were synthesized using different surfactants and carriers. In addition, how the size of magnetite particles affect the ferrofluid’s magnetic and thermodynamic properties were analyzed. Preliminary results show that ferrofluids can be synthesized using various methods but the magnetic properties are not the same in each synthesis. Carriers were found to thin out the ferrofluid and provide a medium that creates less friction so that the ferrofluid can move around easier when a magnetic field is applied. Techniques like scanning (SEM) and transmission (TEM) electron microscopy and powder x-ray diffraction (XRD) were utilized to determine magnetite particle size.

*KA 59 Mechanochemical Synthesis of ZnFe<sub>2</sub>O<sub>4</sub> as a Function of “Ball to Powder Ratio” (BPR)*

**Cabarcas, Jari; Chavez, Ermides; Babilonia, Yari;** Universidad de Puerto Rico **Uwakweh, Oswald;** Recinto Universitario de Mayagüez

Mechanochemical reactions of ZnO and  $\alpha$ -Fe<sub>2</sub>O<sub>3</sub> were carried out in a planetary mill to produce zinc ferrite (ZnFe<sub>2</sub>O<sub>4</sub>) nanocrystallites at room temperature by using a “ball to powder ratio” (BPR) of 20:1 and 40:1, under identical processing conditions entailing initial addition of 0.6 mL of acetone as surfactant with hardened stainless steel grinding materials. The average crystal sizes of the particles as determined from X-ray diffraction measurements varied as a function of milling time, with the value of 7.36 nm achieved for the 35 hours milled materials. The diffraction peaks of the milled samples are broadened, which can be the result of the reduced grain size and the atomic level strain introduced during milling. The development of superparamagnetic behavior of the particles is confirmed by the presence of a central peak in the Mössbauer spectra for 50h and 10h corresponding to BPR= 20:1 and BPR=40:1 respectively. This result has been explained on the basis that at a high BPR, the collision energy is high and therefore leads to enhanced reduction in crystal size and the chemical reaction to single phase ZnFe<sub>2</sub>O<sub>4</sub> having the particle size dependent superparamagnetic behavior.

*KA 60 Stoichiometry of Fe<sub>3</sub>O<sub>4</sub> Nanoparticles Determined by Mössbauer Spectroscopy*

**Hah, Hien-Yoong; Cole, M.; Gray, S.; Johnson, Charles; Johnson, Jacqueline;** The University of Tennessee Space Institute **Kolesnichenko, Vladimir; Kucheryavy, Pavel; Goloverda, Galina;** Xavier University of Louisiana  
The detailed composition of nanoparticles is dependent on the method of preparation. Previous Mössbauer studies of Fe<sub>3</sub>O<sub>4</sub> nanoparticles have shown that the samples were not pure Fe<sub>3</sub>O<sub>4</sub>. In most cases they were  $\gamma$ -Fe<sub>2</sub>O<sub>3</sub>, which has the same spinel structure as Fe<sub>3</sub>O<sub>4</sub> but with the Fe<sup>2+</sup> ions oxidized to Fe<sup>3+</sup> and vacancies to ensure charge neutrality. In other cases the oxidation was incomplete and the structure contained defects on the octahedral (B) sites. In this work the samples of diameters 5.3 and 10.6 nm were prepared from colloidal magnetite in diethylene glycol under an inert atmosphere. The Mössbauer spectra showed that they are superparamagnetic with blocking temperatures, T<sub>B</sub>, of 50 K and 120 K respectively. The spectra at 6 K, the lowest temperature studied, were close to those of bulk crystalline Fe<sub>3</sub>O<sub>4</sub>, in particular showing lines due to Fe<sup>2+</sup> which were absent in many previous studies.

*KA 61 Ytterbium-doped Barium Zirconate Thin Films by Pulsed Laser Deposition for Intermediate Temperature Solid Oxide Fuel Cell Applications*

**Camata, Enrico; Skinner, Alex; Remington, Eric; Camata, Renato;** University of Alabama at Birmingham  
Ytterbium-doped barium zirconate (BZYb) is predicted to have high protonic conductivity and good potential as a thin-film electrolyte material for intermediate temperature (500-750° C) solid oxide fuel cells. We have synthesized BZYb thin films by pulsed laser deposition using ablation targets prepared by mixing barium zirconate (BaZrO<sub>3</sub>) and ytterbium oxide (Yb<sub>2</sub>O<sub>3</sub>) powders. Powders had their masses varied to produce targets with 5, 10, and 15 mol.% of Yb in BaZrO<sub>3</sub>. Targets were pressed at 2800 psi and annealed at 1200° C for 12 hours in air. Thin films 1-2  $\mu$ m thick were deposited on Si and MgO substrates at 600° C using a KrF excimer laser with energy density of 1-2 J/cm<sup>2</sup> and repetition rate of 30 Hz. Deposition took place at a pressure of 50 mTorr of O<sub>2</sub>

in a vacuum system with base pressure below  $5.0 \times 10^{-7}$  Torr. X-ray diffraction from as-deposited films show patterns of polycrystalline cubic  $\text{BaZrO}_3$  on both, Si and MgO substrates. A substantial amount of amorphous material is present in as-deposited samples. Post-deposition annealing in air at  $800^\circ\text{C}$  greatly improves film crystallinity with virtual elimination of the amorphous phase. Energy dispersive X-ray measurements indicate the successful incorporation of Yb in the films in concentrations of 3.1, 5.5, and 8.8 mol.% for targets prepared with 5, 10, and 15 mol.% of Yb, respectively.

#### KA 62 *Effects of Geographical Shape on Power Grid Intentional Islanding Models*

**Gurfinkel, Aleks; Xu, Yan; Rikvold, Per Arne;** Florida State University

Power grids are interconnected networks of generators and loads that are susceptible to rolling blackouts cascading across the system. To contain the spread of power failures, the *intentional islanding* technique deactivates certain electrical connections, partitioning the power grid into temporarily disconnected clusters with the capacity to act as independent power grids with local generating capacity. Optimized choices of intentional islanding clusters for networks of a given topology (pattern of edges) can be found with the application of network theory. We employ a simulated annealing Monte Carlo method to maximize the internal connectivity of the clusters while minimizing the variance of their power surplus. To serve as test cases in the development of adaptable islanding procedures, it is useful to generate large numbers of randomized power grid networks possessing the topological and statistical properties of real power grids. An important factor affecting the topological structure of power grid networks is the geographical shape of the territory in which the network is embedded. In this poster, we compare the success of intentional islanding for models of long, thin geometries (exemplified by the Florida power grid) and geometries with a square aspect ratio.

#### KA 63 *Domain Coarsening on the Hyperbolic Plane*

**Raffield, Jesse;** Florida State University **Richards, Howard;** Marshall University **Rikvold, Per Arne;** Florida State University

In statistical physics, the Ising model is used to study systems that vary in application from sociology to condensed matter. With such a rich diversity of use, it has become one of the most studied interacting models. One of its less studied, but also very rich, variations is that of an Ising model that is embedded in the hyperbolic plane. The motivation for this study is to cast light on how systems of negative curvature behave; examples of such are coral growth and the propagation of the internet. The primary characteristic of the hyperbolic Ising model that we seek to study, is the action of domain coarsening using conserved-order-parameter dynamics. That is to say, we are in search of an exponent that determines the behavior of domain coarsening in the hyperbolic plane. Just as a Euclidean lattice requires a Euclidean metric, so too does a hyperbolic lattice require a proper metric of its own. To this end, two such representations are employed; the first is based in graph theory and is known as the “taxi-cab” metric while the second involves gyro-vectors and analytical geometry. Using Monte-Carlo simulations in conjunction with each geometrical basis, the domain coarsening exponent is estimated to a reasonable degree and is found to be smaller than its Euclidean counterpart.

#### KA 64 *Computational study of the ZGB model with a long-range interaction*

(Supported in part by NSF DMR-1104829.)

**Chan, Chor-Hoi; Rikvold, Per Arne;** Florida State University

The Ziff-Gulari-Barshad (ZGB) model is widely used to study the oxidation of carbon monoxide (CO) on a catalyst surface. The model exhibits a non-equilibrium, discontinuous phase transition between a reactive and a CO poisoned phase. If one allows a nonzero rate of CO desorption ( $k$ ), the line of phase transitions is terminated at a critical point ( $k_c$ ). In this work, instead of restricting the CO and atomic oxygen (O) to react only when they are absorbed in close proximity, we consider a theoretical model that allows CO and O atoms adsorbed far apart on the lattice to react to form carbon dioxide ( $\text{CO}_2$ ). We employ Monte Carlo simulations to study changes in the physical properties of the system, especially the universality class of the critical point. Through this study we hope to gain further understanding of the ways that a long-range interaction can affect an originally short-range interacting non-equilibrium system.

### KA 65 *What's in Your Wineglass*

**Woolbright, Stephen; Schelp, Rich;** Erskine College

You probably have done the trick of rubbing the rim of a wineglass, partially filled with water, to produce a crisp tone. We took this old instrument and applied a new question: What would happen to the frequency if we used liquids with different densities? A.P. French constructed a wineglass model which predicts that  $(f_0/f)^2 = 1 + kF^4$ , where  $f_0$  is the frequency of the empty wineglass,  $F$  is the wineglass fullness fraction,  $f$  is the frequency at that fullness fraction, and  $k$  is a constant that is proportional to the density of the liquid [1]. We addressed this question experimentally using five liquids with densities varying from  $0.7 - 1.4 \text{ g/cm}^3$ . To determine how the frequency changed, we filled a wineglass to several different heights for each liquid. At each height, we made a digital recording of the sound produced and used FFT analysis software to determine its frequency. Our results show that the denser a liquid is the lower the frequency of the sound the wineglass produces. The results also confirm that A.P. French's model correctly predicts the relationship between frequency and density.

[1] A.P. French, *In Vino Veritas: A Study of Wineglass Acoustics*, Am. J. Phys. 51, 8 (1983).

### KA 66 *Angular Momentum Flux in the Scalar Self-Force Problem*

**Cupp, Samuel;** Austin Peay State University **Diener, Peter;** Louisiana State University

The scalar self-force problem consists of a scalar point charge orbiting a supermassive black hole. The object is small enough that the perturbation of space-time due to its mass is inconsequential, and the only forces are gravity and the self-force. The self-force is a force on the inspiraling particle that results from the back-scattering of the object's own field off of curved space-time. I derived an accurate calculation of the angular momentum flux for the scalar self-force problem and implemented it into a preexisting (3 spatial +1 time) dimensional code. We then compared our results to very precise frequency domain calculations. The angular momentum flux calculations yield results that converge to the actual value of  $0.0124682173 M^2$ . However, the calculations currently converge at about .7 order, and the reason for this extremely slow convergence is currently unknown.

### KA 67 *Exclusive semileptonic B meson decays at Belle*

**Wang, Xiao Long;** Virginia Tech, Belle

I will report on the results from the Belle experiment on exclusive and inclusive  $B$  meson semileptonic decays to charmed mesons as a probe of the CKM matrix element  $|V_{cb}|$ . The exclusive modes include  $B \rightarrow D_s^{(*)} \ell \nu$ . The discrepancy between the inclusive and sum-of-exclusive branching fractions will be reviewed.

### KA 68 *The Belle II Experiment at SuperKEKB*

**Wang, Xiao Long;** Virginia Tech, Belle II

I will describe the Belle II experiment and the SuperKEKB project under construction at the High Energy Accelerator Research Organization (KEK) in Japan. At this next-generation flavor factory, the Belle II detector will collect about 50 times more data than Belle, i.e., about  $50 \text{ ab}^{-1}$ . This data set will permit us to search for evidence of new interactions and particles and to make more precise measurements of Standard Model properties such as  $CP$  asymmetries in the decays of heavy mesons and leptons, including missing-energy decay modes such as  $B \rightarrow \tau \nu$  that are inaccessible to the LHC experiments.

### KA 69 *True Neutrality as a New Type of Flavour*

**Sharafiddinov, Rasulkhodzha;** Uzbekistan Academy of Sciences

A classification of leptonic currents with respect to C-operation requires the separation of elementary particles into the two classes of vector C-even and axial-vector C-odd character. Their nature has been created so that to each type of lepton corresponds a kind of neutrino. Such pairs are united in families of a different C-parity. Unlike the neutrino of a vector type, any C-noninvariant Dirac neutrino must have his Majorana neutrino. They constitute the purely neutrino families. We discuss the nature of a corresponding mechanism responsible for the availability in all types of axial-vector particles of a kind of flavour which distinguishes each of them from others by a true charge characterized by a quantum number conserved at the interactions between the C-odd fermion and the field of emission of the corresponding types of gauge bosons. This regularity expresses the

unidenticality of truly neutral neutrino and antineutrino. Thereby, such a true flavour together with the earlier known lepton flavour predicts the existence of leptonic strings and their birth in single and double beta decays as a unity of symmetry laws.

---

## SESSION LB: Condensed Matter Physics II

08:30 Saturday Morning

Salon AB

Chair: Laurie McNeil, University of North Carolina - Chapel Hill

08:30 LB 01 *Heatless Motive Force for Producing Grid Turbulence in Liquid Helium near Absolute Zero*

(We thank W.F. Vinen for many useful discussions. Work supported in part by US NSF DMR #0602778 and #1007937 and UK EPSRC Grants No. EP/H04762X/1 and EP/I003738/1.)

**Ihas, Gary; Thompson, Kyle; Chapurin, Roman;** University of Florida **Munday, Lydia;** Lancaster University **Labbe, Greg;** University of Florida **McClintock, Peter;** Lancaster University

Flow through a grid is a standard method to produce isotropic, homogeneous turbulence for laboratory study. This technique has been used to generate quantum turbulence (QT) above 1 K in superfluid helium, (S. R. Stalp, L. Skrbek, and R. J. Donnelly, *Phys. Rev. Lett.* **82**, 4831 (1999).) where QT seems to mimic classical turbulence. Efforts have been made recently (G. G. Ihas, G. Labbe, S-c. Liu, and K. J. Thompson, *J. Low Temp. Phys.* **150**, 384 (2008).) to make similar measurements near absolute zero, where there is an almost total absence of normal fluid and hence classical viscosity. This presents the difficulty that most motive force devices produce heat which overwhelms the phenomena being investigated. The process of designing and implementing a “dissipation-free” motor for pulling a grid through superfluid helium at millikelvin temperatures has resulted in the development of new techniques which have broad application in low temperature research. Some of these, such as Meissner-effect magnetic drives, capacitive and inductive position sensors, and magnetic centering devices (bearings) will be described.

08:42 LB 02 *The Design and Testing of a Device to Limit Superfluid Helium Film Flow*

(Work supported by DOE Grant No. DE-FG02-97ER41041 and a contract from Oak Ridge National Laboratory.)

**Haase, David G.; Frame, Dillon K.; Rowland, James R.;** North Carolina State University

A proposed new measurement of the electric dipole moment of the neutron (the nEDM project) uses a volume of superfluid liquid  $^4\text{He}$  to trap neutrons from the Spallation Neutron Source as ultracold neutrons. Polarized  $^3\text{He}$  atoms dissolved in the liquid serve as a co-magnetometer. The measurement process will require the distillation of  $10^{-10}$  concentrations of depolarized  $^3\text{He}$  from liquid  $^4\text{He}$ . Unfortunately, a superfluid  $^4\text{He}$  film flows up the walls of its container where it eventually evaporates and would overwhelm the  $^3\text{He}$  vapor removal. Following a design employed by NASA on the cryogenic helium-cooled XRS satellite [1] we have had manufactured at NCSU 300 micron thick, 0.75 inch square silicon wafers which include gas flow orifices and rows of etched ridges. The reduced radius of curvature of the superfluid film at the atomically sharp ridges reduces the film thickness to stop film flow. We have designed and constructed a closed-cycle cryocooler-based cryostat to test and to characterize these silicon “film pinners.” We will discuss the design and operation of the cryostat and initial tests of the etched pinners.

[1] P. J. Shirron and M. J. DiPirro, *Adv. in Cryo. Engineering*, vol. 43, p. 949, 1998.

08:54 LB 03 *Diverging Thermodynamic Derivatives in Critical Phenomena in a Binary Liquid Mixture*

**Baird, James;** University of Alabama in Huntsville

The opposite sides of the coexistence curve of a binary liquid mixture with a miscibility gap converge at the critical solution temperature where certain of the thermodynamic derivatives go to infinity [1]. We examine three

cases of solids in contact with a mixture of isobutyric acid + water, which has a critical solution temperature near 26 C: (a) The temperature derivative of the solubility,  $s$ , of a metal oxide goes to infinity as the temperature,  $T$ , approaches the critical temperature [2]. (b) When charcoal comes into contact with the liquid mixture, the derivative of isobutyric acid mole fraction with respect to chemical potential goes to infinity as  $T$  approaches the critical temperature [3]. (c) When the hydroxide form of an anion exchange resin comes into contact with isobutyric acid + water, the isobutyrate anion exchanges with the hydroxide ion. If the fraction of resin sites occupied by isobutyrate anions is assumed to be governed by the Langmuir adsorption isotherm, then the derivative of isobutyric acid mole fraction with respect to resin site mole fraction diverges as  $T$  approaches the critical temperature. We will show that all of these diverging derivatives follow as a consequence of the principle of critical point universality [1].

[1] R. B. Griffiths and J. C. Wheeler, Phys. Rev. A 2, 1047 (1970).

[2] B. Hu, J. K. Baird, R. D. Richey, and R. G. Reddy, J. Chem. Phys. 134, 154505 (2011).

[3] T. J. Giesy, A. S. Chou, R. L. McFeeters, J. K. Baird, and D. A. Barlow, Phys. Rev. E 83, 061201 (2011).

09:06 LB 04 *Superconducting Properties of Nb/Ni Bilayers*

**Ahrenholz, Timothy; Davis, Emily; Broussard, Phillip**; Covenant College

We grew Nb/Ni bilayers in order to observe their behavior as it compares to Usadel theory. The bilayers themselves were grown in a magnetron sputtering system, each consisting of a 33 nm film of Nb and a 0-7 nm film of Ni. These films were deposited on Si wafers. Measurements of the thicknesses of the films were performed with a contact profilometer. We measured the transition temperatures ( $T_c$ ) of the films by cooling them as low as 5 K in a Janis Cryocooler. We measured the  $T_c$  with four different methods to insure accuracy: resistively, inductively, through third harmonic analysis, and resistively from upper critical field measurements. The  $T_c$  with respect to Ni layer thickness for each of these measurements seemed to confirm Usadel theory's predictions to a great extent. In the case of the resistive measurements, the  $T_c$  dropped from 8.31 K to 6.66 K as the thickness of Ni went from 0 nm to 0.48 nm, but then it rose to 7.28 K as Ni thickness reached 3.97 nm, and thereafter remained constant. This pattern of behavior was evident across each of the measurements of  $T_c$ .

09:18 LB 05 *Predicting the temperature for the solid-solid phase transition in ZnS and CdS*

**Barlow, Douglas**; Embry Riddle Aeronautical University

At atmospheric pressure, many of the II-VI semiconducting alloys are known to undergo a zinc-blende to wurtzite solid-solid transition at elevated temperatures below the melting point. Few experimental values for these transitions temperatures have been reported. We show here that chemical potentials for one of the components in a solid solution with the other can be used to estimate the transition temperature. The non-ideal behavior of the solvent component is addressed via an activity coefficient which is computed using the quasi-chemical model. The chemical potentials for each case, zinc-blende and wurtzite are then taken to be equal at the transition temperature. Predicted transition temperatures are reported here, and compared with the experimental values for ZnS and CdS.

09:30 LB 06 *Highly tunable electron transport in epitaxial topological insulator  $(\text{Bi}_{1-x}\text{Sb}_x)_2\text{Te}_3$  thin films*

**Guan, Tong**; Chinese Academy of Sciences, Florida State University **He, Xiaoyue; Wu, K.; Li, Y.**; Chinese Academy of Sciences

Three dimensional topological insulators have emerged as a novel type of quantum materials that may lead to ground-breaking applications such as quantum computation and spintronic devices. These applications, however, often require an insulating bulk. A lot of progress has been made in suppressing the bulk conductivity. Here we report the growth of single crystalline  $(\text{Bi}_{1-x}\text{Sb}_x)_2\text{Te}_3$  films on  $\text{SrTiO}_3(111)$  substrates by molecular beam epitaxy (MBE). A full range of Sb-Bi compositions have been studied in order to obtain the lowest possible bulk conductivity. For the samples with optimized Sb compositions ( $x = 0.5 \pm 0.1$ ), the carrier type can be tuned from n-type to p-type with the help of a back-gate. Linear magnetoresistance has been observed at gate voltages close to the maximum in the longitudinal resistance of a  $(\text{Bi}_{1-x}\text{Sb}_x)_2\text{Te}_3$  sample. These highly tunable  $(\text{Bi}_{1-x}\text{Sb}_x)_2\text{Te}_3$  thin films provide an excellent platform to explore the intrinsic transport properties of the three

dimensional topological insulators.

09:42 LB 07 *Magnetic and Structural Investigations on As-grown and Annealed Pulsed Laser Deposited SnO<sub>2</sub>:Co Thin Films*

(Grant no. NSF DMR-0605734)

**Stoian, Gratiela M.**; Florida State University **Stampe, P.A.**; **Kennedy, R.J.**; Florida A&M University **Xin, Y.**; National High Magnetic Field Laboratory **von Molnar, Stephan**; Florida State University Dilute Magnetic Semiconductor SnO<sub>2</sub>:Co films were deposited on r-cut sapphire substrates via PLD from a doped target with a nominal Co concentration of 5 at.%. To study the role of oxygen vacancies and other defects in tuning the ferromagnetic (FM) and electrical properties of these materials, films were deposited at different growth rates, temperatures and oxygen pressures. In addition, some films were annealed at various conditions. For samples grown at optimal conditions, magnetometer measurements show that films are FM at room temperature for thicknesses between 30 nm and 100 nm, with a saturation magnetization of approximately 20 emu/cm<sup>3</sup>. Crystallinity improves as the thickness decreases and the moment per surface area varies linearly with the film thickness increase, suggesting the magnetism in our materials is a volume property of the films rather than a surface effect. Moreover, we have also noticed a decrease of the saturation magnetization with increasing growth rate. Annealing films grown at a higher deposition rate than optimal under the same conditions used for their growth, led to an initial rapid increase in the saturation magnetization for short annealing times followed by constant saturation magnetization after further annealing.

09:54 LB 08 *The Density of States: Counting that Counts*

**Brown, Gregory**; Florida State University, Oak Ridge National Laboratory

Wang-Landau method and associated Multicanonical Monte Carlo methods make it possible to calculate the density of states  $g(E)$  for thermodynamic systems. This is particularly useful for first-principles calculations, where temperature-dependent quantities like the specific heat and susceptibility can be calculated from, say, 50000 configurations. We have successfully employed an approach combining the classical Heisenberg model of magnetism with first-principles LSMS computations to calculate  $T_c$  in transition metal alloys. The thermodynamic properties of the system can be calculated directly from the  $\ln[g(E)]$  and its derivatives.

---

## SESSION MB: Particle Physics II

*10:45 Saturday Morning*

Salon AB

Chair: Roxanne Springer, Duke University

10:45 MB 01 *Preliminary results from Mississippi State Axion Search*

(Supported by Mississippi State Instrumentations Grant)

**Mohanmurthy, Prajwal**; **Riehle, Robertsen**; **Dutta, Dipangkar**; Mississippi State University, MASS

Mississippi State Axion Search is an exotic particle search experiment using a novel light shining through a wall technique. The experimental setup consists of two tuned vacuum cavities placed under a very strong magnetic field and separated by a wall. While one of the cavities houses a strong EM field generator, the other (dark) cavity houses the detector systems. The electronics consists of multi-stage amplifier system, each based on  $SR - 510$  lock in amplifiers and  $PCI - D$  high speed data cards. The experiment is scheduled to run up to April 2013. The theory leading up to light axions will be previewed highlighting different experimental approaches to search for axions which spans 8 orders of magnitude in mass and a wide plethora of experiments investigating each approach, with their results, will be discussed. Projected sensitivity of MASS for light axions and para-photons besides certain other candidate dark matter particles will be illustrated showing its impact on a wider scale amongst other low cost axion search experiments. Results from the systematics and background studies

will be presented.

10:57 MB 02 *Search for Axions in the 70cm Range*  
(Mississippi State Consortium)

**Riehle, Robertsen**; Mississippi State University, MASS

In 1967 Andrei Sakharov introduced three conditions to produce a universe with a non-zero baryon number. One of those conditions was that charge and charge-parity (CP) symmetry needed to be violated. CP symmetry has not been observed in the strong sector although the Standard Model of Particle Physics allows it. In 1977, Peccei and Quinn proposed a solution to this low upper bound on the observed strong force CP violation. The solution required a new particle called an axion. Finding and understanding the axion could solve the strong CP problem.

The MASS experiment at Mississippi State University utilizes a dipole magnet, a radio field and a conducting wall dividing an evacuated cavity into two. If axions are present, they could be observed beyond the wall in the “dark” end of the cavity. This experiment is still in building and testing phase.

11:09 MB 03 *Vector Currents of Massive Neutrinos of an Electroweak Nature*

**Sharafiddinov, Rasulkhozha**; Uzbekistan Academy of Sciences

The mass of an electroweakly interacting neutrino consists of the electric and weak parts responsible for the existence of its charge, charge radius and magnetic moment. Such connections explain the formation of para-neutrinos, for example, at the polarized neutrino electroweak scattering by spinless nuclei. We derive the structural equations which relate the self components of mass to charge, charge radius and magnetic moment of each neutrino as a consequence of unification of fermions of a definite flavor. They indicate to the availability of neutrino universality and require follow its logic in a constancy law dependence of the size implied from the multiplication of a weak mass of neutrino by its electric mass. According to this principle, all Dirac neutrinos of the vector nature regardless of the difference in masses, have the same charge, an identical charge radius as well as an equal magnetic moment. Thereby, it opens the possibility for establishment of the laboratory limits of weak masses of the investigated types of neutrinos. Finding estimates show clearly that the earlier measured properties of these particles may testify in favor of the unified mass structure of their interaction with any of the corresponding types of gauge fields.

11:21 MB 04 *Particle Trapping in Stable Islands of Transverse Phase Space*

**Frye, Christopher**; University of Central Florida

At CERN, particles are transferred from the Proton Synchrotron (PS) to the Super Proton Synchrotron (SPS) as they accelerate to high energies for subsequent fixed target or neutrino experiments. Since the SPS has a circumference eleven times that of the PS, beams from the PS must be “stretched out” in order to fill the SPS. Traditional methods of carrying out this beam transfer, such as fast extraction and continuous transfer, create either strong transient effects (fast extraction) or suffer from large losses of particles during transfer and a lack of control over optical parameters of the extracted beam (continuous transfer). As a result, a novel method called multi-turn extraction (MTE) has been investigated and implemented in recent years, in which nonlinear magnetic fields create stable islands in the beam’s horizontal phase space, thus separating the beam into parts for clean extraction. We analyze, both analytically and through simulations, a simple model of this phenomenon in order to understand the separate effects of moving and enlarging these phase-space islands. We then apply our conclusions to optimize beam-splitting in a more realistic model.

11:33 MB 05 *Production of Two Heavy Quarks With Different Masses at One-loop with Eikonal Approximation*  
(This material is based upon work supported by the National Science Foundation under Grant No. PHY 1212472.)

**Martin, Elwin**; Georgia Institute of Technology **Kidonakis, Nikolaos**; Kennesaw State University

The eikonal approximation provides a powerful tool for calculating hard scattering cross sections in QCD. In particular, we consider the exchange of soft-gluons between quarks in hard scattering. We present the results for the one loop calculation for two quark production with different masses. These calculations begin with the



Feynman diagram and use the eikonal approximation for soft-gluon emission. The integration is then Feynman parametrized and the UV poles are isolated. The UV structure also allows us to recover the results for quark-antiquark production.

11:45 MB 06 *Deconfinement Transition in Equilibrium Lattice Gauge Theory with Realistic Boundary Conditions*

**Wu, Hao**; Florida State University **Berg, Bernd**; Florida State University

Heavy-ion collision experiments carried out at the Brookhaven National Laboratory provide evidence that matter can be driven from a confined, low-temperature phase into a deconfined high-temperature phase of liberated quarks and gluons. Understanding of the deconfinement transition can bring our knowledge of strongly-interacting matter to a deeper level.

*Ab initio* equilibrium studies of the thermodynamic equation of state in the deconfined phase are possible in the framework of lattice gauge theory. It is most desired in such studies to work on as large lattices as possible in order to approach the infinite volume thermodynamic limit. To accomplish it quickly, most of them have implemented periodic boundary conditions on the physical systems. However, the physical volumes created at the Brookhaven National Laboratory are small and exploratory work for pure  $SU(3)$  lattice gauge theory suggests that boundary effects cannot be neglected. In this work we studied the  $SU(3)$  deconfined equilibrium phase in small volumes with inside and outside temperatures in the  $SU(3)$  scaling region, using a lattice geometry of the double-layered torus. Our results show substantial finite size effects on the deconfining transition temperature under realistic boundary conditions.

11:57 MB 07 *Creating a Public Data Access Website for Double Chooz*

(Thank you to John Parsons and Mike Shaevitz at Columbia University and to the NSF.)

**Carter, Maya**; Stetson University

My talk describes the creation of a public data access webpage that will allow people unaffiliated with the Double Chooz experiment to understand exactly how the value of  $\theta_{13}$  (the final mixing angle for neutrino oscillation) was measured by the experiment. Double Chooz is a two detector neutrino experiment based in Chooz, France that has run since 2011. The website has all the final values found by Double Chooz and the fitting macros that found those values. I will explain the method used for choosing which macros and how much information went up on the website.

---

## SESSION MC: National High-Field Magnet Laboratory II

*10:45 Saturday Morning*

Adams-Park

Chair: Timothy Murphy, National High-Field Magnet Laboratory

10:45 MC 01 *Electronic Multicriticality in B-layer Graphene*

(Supported in part by the NSF CAREER Award under Grant DMR-0955561.)

**Throckmorton, Robert**; **Cvetkovic, Vladimir**; **Vafeek, Oskar**; Florida State University, National High Magnetic Field Laboratory

We use renormalization group (RG) methods to investigate the symmetry-breaking phases of bilayer graphene. We derive the flow equations for different coupling constants that appear in a low-energy effective theory for the system, and show how they may be used to determine the different symmetry-breaking phases in the system. We are able to map out all of the possible phases that the system is unstable to. We also apply our methods to the special case of finite-range, monotonically-decreasing, density-density interactions. We map out which phase(s) that the system is unstable to as a function of the overall interaction strength and of the range. We find that

the system is unstable to an antiferromagnetic state for short-range interactions and to a nematic state, in which the parabolic degeneracy of the low-energy modes splits into two Dirac-like cones, for long ranges. Finally, we investigate, within the framework of variational mean field theory, the behavior of the antiferromagnetic state in the presence of a magnetic field applied perpendicular to the sample. We show how to determine the energy gap in the system, and find a slight non-monotonic behavior at low fields and a quasi-linear behavior at high fields. We then compare this result to experimental findings.

10:57 MC 02 *Effects of Lateral Diffusion on the Dynamics of Desorption*

**Juwono, Tjipto; Abou Hamad, Ibrahim; Arne Rikvold, Per;** Florida State University

The adsorbate dynamics during simultaneous action of desorption and lateral adsorbate diffusion is studied in a simple lattice-gas model by kinetic Monte Carlo simulations. It is found that the action of the coverage-conserving diffusion process during the course of the desorption has two distinct, competing effects: a general acceleration of the desorption process, and a coarsening of the adsorbate configuration through Ostwald ripening. The balance between these two effects is governed by the structure of the adsorbate layer at the beginning of the desorption process. It is found that when starting with larger cluster sizes, the acceleration effect of diffusion dominates, while starting with smaller cluster sizes results in the dominance of coarsening. It is also found that the initial size distribution of the adsorbate determines both the quantitative and the qualitative features of the distribution as it develops during the desorption process.

11:09 MC 03 *Gauge Fields and Interlayer Coherence in Bilayer Composite Fermion Metals*

**Cipri, Robert; Bonesteel, N.E.;** Florida State University, National High Magnetic Field Laboratory

The  $\nu=1$  ( $=1/2+1/2$ ) bilayer quantum Hall system exhibits at least two distinct phases as a function of layer spacing,  $d$ . In the limit of large layer spacing ( $d \gg l$ , where  $l$  is magnetic length) the system decouples into two distinct compressible  $\nu=1/2$  “composite Fermi liquid” states. In the opposite limit of small layer spacing ( $d \ll l$ ) the system enters an incompressible bilayer quantum Hall state (the “111” state). After decades of study, the transition between these two states is still poorly understood. Recently, Alicea et al. [1] have proposed an interesting new state which might exist in this system for intermediate layer spacing ( $d \sim l$ ). In this so-called “interlayer phase coherent” state, composite fermions tunnel coherently between layers and form well-defined bonding and antibonding Fermi seas, despite the fact that there is no actual tunneling of physical electrons. We study the effect of the Chern-Simons gauge fields associated with the composite fermions on the formation of such an interlayer phase coherent state. We show that scattering from these gauge fields leads to layer-dependent fluctuations in the Aharonov-Bohm phase of the composite fermions which strongly suppress interlayer phase coherence. This suppression manifests itself through the appearance of a contribution to the ground state energy which is logarithmically singular in the order parameter characterizing this interlayer coherence.

[1] J. Alicea, O. I. Motrunich, G. Refael, M. P. A. Fisher, Phys. Rev. Lett. 103, 256403 (2009)

11:21 MC 04 *Field-induced spin-flop transitions in single-crystalline  $\text{La}_{0.25}\text{Pr}_{0.75}\text{Co}_2\text{P}_2$*

**Xu, Tongshuai;** Florida State University, Shandong University **Kovnir, Kirill; Chai, Ping; Shatruk, Michael;** Florida State University **Xiong, Peng;** Florida State University

We report measurements of anisotropic magnetization and magnetoresistance (MR) on single crystals of  $\text{La}_{0.25}\text{Pr}_{0.75}\text{Co}_2\text{P}_2$ , a novel magnetic alloy with the  $\text{ThCr}_2\text{Si}_2$ -type structure, which is a parent structure of the ferro-pnictide high-temperature superconductors. The material exhibits two magnetic transitions in the  $c$ -axis direction at 240 K and 10.5 K. Below 10K, the magnetization and MR measurements provide corroborating evidence that applying a magnetic field along the  $c$ -axis induces two successive spin-flop transitions at 0.5 T and 5.5 T. For a magnetic field applied in the  $ab$  plane, spins cannot be fully polarized at up to 7 T and the MR changes sign from negative to positive at  $\sim 20$  K with increasing temperature. The observations are consistent with a magnetic configuration, in which the Pr and Co magnetic moments are oriented along the  $c$  axis and ordered ferromagnetically within the  $ab$  plane but antiferromagnetically along the  $c$  axis. Details of the microscopic origin of the spin-flop transitions will be discussed.

11:33 MC 05 *Carrier density dependence of spin lifetime in Fe/AlGaAs heterostructures*

**Kim, Joon-II; Misuraca, Jennifer; Kountouriotis, Konstantinos; von Molnar, Stephan; Xiong, Peng;** Florida State University **Meng, Kangkang; Lu, Jun; Chen, Lin; Yu, Xuezhe; Zhao, Jianhua;** Chinese Academy of Sciences

Electrical Hanle-type measurements have been performed to determine spin lifetimes at various carrier densities in Si:Al<sub>0.3</sub>Ga<sub>0.7</sub>As, a persistent photoconductor (PPC). The carrier density of this material can be tuned, changing it from insulating to metallic *in situ* via photo excitation. Utilizing this PPC effect, we conduct electrical measurements of spin accumulation and transport under the same experimental conditions without the necessity of making replicas to realize different doping levels. We report the carrier density dependence of the spin lifetime derived from Hanle measurements with spin devices formed on wafers which have different graded junctions and Si doping levels. Carrier densities ranged from  $3.5 \times 10^{16}$  to  $2.4 \times 10^{17}$  cm<sup>-3</sup> and from  $7.2 \times 10^{16}$  to  $6.5 \times 10^{17}$  cm<sup>-3</sup> in two different samples. The spin lifetimes (determined using Lorentzian fits to the Hanle curves) ranged from 0.5 to 2.8 ns. From optical studies, the spin lifetime at zero bias and at low temperature in n-GaAs was reported to be larger than 100 ns on the insulating side and ~80 ns on the metallic side. Based on our measurements in Si:Al<sub>0.3</sub>Ga<sub>0.7</sub>As, the extrapolated spin lifetime at zero bias and at 5 K is found to be only ~2.3 ns on the insulating side and decreases with increasing bias current.

11:45 MC 06 *Measurements of Molecule-Based Magnets using micro-SQUID on a Waveguide*

**Yue, Guang;** Florida State University, National High Magnetic Field Laboratory **Wernsdorfer, Wolfgang;** Institut Neel **Chiorescu, Iriuel;** Florida State University, National High Magnetic Field Laboratory

We describe a setup design which plans to use a dc micro-SQUID to measure the magnetization signal of a magnetic sample while the spins are excited by microwave pulses. Such on-chip techniques are gathering more and more interest. In a first approach, the SQUID chip containing the studied sample, will be placed on top of another chip containing the waveguide. Computer simulations are done to verify that the field strength is sufficiently strong and uniform in this case. In another approach, we integrate a microwave waveguide on the same chip as the SQUID.

The presented setup will be able to sense the magnetic flux generated by rotating spins, without the need of analyzing the output microwave signal. The microwave will only serve as an input pulse, to excite the spin dynamics.

11:57 MC 07 *Magnetic Dipolar Interactions in Nanoparticle Assemblies*

**Chandra, Manabendra; Knappenberger, Kenneth;** Florida State University

I will present evidence of a magnetic dipolar contribution to the nonlinear optical (NLO) response of colloidal metal nanostructures. Second-order NLO responses from several small assemblies of solid gold nanospheres (SGN) were examined using polarization-resolved second harmonic generation (SHG) spectroscopy at the single-particle level. Unambiguous circular dichroism in the SH signal was observed for many of the nanostructures, indicating that the plasmon field located within the interparticle gap was chiral. Detailed analysis of the polarization line shapes of the SH intensities obtained by continuous polarization variation suggested that the effect resulted from strong magnetic-dipole contributions to the nanostructure's optical properties.

12:09 MC 08 *Relaxation Dynamics of Electronically Excited Metal Nanoclusters*

**Green, Thomas; Knappenberger, Kenneth;** Florida State University

Recent advances describing optical properties and relaxation dynamics of electronically excited nanoclusters are presented. Femtosecond time-resolved transient absorption and magneto-photoluminescence data were used to study properties of excited states located near the HOMO-LUMO energy gap for anionic and neutral Au<sub>25</sub>(SCH<sub>2</sub>CH<sub>2</sub>Ph)<sub>18</sub>. With these data, we show the optical properties of these nanoclusters are charge-state dependent. Transient absorption measurements employing NIR probe pulses reveal a previously unobserved relaxation process for neutral nanoclusters with a lifetime of several hundred picoseconds. Information regarding the electronic g-factor and photoluminescence rates of these clusters were obtained from temperature- and magnetic field-dependent measurements. Together these data indicate neutral nanocluster emission proceeds

through multiple channels, including both high- and low-spin states. Quantum-confined, ligand-protected gold nanoclusters represent a class of nanomaterials with potential application across a wide range of fields. These results will impact several technologies, including: optical imaging, energy conversion, and catalysis, which all feature the nanocluster platform.

12:21 MC 09 *Scalable Lipid Multilayer Microarraying*

(Acknowledges funding from the state of Florida)

**Lowry, Troy; Lenhart, Steven;** Florida State University

A need exists for scalable, high throughput screening of both lipophilic drug candidates and biosensors. Surface-supported lipid multilayer nanostructures are lipid molecules thicker than a bilayer with controlled thickness physisorbed to a substrate and have promising applications in scalable drug screening...<sup>1</sup> and biosensing...<sup>2</sup> Uniform lipid nanostructures with multilayers of controlled thickness are essential for drug screening in order to control the dosage of drug candidates and for adhesion of cells. Methods for controlling lipid multilayer thickness have been shown using DPN nanolithography<sup>2</sup> and multilayer stamping.<sup>3</sup> In order for scalability to be achieved, multiple different lipid multilayers need to be arrayed onto the same surface. In this work, liposomal lipid concentrations are microarrayed onto an 'ink-palette' made of PDMS and in combination with multilayer stamping, lipid nanostructures are patterned onto a substrate. Characterization of the patterns is shown using fluorescence and atomic force microscopy. The method is used to test how different lipid-drug combinations alter the efficacy of drugs.

1 Kusi-Appiah, A. E., Vafai, N., Cranfill, P. J., Davidson, M. W. & Lenhart, S. Lipid multilayer microarrays for in vitro liposomal drug delivery and screening. *Biomaterials* **33**, 4187-4194, doi:10.1016/j.biomaterials.2012.02.023 (2012).

2 Lenhart, S. *et al.* Lipid multilayer gratings. *Nat. Nanotechnol.* **5**, 275-279, doi:10.1038/nnano.2010.17 (2010).

3 Nafday, O. A., Lowry, T. W. & Lenhart, S. Multifunctional Lipid Multilayer Stamping. *Small* **8**, 1021-1028, doi:10.1002/smll.201102096 (2012).

# Index

- Abdel-Fattah, Mahmoud , 27, 30  
Abou Hamad, Ibrahim , 24, 58  
Abrahamsen, Dylan , 41  
Adhikari, Sushovit , 45  
Ahrenholz, Timothy , 9, 49, 54  
Akpovo, Charlemagne , 7, 30  
Al Ghoul, Hussein , 15  
Alexander, Alonzo B. , 13  
Alexander, J.A. , 10  
Allen, S.D. , 44  
Allgower, Chris , 34  
Almagri, Abdulgader , 13  
Anderson, Dakotah , 39  
Anderson, Eamon , 36  
Andrew, Keith , 12, 38  
Anker, Jeffrey , 39  
Appavoo, Kannatassen , 48  
Arce, Ayana , 1  
Arne Rikvold, Per , 58  
Assi, Hiba , 24  
Atkinson, William , 11  
Austin, Jasmine , 27  
Avila, M.L. , 31  
Babilonia, Yari , 50  
Baby, L.T. , 16, 17, 32  
Bahmani, Fatemeh , 12  
Baibekov, E. , 9  
Baird, James , 53  
Baker, Jessica , 17, 32  
Baker, Robert , 37  
Barbara, B. , 9  
Barlow, Douglas , 54  
Barreda, Jorge , 4, 48  
Beaudoin, Christopher , 39  
Beedle, C.C. , 6, 47  
Beiersdorfer, P. , 7  
Belarge, Joseph , 32  
Belyanin, A. , 4  
Bender, P. , 31, 32  
Berg, Bernd , 57  
Bermes, Karen , 44  
Bertaina, Sylvain , 5, 9, 40  
Besara, T. , 5  
Betzwieser, Joe , 28  
Bililign, Solomon , 46  
Blackmon, J. , 32  
Blessing, Susan , 41  
Bollen, Georg , 37  
Bonesteel, N.E. , 58  
Borchers, Nick , 23  
Boye, D.M. , 49  
Brewer, N.T. , 31  
Brooks, James , 3, 5  
Broussard, Phillip , 9, 49, 54  
Brown, Gregory , 55  
Brown, Staci , 7, 30  
Brunt, Christopher , 20  
Bullock, N.A. , 44  
Cabarcas, Jari , 50  
Camata, Enrico , 50  
Camata, Renato , 50  
Canfield, Brian K. , 27  
Carpenter, M. , 31  
Carter, Maya , 57  
Chai, Ping , 58  
Chambers, Erin , 34  
Chandra, Manabendra , 59  
Chan, Chor-Hoi , 51  
Chapurin, Roman , 53  
Chavez, Ermides , 50  
Chen, Lin , 59  
Chen, Wei-Chia , 31  
Chen, X. , 31  
Cherian, J.G. , 4  
Chiara, C. , 31  
Chiorescu, Irinel , 5, 40, 59  
Cho, Hyoyeong , 30  
Cho, Won Sang , 22  
Christen, D.K. , 10  
Cipri, Robert , 58  
Clark, R. , 31  
Cohn, Robert W. , 29  
Colella, Antonio , 21  
Cole, M. , 48, 50  
Coniglio, William , 3  
Craft, Sean , 44  
Cramer, Mark , 12  
Cruz, Linda , 12, 38  
Cupp, Samuel , 52  
Curtis, Jeremy , 4, 9  
Cvetkovic, Vladimir , 57  
Daniels-Race, Theda , 10, 11  
Das, Susmita , 10  
Davidson, II, Roderick B. , 47

Davis, Emily , 9, 49, 54  
 Davis, Lloyd M. , 27  
 Daw, Murray , 25  
 Diener, Peter , 52  
 Divakar, Madhavi , 10  
 Dobramysl, Ulrich , 24  
 Dobrokhotov, Vladimir , 10  
 Donaldson, A.B. , 46  
 Dorosz, Sven , 25  
 Drake, Paul , 43  
 Duston, Christopher , 13  
 Dutta, Dipangkar , 16, 42, 55  
 Ebong, Imeh , 17  
 Engelhardt, Larry , 14, 18, 38, 42  
 Ethier, Jacob , 35  
 Evans, Nicholas , 8  
 Fallon, P. , 31  
 Fiddler, Marc , 46  
 Field, Rick , 19, 35  
 Flaig, Markus , 43  
 Fowler, Nicholas , 42  
 Frame, Dillon K. , 53  
 Frlez, Emil , 20  
 Frye, Christopher , 56  
 Fry, Jason , 36  
 Fudala, Rafal , 30  
 Gaerlan, Mikhail , 42  
 Gafarov, O. , 10  
 Gainer, James , 22  
 Gambarelli, S. , 9  
 Gao, Yang , 25  
 Gapud, A.A. , 10  
 Gardiner, Hannah , 36  
 Garland, Scott , 38  
 Gates, James Sylvester , 21  
 Gay, Dennis , 17, 32  
 Germann, James A. , 27  
 Germiller, Austin , 24  
 Ghimire, Bishwas , 44, 45  
 Gibson, Steven , 20  
 Gill, W. , 46  
 Goloverda, Galina , 50  
 Gomez, Alicia , 41  
 Gordon, Emily , 35  
 Graf, David , 3  
 Gray, S. , 48, 50  
 Green, Thomas , 59  
 Grosskopf, Michael , 43  
 Group, Craig , 19, 35  
 Gryczynski, Ignacy , 30  
 Gryczynski, Zygmunt , 30  
 Guan, Tong , 4, 54  
 Gurfinkel, Aleks , 51  
 Haase, David G. , 53  
 Haglund, Richard , 47, 48  
 Hah, Hien-Yoong , 48, 50  
 Hall, Jessica , 10  
 Hamilton, J.H. , 31  
 Hamilton, L. , 31  
 Hampton, D.G. , 49  
 Handy, Timothy , 42  
 Hartanto, Heribertus , 2  
 Hasan, Farhana , 10  
 Hasnaoui, Karim , 33  
 Heath, Jonathan , 39  
 Height, J. , 46  
 Hellstrom, Eric , 5  
 Henderson, Alyssa , 19, 35  
 Hennrich, F. , 6  
 Hess, Dennis W. , 10  
 He, Xiaoyue , 4, 54  
 Hill, S. , 6, 47  
 Hilton, D.J. , 4, 9  
 Hoang, Trang , 22  
 Hoch, M.J.R. , 5  
 Hodge, John , 43  
 Hoffman, C. , 31  
 Holley, Adam , 36  
 Howard, Ward , 20  
 Huff, Ashley , 41  
 Hu, Longqian , 4  
 Hwang, J.K. , 31  
 Hynds, Taylor , 40  
 Ihas, Gary , 53  
 Intoy, Ben , 25  
 Jackson, Ashley , 27  
 Jackson, Christopher , 2  
 Janssens, R.V.F. , 31  
 Jenkins, Charles , 23  
 Jiang, Jianyu , 5  
 Johnson, C.E. , 48  
 Johnson, Charles , 50  
 Johnson, E.D. , 32  
 Johnson, J.A. , 48  
 Johnson, Jacqueline , 50  
 Johnson, Lewis , 7, 30  
 Johnson, T.L. , 34  
 Jolly, Christian , 20  
 Jones, Daniel , 45  
 Jones, Robert , 6

**Joung, Daeha** , 18  
**Jung, Sungsoo** , 27, 30  
**Juwono, Tjipto** , 58  
**Kabza, Konrad** , 45  
**Kamarás, K.** , 6  
**Kametani, Fumitake** , 5  
**Kanakamedala, Kalyan** , 10  
**Keiper, Timothy** , 48  
**Keiter, Paul** , 43  
**Kennedy, R.J.** , 55  
**Kidonakis, Nikolaos** , 56  
**Kim, Bomi** , 36, 37  
**Kim, Harold** , 26  
**Kim, Joon-Il** , 48, 59  
**Kim, Wan-Joong** , 27, 30  
**King, Jason K.** , 27  
**Kintzel, Edward** , 12, 38  
**Klein, Susan** , 34  
**Knappenberger, Kenneth** , 59  
**Kolesnichenko, Vladimir** , 50  
**Kono, J.** , 4  
**Koshchiy, E.** , 16, 31, 32  
**Kountouriotis, Konstantinos** , 59  
**Kovalev, A.** , 6  
**Kovalskiy, Andriy** , 49  
**Kovnir, Kirill** , 58  
**Kuchera, A.N.** , 32  
**Kucheryavy, Pavel** , 50  
**Kuhns, P.L.** , 5  
**Kuntscher, C.A.** , 6  
**Kuranz, Carolyn** , 43  
**Kuvin, Sean** , 17, 32  
**Labbe, Greg** , 53  
**Lai, J.** , 32  
**Larbalestier, David** , 5  
**Larin, Alexander** , 10  
**Lauritsen, T.** , 31  
**Learn, Ryan** , 37  
**Lehman, Martin** , 16  
**Lenhert, Steven** , 60  
**Leonard, Katie** , 13  
**Leszczewicz, Jason** , 12  
**Lewis, Dawn** , 7, 30  
**Liang, Jason** , 19  
**Liang, Zhiyong** , 44  
**Lim, Halston** , 19  
**Lim, Kyung Taek** , 14  
**Lincoln, David** , 37  
**Lingle, Mark** , 14  
**Linhardt, L.** , 32  
**Liu, Junjie** , 47  
**Li, Wenzhi** , 17  
**Li, Y.** , 4, 54  
**Lowry, Troy** , 60  
**Luo, Y.X.** , 31  
**Lu, Jun** , 59  
**Macchiavelli, A.** , 31  
**Macon, K.** , 32  
**Maheswaranathan, Ponn** , 49  
**Malkin, B.** , 9  
**Martens, Mathew** , 40  
**Martens, Matthew** , 5  
**Martinez, Jorge** , 7, 30  
**Martin, Elwin** , 56  
**Martin, Kate** , 39  
**Matchev, Konstantin** , 22  
**Matos, M.** , 32  
**Mayo, Daniel** , 47  
**McClintock, Luke** , 4, 9  
**McClintock, Peter** , 53  
**McCutchan, E.** , 31  
**McGahan, Christina** , 48  
**McGill, S.A.** , 4  
**McLaughlin, Chatham David** , 33  
**Melnitchouk, Wally** , 35  
**Mendoza, William** , 14  
**Meng, Kangkang** , 59  
**Merten, J.A.** , 44  
**Mezonlin, Ephrem** , 13  
**Mickens, Ronald E.** , 25, 26  
**Migirditch, Sam** , 14  
**Misuraca, Jennifer** , 59  
**Mitchell, G.E.** , 34  
**Mitchell, J.F.** , 5  
**Mitra, T.** , 9  
**Moerland, Daniel** , 40  
**Mohanmurthy, Prajwal** , 16, 42, 55  
**Moldenhauer, Jacob** , 18, 42  
**Moore, Keith** , 36  
**Muller, A.** , 9  
**Munday, Lydia** , 53  
**Murphy, Timothy** , 3  
**Mu, Richard** , 47  
**Neu, Chris** , 2  
**Novikov, Ivan** , 35, 36  
**Oakley, R.T.** , 6  
**Odrzywolek, Andrzej** , 42  
**Oelgoetz, Justin** , 44, 49  
**Oganessian, Yu.Ts.** , 31  
**Oksuzian, Yuri** , 19, 35

**Onken, Drew** , 49  
**Osborn, Joe** , 15  
**Oyedeji, 'Kale** , 25  
**Pálka, Karel** , 49  
**Palmer, Jahi** , 12, 38  
**Palmquist, Shane** , 12, 38  
**Palm, Eric** , 3  
**Parigger, C.G.** , 44–46, 48  
**Park, Hye-Sook** , 43  
**Park, Hyunhang** , 23  
**Park, Jin Gyu** , 44  
**Park, Ju-Hyun** , 3  
**Paschalis, S.** , 31  
**Penumadu, Dayakar** , 12, 28  
**Peplowski, Patrick** , 32  
**Perdikakis, Georgios** , 17, 32  
**Petri, M.** , 31  
**Phillips, David** , 15  
**Piekarewicz, Jorge** , 31, 33  
**Pindzola, M.S.** , 30  
**Pino, James** , 36, 37  
**Pleimling, Michel** , 23–25  
**Plewa, Tomasz** , 37, 42, 43  
**Polyanskii, Anatolii** , 5  
**Poroseva, Svetlana V.** , 24  
**Potts, Jay** , 36  
**Powers, Adam** , 42  
**Prosper, Harrison** , 1  
**Pudukodu, Harish** , 19  
**Quackenbush, Seth** , 22  
**Raffield, Jesse** , 24, 51  
**Ramayya, A.V.** , 31  
**Ramdon, Roopchan** , 30  
**Rasmussen, J.O.** , 31  
**Ray, Amy** , 42  
**Redshaw, Matt** , 37  
**Reed, K.J.** , 7  
**Reina, Laura** , 2  
**Remington, Bruce** , 43  
**Remington, Eric** , 50  
**Reno, J.L.** , 4  
**Rericha, Erin** , 26  
**Reviol, W.** , 31  
**Reyes, A.P.** , 5  
**Rezaee, M.R.** , 45  
**Rhodes, Christian** , 39  
**Richards, Howard** , 24, 51  
**Rich, Ryan** , 30  
**Riehle, Robertsen** , 42, 55, 56  
**Rikvold, Per Arne** , 24, 51  
**Ringle, Ryan** , 37  
**Roberts, Winston** , 40  
**Rogachev, G.V.** , 16, 31, 32  
**Rojas, Alexander** , 32  
**Rondinone, Adam** , 29  
**Rosenfeld, Spencer** , 40  
**Rowland, James R.** , 53  
**Rubinov, Paul** , 19, 35  
**Samarakoon, Duminda K.** , 10  
**Santiago-Gonzalez, Daniel** , 16, 17, 32  
**Santiago, Manuel** , 36, 37  
**Sarantites, D.** , 31  
**Sarkar, Anirban** , 11  
**Sasaki, T.** , 44  
**Sato, Nobuo** , 3  
**Schelp, Rich** , 52  
**Schlottmann, Pedro** , 3  
**Scholberg, Kate** , 19  
**Schwarz, Stefan** , 37  
**Scime, Earl** , 43  
**Seo, Jaetae** , 27, 30  
**Serniak, Kyle** , 5, 40  
**Serpico, Jonathan** , 36  
**Seweryniak, D.** , 31  
**Shabestari, Mitra** , 42  
**Shafranovsky, E.** , 48  
**Shapera, Ethan Paul** , 48  
**Sharafiddinov, Rasulkhozha** , 52, 56  
**Shatruk, Michael** , 58  
**Sheehy, Daniel** , 18  
**Shiddiq, Muhandis** , 47  
**Shields, Austin** , 24  
**Shim, J.** , 9  
**Shriner, Jr., J.F.** , 34  
**Shrock, Robert Ellsworth** , 24  
**Shuler, Ezekiel** , 18, 38, 42  
**Siegrist, T.M.** , 3, 5  
**Silano, J.A.** , 41  
**Silversmith, A.J.** , 49  
**Singh, Sujeeta** , 46  
**Siraj, Noureen** , 10  
**Skinner, Alex** , 50  
**Smith, A.J.** , 7  
**Smith, R. Seth** , 46  
**Snow, Mike** , 36  
**Sowell, Dewayne** , 10  
**Stampe, P.A.** , 55  
**Stillwell, Ryan** , 3  
**Stoian, Gratiela M.** , 55  
**Stone, Keenan** , 18, 42



**Sullivan, Zack** , 22  
**Surmick, D.M.** , 46  
**Swafford, L.D.** , 48  
**Täuber, Uwe C.** , 24  
**Tabibi, Bagher** , 27, 30  
**Tabor, Samuel** , 31, 32  
**Tai, Pei-Luan** , 31, 32  
**Talbert, Justin** , 49  
**Tarantini, Chiara** , 5  
**Tedela, Getachew** , 46  
**Ter-Akopian, G.M.** , 31  
**Thapa, Bidhan** , 44  
**Thavayoganathan, Kirubaa** , 38  
**Thirunavukkuarasu, K.** , 6  
**Thomas, Edward** , 43  
**Thomas, John** , 29  
**Thompson, Kyle** , 53  
**Throckmorton, Robert** , 57  
**Titus, James B.** , 13  
**Tokumoto, T.T.** , 4  
**Tozer, Stanley** , 3, 6  
**Trennepohl, C.J.** , 49  
**Tripathi, Vandana** , 31, 32  
**Tsaris, Aristeidis** , 15  
**Tsukerblat, B.** , 9  
**Ullrich, Susanne** , 7, 8  
**Uwakweh, Oswald** , 50  
**Vafek, Oskar** , 57  
**Valverde, Adrian** , 37  
**Van Winkle, David** , 46  
**Vargas, Guillermo** , 47  
**Vasquez, Rafael** , 3  
**Veeraraghavan, Venkatesh** , 2  
**Vlček, Miroslav** , 49  
**Volya, Alexander** , 14, 32, 41  
**von Molnar, Stephan** , 4, 55, 59  
**VonMoss, Justin** , 32  
**Walsh, Robert** , 5  
**Wang, Andrew** , 30  
**Wang, E.H.** , 31  
**Wang, Lingfei** , 4  
**Wang, X.** , 4  
**Wang, Xiao Long** , 20, 52  
**Wang, Xiao-Qian** , 10  
**Warnberg, D.** , 48  
**Warner, Isiah** , 10  
**Weiss, Jeremy** , 5  
**Wei, Ling** , 46  
**Wernsdorfer, Wolfgang** , 59  
**Westmark, David** , 2  
**Whalen, J.B.** , 5  
**Whalen, Jeffrey** , 3  
**Whitson, Kristin** , 36, 37  
**Whitson, Stefanie** , 36, 37  
**Widejko, Ryan** , 36  
**Wiedenhöver, Ingo** , 16, 17, 32, 40, 41  
**Williams, K.M.** , 43  
**Williams, Michael D.** , 10  
**Willoughby, William** , 8  
**Wilson, David** , 19, 35  
**Winter, Laurel** , 3  
**Winter, Stephen** , 6  
**Witte, M.** , 44  
**Womble, Phillip** , 45  
**Woodard, Richard** , 13  
**Woodruff, Simon** , 43  
**Woods, A.C.** , 45, 46  
**Woods, Lilia** , 17  
**Wood, Dylan** , 44  
**Wood, John** , 2  
**Woolbright, Stephen** , 52  
**Woracek, Robin** , 12  
**Wu, Hao** , 57  
**Wu, J.Z.** , 10  
**Wu, K.** , 4, 54  
**Wu, W.** , 4  
**Xin, Y.** , 55  
**Xiong, Peng** , 4, 48, 58, 59  
**Xu, Tongshuai** , 58  
**Xu, Yan** , 24, 51  
**York-Winegar, James** , 49  
**Yoshida, Sanichiro** , 44, 45  
**Young, Stephen** , 12  
**Yuan, S.** , 5  
**Yue, Guang** , 59  
**Yukich, John** , 14  
**Yu, Hui** , 8  
**Yu, Liuqi** , 4  
**Yu, William** , 30  
**Yu, Xuezhe** , 59  
**Zhang, Xiaohang** , 4  
**Zhao, Jianhua** , 59  
**Zheng, H.** , 5  
**Zheng, Jim P.** , 48  
**Zhiglo, Andrey** , 37  
**Zhu, S.J.** , 31  
**Zhu, S.** , 31  
**Zia, R.K.P.** , 23  
**Ziegler, Jed I.** , 47  
**Zvanut, Mary Ellen** , 8

---

---

---

# SPONSORS

